THE MECHANOTRANSDUCTION OF HYDROSTATIC PRESSURE BY MESENCHYMAL STEM CELLS

A Thesis

Submitted to the Faculty

of

Purdue University

by

Seyedeh Ghazaleh Hosseini

In Partial Fulfillment of the

Requirements for the Degree

of

Master of Science in Biomedical Engineering

December 2018

Purdue University

Indianapolis, Indiana

THE PURDUE UNIVERSITY GRADUATE SCHOOL
STATEMENT OF COMMITTEE APPROVAL

Dr. Diane R. Wagner, Chair

Department of Mechanical Engineering

Dr. Julie Ji

Department of Biomedical Engineering

Dr. Sungsoo Na

Department of Biomedical Engineering

Approved by:

Dr. Julie Ji

Head of the Graduate Program

ACKNOWLEDGMENTS

First of all, I would like to appreciate Dr. Diane Wagner for her support as an advisor. She always encouraged and motivated me and taught me a lot about work and also life. I would like to thank my committee members, Dr. Julie Ji and Dr. Sungsoo Na, for their support and suggestions. I also would like to thank the funding source, which is National Science Foundation grant # 1563721.

Thanks to all my colleagues in Dr. Wagner's lab past and present, including, Komal Yadav, Huseyin Arman, Dr. Nizeet Aguilar, and Dr. Sonali Karnik, Amin Joukar, and Hessam Noori. Special thanks go to Sherry Clemens for helping me with all the administrative work.

I would like to give my most appreciation to my mother, father, sister, and friends who have supported me through all the hardships and have been warmth of my heart.

TABLE OF CONTENTS

Page

Page

Page

LIST OF TABLES

LIST OF FIGURES

Figure Page

Figure Page

LIST OF ABBREVIATIONS

Agc	Aggrecan
AMP-B	Amphotericin B
ASC	adipose-derived stem cell
ATP	Adenosine triphosphate
bFGF	basic fibroblast growth factor
BMP	bone morphogenetic proteins
Ca^{++}	Calcium ions
cDNA	complimentary deoxyribonucleic acid
Col2	Collagen II
DMMB	dimethylmethylene blue
DNA	deoxyribonucleic acid
DTT	Dithiothreitol
ECM	extracellular matrix
ESC	embryonic stem cell
FAK	focal adhesion kinase
GAG	glycosaminoglycan
HGF	hepatocyte growth factor
HP	hydrostatic pressure
IGF	insulin-like factor
iPSC	induced pluripotent stem cells
MAP	mitogen-activated protein
MSCs	mesenchymal stem cells
NAD	Nicotinamide adenine dinucleotide
OA	Osteoarthritis

PEEK	polyether ether ketone
PGA	polyglycolic acid
PLA	poly lactic acid
PLGA	poly(lactic-co-glycolic) acid
RA	rheumatoid arthritis
RT-PCR	real time-polymeric chain reaction
SERC	sarcoendoplasmic reticulum Ca^{++} stores
TGF	transforming growth factor
VGCC	voltage gated Ca^{++} channels

ABSTRACT

Hosseini, Seyedeh Ghazaleh M.S.B.M.E., Purdue University, December 2018. The Mechanotransduction of Hydrostatic Pressure by Mesenchymal Stem Cells. Major Professor: Diane R. Wagner.

Mesenchymal stem cells (MSCs) are responsive to mechanical stimuli that play an essential role in directing their differentiation to the chondrogenic lineage. A better understanding of the mechanisms that allow MSCs to respond to mechanical stimuli is important to improving cartilage tissue engineering and regenerative medicine. Hydrostatic pressure (HP) in particular is known to be a primary mechanical force in joints. However, little is known about the underlying mechanisms that facilitate HP mechanotransduction. Understanding the signaling pathways in MSCs in transducing HP to a beneficial biologic response and their interrelationship were the focus of this thesis. Studies used porcine marrow-derived MSCs seeded in agarose gel. Calcium ion Ca^{++} signaling, focal adhesion kinase (FAK) involvement, and sirtuin1 activity were investigated in conjunction with HP application.

Intracellular Ca^{++} concentration was previously shown to be changed with HP application. In our study a bioreactor was used to apply a single application of HP to the MSC-seeded gel structures and observe Ca^{++} signaling via live imaging of a fluorescent calcium indicator in cells. However, no fluctuations in Ca^{++} concentrations were observed with 10 minutes loading of HP. Additionally a problem with the bioreactor design was discovered. First the gel was floating around in the bioreactor even without loading. After stabilizing the gel and stopping it from floating, there were still about 16 μm of movement and deformation in the system. The movement and deformation was analyzed for the gel structure and different parts of the bioreactor.

Furthermore, we investigated the role of FAK in early and late chondrogenesis and also its involvement in HP mechanotransduction. A FAK inhibitor was used on MSCs from day 1 to 21 and showed a dose-dependent suppression of chondrogenesis. However, when low doses of FAK inhibitor added to the MSC culture from day 21 to 42, chondrogenesis was not inhibited. With 4 hour cyclic HP, FAK phosphorylation increased. The beneficial effect of HP was suppressed with overnight addition of the FAK inhibitor to MSC medium, suggesting FAK involvement in HP mechanotransducation by MSCs.

Moreover, sirtuin1 participation in MSC chondrogenesis and mechanotransduction was also explored. The results indicated that overnight sirtuin1 inhibition increased chondrogenic gene expression (Agc, Col2, and Sox9) in MSCs. Additionally, the activity of sirtuin1 was decreased with both 4 hour cyclic hydrostatic pressure and inhibitor application. These two together demonstrated that sirtuin1 inhibition enhances chondrogenesis.

In this research we have investigated the role of Ca^{++} signaling, FAK involvement, and sirtuin1 activity in the mechanotransduction of HP in MSCs. These understandings about the mechanisms regulating the chondrogenesis with respect to HP could have important implications for cartilage tissue engineering and regenerative studies.

1. INTRODUCTION

1.1 Articular Cartilage Composition and Structure

1.1.1 Composition of Articular Cartilage

Articular cartilage is a connective tissue lining the outer surfaces of bones in diarthrosis joints; tissue thickness can vary from 1.5 to 3 mm [1]. Articular cartilage is made up of two different phases; solid and liquid. The solid phase itself is composed of two main parts.

The first part is cells, which forms 1% of the total tissue volume and can modify the other part of the solid phase, which is extra cellular matrix (ECM) [2]. The only type of cells in cartilage are chondrocytes, which sense and react to different kinds of mechanical stimuli in their secreted microenvironment. Moreover, they form various morphologies in different zones of articular cartilage. The dense ECM around the cells does not allow them to migrate or proliferate significantly [3], limiting regeneration when injury happens.

The ECM is composed of different organic proteins and proteoglycans and a small amount of fibronectin. The main proteins in articular cartilage ECM are collagens. As the cartilage matures, the random distribution and uniform size of collagen transforms to have an oriented distribution with non-uniform size [4]. Moreover, type II collagen is the most prevalent in mature tissue, in comparison to collagen type VI, IX, X, and XI. Collagen II comprises 15%-20% wet weight of the cartilage and contributes to the tensile properties and macromolecular entrapment of cartilage [3]. In addition, collagens IX and XI form fibrils when crosslinked with collagen II and results in a mesh structure that also plays roles in tensile properties [4]. Beside collagen II,

collagen VI has been shown to be a part of the mechanotranduction mechanism of chondrocytes [5].

Proteoglycans, a special group of glycoproteins found in hyaline cartilage, provide the compressive and flow-dependent viscoelastic properties of cartilage. Swelling and shrinking of proteoglycans plays a role in the degree of tissue hydration, and thereby the compressive properties of the tissue [6]. Proteoglycans can also associate as a large chain with small branches of glycosaminoglycans (GAGs) [7].

The liquid phase of cartilage contains interstitial water and electrolytes forming 60%-80% of the wet weight. Due to negative charge of the tangled aggrecans, a high density of ions is seen in the liquid phase. The role of this liquid is to exchange nutrients with synovial fluid, lubricate the joint, and contribute to compressive resistance and deformation [7].

1.1.2 Structure of Articular Cartilage

There are four different zones in articular cartilage, with variations in matrix composition, morphology, mechanical, cellular and metabolic parameters. Every zone acts differently in function and has different properties (Figure 1.1).

The top zone at the articular surface, called the superficial zone, occupies 10% to 20% of the thickness. However, this zone comprises a high density of collagen in comparison to other zones. On the other hand, the oriented collagen fibrils in this area are thinner than in the other underlying layers. There are fewer proteoglycans in this region in comparison to other zones. The fibroblast-like chondrocytes present in this zone are flattened and oriented parallel to the direction of shear stress that they sense. It is believed that this composition and organization provide tensile strength, shear resistance, and fluid permeability during articulation [8].

The transitional zone or middle zone is below the superficial zone and contains the highest amount of proteoglycans in the tissue. The collagen and water content

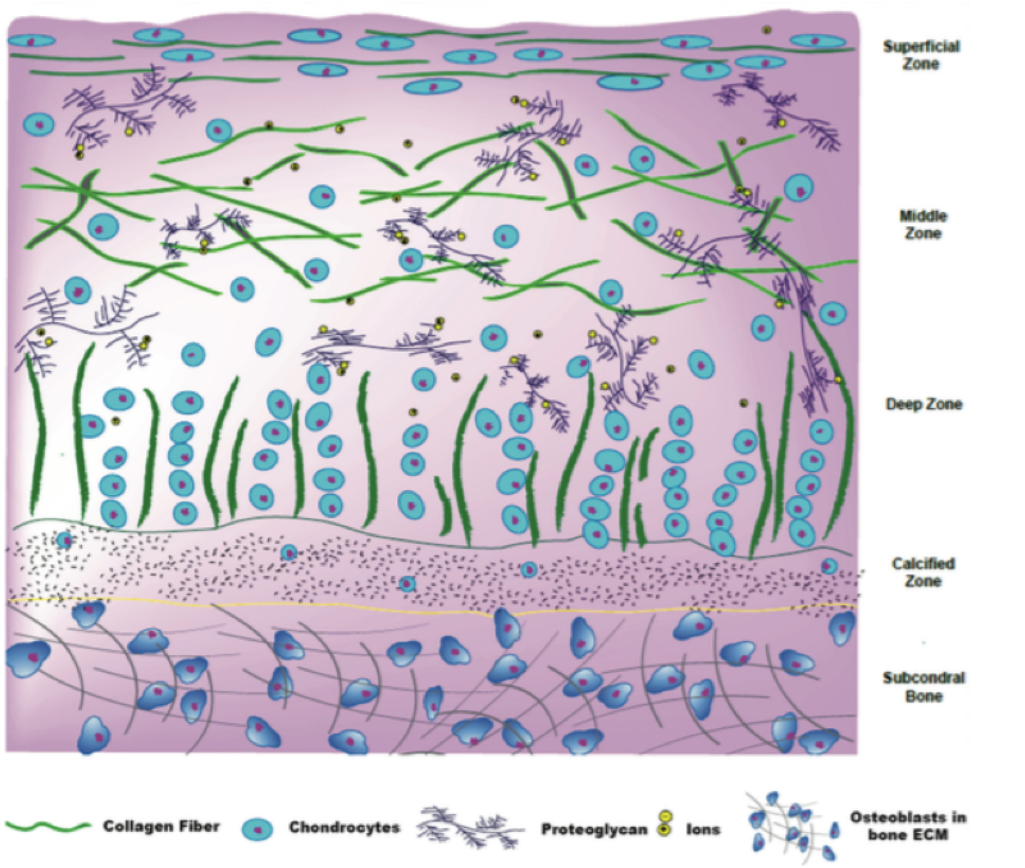

Fig. 1.1.: Schematic of composition and structure of articular cartilage (not drawn to scale). There are four zones with different structures in articular cartilage: superficial, middle, deep, and calcified [7].

decreases and collagen fiber size increases in this zone compared to the superficial zone. Chondrocytes display a rounded morphology in this zone [7].

The deep zone has a different composition and organization of cell and collagen fibril morphology. Collagen fibers have a larger diameter and are organized perpendicular to the articulating surface in this zone. Chondrocytes form columns parallel to the arranged collagen fibers with 10-fold higher synthesizing activities than cells in the superficial zone [9].

The calcified zone is a transition from articular cartilage to the outer surface of bone. Collagen type X is observed in this zone and plays roles in mineralization and

strength of the tissue. The number of chondrocytes in this zone is few and those that are present are inert and embedded in a calcified ECM.

Alternately, cartilage matrix can be categorized into three classes based on the distance from the chondrocyte; territorial, interterritorial, and pericellular. Pericellular is the closest region to each cell and is composed of collagen VI, proteoglycans, and some other proteins. The collagen and proteins in this area protect individual cells from mechanical loadings and are also responsible for a cells response to different kinds of loading. The next furthest region from the cells, interterritorial, contains the largest fibrils and takes the most volume in the matrix. The territorial part is the farthest region and has less organized collagen fibrils [10].

1.1.3 Mechanical Properties of Articular Cartilage

Articular cartilage accounts for a smaller volume than muscles, tendons, ligaments, and also bones. However, this small tissue plays a key role in distributing mechanical forces, joint lubrication and friction, shock absorbance, and dispersing compression. Other characteristics such as the interaction between the liquid and solid phase affect the viscoelastic properties of the cartilage. Outflow of the interstitial liquid from the porous collagen-proteoglycan matrix lubricates the joint during loading [11].

The composition of cartilage ECM is also critical in regulating the biomechanical characteristics of this tissue. Tensile behavior, as an example of biomechanical properties, is mainly determined by collagens. As stated earlier, collagens are varied in diameter and organization in different zones. This explains the variation of tensile properties in different zones of the cartilage. For instance, the tensile modulus can be as low as 5.4 MPa in the middle zone and as high as 10.1 MPa in superficial zone in human cartilage. This may be a result of more abundant and organized cartilage in the superficial zone as opposed to the middle zone [12].

Another important biomechanical characteristic in cartilage is compressive properties, as this tissue bear frequent compression during physiological activities. The compressive modulus depends on the depth and location of the tissue.

1.1.4 Articular Cartilage Injuries

Articular cartilage injuries can be caused by destructive trauma or degenerative joint diseases. The defects can be classified into two main categories; partial thickness and full thickness cartilage defects. The former − partial thickness defect − is only a defect of the articular cartilage and does not penetrate into the subchondral bone, and therefore does not extend to the blood or progenitor cells that are available in bone marrow for repair. The repair cannot be effective due to the lack of migrating chondrocytes. Although there are some metabolic and enzymatic activities to regenerate the ECM components and induce the chondrocyte to proliferate and produce matrix, chondrocytes are not sufficiently active to heal the defect completely. Thus, the defect persists and could reduce the functionality of the cartilage leading to tissue degeneration [13].

Full thickness defects, also called osteochondral defects, extend through the whole cartilage thickness and penetrate the calcified zone and even the subchondral bone. In this type of defect, the defect area reaches the progenitor cells, blood cells, and macrophages for immune response and the healing reagents [13]. Consequently, in response to the injury, the defect area is filled with a fibrin clot and the inflammatory response cascade is activated. The mesenchymal stem cells (MSCs) from bone marrow migrate to the fibrin clot after 1 week and will differentiate and produce their own matrix gradually [13]. Their matrix is proteoglycan-rich ECM and is may be considered as a repair for the defect. However, this repair is more fibrous than hyaline cartilage, having weaker mechanical characteristics and also higher permeability [14]. Accordingly, this repair is transient and incomplete and causes tissue degeneration few months later. As the repair tissue is not stable cartilage, regeneration of the cartilage

functionality and properties is not complete or sufficient. Consequently, bone-to-bone articulation, pain, inflammation, and disabilities may eventually occur [15].

1.2 Treatment Options for Articular Cartilage Injuries

Considering the lack of cartilage tissue regeneration and self-healing, the shortage of treatment options for giving the true function back to injured cartilage, and the increasing need for curative therapies, researchers have focused on substitutions for this tissue.

1.2.1 Microfracture

Microfracture is a well-known and effective surgery to heal small injuries in articular cartilage. This procedure is inspired by a natural physiological response of the body to heal full-thickness defects by signaling the cells in the bone marrow for wound healing. Micro-scale holes are drilled in the underlying subchondral bone. These small holes allow progenitor cells to be released from the bone marrow. When the inflammatory response is activated, cells fill the defect in a fibrin clot. This process works effectively for defects less than 2 cm^2 and has some advantages like minimally invasive nature, short time for surgery and recovery, and low site morbidity [16]. Despite these attractive features, the healing responses are different in patients due to personal physical conditions. Smaller injuries, younger patients, and earlier therapy lead to a better repair as mesenchymal stem cells in bone marrow are more abundant and active in these situations [17]. Moreover, tissue regeneration is not ideal, as a weak fibrocartilage is made, and consequently the failure rate is high [18].

1.2.2 Autologous Chondrocyte Implantation

One other common technique for cartilage repair is autologous chondrocyte implantation (ACI). This method is often suggested to patients with a failure in mi-

crofracture surgery and wounds between 1 cm^2 and 12 cm^2 [19]. Two separate surgeries are done in this procedure; one for harvesting healthy cartilage, and the other one to implant chondrocytes in the defect site. The first surgery includes collecting a small piece of non-injured cartilage from the low weight-bearing part of the patients knee. This piece of cartilage contains chondrocytes that can be harvested and cultured out of the body for 3 to 5 weeks to attain about 12 million cells for the second surgery. The second surgery is a reimplantation of the cells to the defected area by injection. In this operation, a patch of patients periosteum is sutured over the defect to retain the chondrocytes at the injured site. This procedure has shown promising results in healing. However, there are some limitations such as being invasive, requiring multiple surgeries, donor site morbidity, dedifferentiation of the harvested chondrocytes, and lack of number of healthy cells in patients [20].

1.2.3 Autografts and Allografts

Autografts and allografts are another available options to heal small lesions in cartilage. In an autograft procedure, a cylindrical section of a healthy cartilage is collected from non-weight bearing or low weight bearing areas of the patient. This piece is then implanted into the defected site of the same person to restore the function of the cartilage. Some advantages such as less donor site morbidity than ACI and promising clinical results make this method attractive. Nevertheless, an insufficient quality or quantity of donor tissue, donor site morbidity, implant surface mismatch with the surrounding tissue, instable graft, and compatibility of low weight bearing cartilage with a high weight bearing site are limitations of autograft surgery [16].

Allografts are tissues from another person, and are available from tissue banks. Although this procedure avoids multiple surgeries and donor site morbidity, there are still the same limitation for this option of therapy which are surface matching, load bearing compatibility. Some other limitations come along with this method,

including immune rejection, inflammations, and the presence of dysfunctional dead cells in allograft tissue [7].

1.2.4 Total and Partial Joint Replacements

All of the above therapies can be used when the injury is not too acute. For severe traumas, disease, or advanced osteoarthritis, total or partial joint replacement is suggested. In this method, it is necessary to remove the damaged joint and then implant the artificial joint. The artificial implant is composed of a metal stem (for stability), a metal shell (made of titanium, stainless steel, or alloys), and a polymeric part (made of polyethylene for smooth sliding). Although this therapy is great for older patients and patients with severe injuries, second surgeries are sometimes performed due to reported infection, implant loosening, implant wear and tear. The other main consideration is that the implant has a finite life and is not ideal for younger or more active patients [15].

1.2.4.1 Tissue Engineering

Regenerative medicine or tissue engineering uses concepts of engineering, biology, chemistry and material science to build a substitution of a tissue. The substitute helps, maintains, or brings back function to the damaged part of the body. Aspects of tissue engineering that have been investigated include various cell types; scaffolds that may be biodegradable, natural, synthetic, hydrogels, polymers, and nanocomposites; and chemical and physical factors including growth factors, cytokines, mechanical loading and electrical stimulation (Figure 1.2) [7].

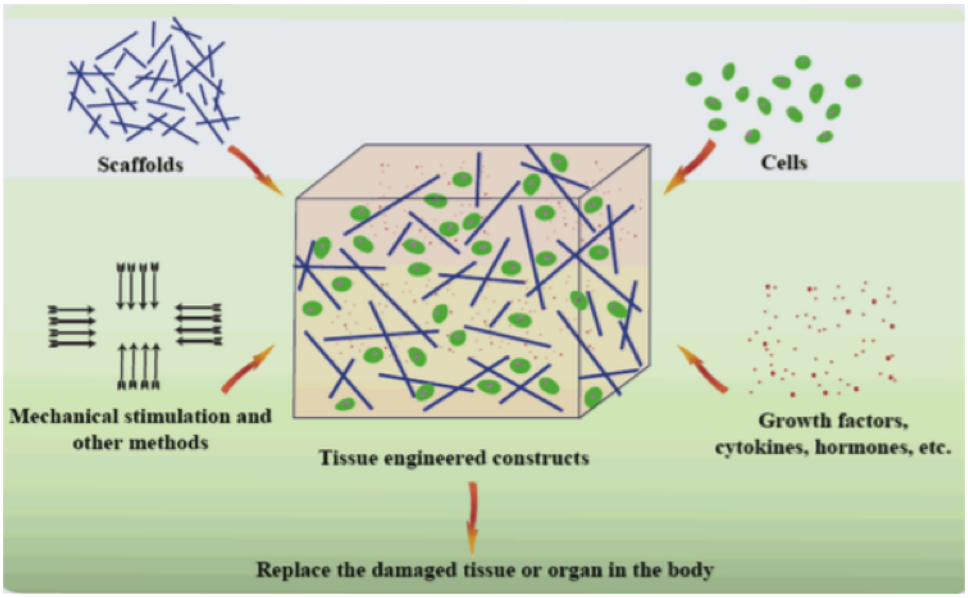

Fig. 1.2.: The concept of tissue engineering. Tissue engineering incorporates many critical factors including cells, scaffolds, bioactive factors, and physical stimuli to assemble biomimetic tissue-engineered constructs for replacing damaged tissues [7].

1.3 Cell Sources for Articular Cartilage Repair and Regeneration

1.3.1 Chondrocytes

The one and only type of cell in cartilage is chondrocytes, having a diameter of 10 to 13 μm [21]. In practice, chondrocytes have been a popular source for regeneration of articular cartilage. Despite some limitations, autologous transplantation is widely used for repairs. The low number of chondrocytes that can be used for therapy, dedifferentiation and lack of capability of chondrocytes in in vitro cell expansion are the main concerns about this type of therapy. The other available sources of chondrocytes such as allogeneic and xenogeneic chondrocytes also have some restrictions. They can potentially trigger immune responses of the patient and also there is a risk for transmission of diseases. Separately seeded zonal chondrocytes may be a source for regenerating the tissue structure, as different zones have different characteristics [8].

1.3.2 Stem Cells

Due to the limitations listed above, investigators have been looking for other available sources for cartilage repair and tissue engineering. Stem cells are considered a promising source due to their availability, accessibility, and capability of differentiating to the chondrogenic lineage. Different kinds of stem cells can be used for tissue regeneration, including mesenchymal stem cells (MSCs) and embryonic stem cells (ESCs).

From a functional point of view, stem cells are distinctive in two ways: first of all, they are capable of proliferating when they are at an undifferentiated state, and secondly, they can differentiate into one or multiple lineages of specific cells (Figure 1.3). Based on the number of lineages to which they are able to differentiate, we can classify them into four groups: totipotent, pluripotent, multipotent, unipotent.

Totipotent stem cells or morula cells can develop a whole human body and are able to differentiate into any type of cell. ECSs are pluripotent cells that can differentiate to any type expect for placental cells. These stem cells are obtained artificially through an in vitro fertilization.

Multipotent stem cells are able to differentiate into multiple related cell types, and can be harvested from many different tissues. This group includes hematopoietic stem cells that can become blood cells, and also mesenchymal stem cells that can differentiate to bone, cartilage, muscle, and fat cells. Finally, unipotent stem cells can only become one type of cell and has the ability to self-renew [15].

1.3.2.1 Mesenchymal Stem Cells

MSCs can be harvested for repair purposes from different tissues in the body, such as bone marrow, fat, synovium, periosteum, muscle, and skin [22]. Autologous MSCs have the ability to proliferate to get enough number of cells, and do not induce an immune responses in comparison to allografts and xenograft alternatives. Moreover,

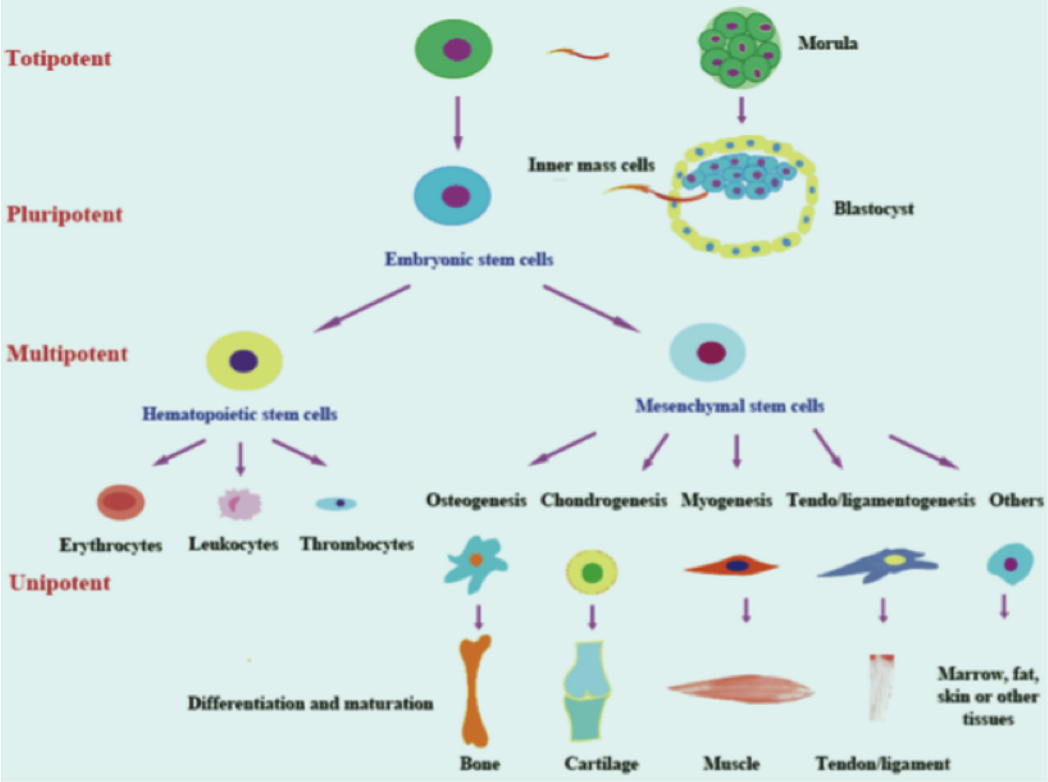

Fig. 1.3.: Totipotent, pluripotent, multipotent, and unipotent stem cells [15].

MSCs can be isolated in a minimally invasive process and have decreased donor site morbidity and pain complaints compared to ACI and tissue autografts [21].

MSCs have the ability to differentiate to multiple types of cell. One of the main cell types that MSCs can be differentiated to are cells that resemble chondrocytes in a process called chondrogenesis [21]. The chemical factors that induce chondrogenesis are transforming growth factors (TGF), insulin-like factors (IGF), dexamethasone, bone morphogenetic proteins (BMP) and fibroblast factors. These can all be provided in the media, and some physical factors such as mechanical stimuli (e.g. cyclic hydrostatic pressure, compression) also enhance chondrogenesis [22–24]. MSCs isolated from bone marrow are widely used due to their accepted ability to differentiate to the chondrogenic lineage and their easy access via the iliac crest.

Other source for mesenchymal stem cells are adipose-derived stem cells (ASCs) from subcutaneous fat that have shown potential for chondrogenic differentiation. Scientists are interested in ASCs because of their abundancy, minimally invasive procedure for isolation, and lower donor site morbidity and pain [25].

MSCs have shown great ability to repair cartilage in in vitro and in vivo studies. However, few clinical trials have been conducted. Walkitani et al. transplanted autologous MSCs in three patients knees after isolating and expanding them in vitro. Improvements were observed after 6 months of reimplantation [26]. Moreover, Chondroen from Osiris Therapeutics Inc. showed potential to prevent osteoarthritis in phase I or II clinical trials using expanded MSCs from human bone marrow. All in all, clinical trials show promise for MSC therapies for cartilage repair and regeneration. However, more study and work is needed to optimize culture conditions and overcome limitations in the differentiation of MSCs for cartilage regeneration [7].

1.3.2.2 Other Cell Sources

Embryonic stem cells are known to have nearly unlimited ability to proliferate and also can potentially differentiate to all cell types. These interesting characteristics make them favorable for cartilage tissue engineering as a cell source. For instance, Koay et al. expanded human ESCs in scaffold free conditions to make cartilage-like structures in agarose wells [27]. Another interesting alternative for cell source in tissue engineering is the dermis of the skin. This autologous option and other cell sources can be dedifferentiated to less mature cells (induced pluripotent stem cells or iPSCs) and then differentiated to the chondrogenic lineage. This process has been shown to produce constructs containing cartilage matrix components like aggrecan, making iPS cells a promising cell source that can be used for tissue engineering purposes [28].

1.3.3 Tissue Engineering Scaffolds for Articular Cartilage Repair and Regeneration

3D scaffolds are crucial to provide the right environment for cells to grow, produce matrix, and differentiate. The scaffold needs to have some essential characteristics; 1) biocompatibility, 2) appropriate degradation as cells produce their own matrix, 3) appropriate mechanical properties [21]. Sources of scaffold for tissue regeneration vary from natural polymers from living organisms to synthetic materials obtained from chemical processes. Some of the most common materials used as scaffolds are described in the following paragraphs.

1.3.3.1 Natural Scaffolds

Natural materials are frequently studied as tissue engineering scaffolds. They have good biocompatibility and may provide cell anchorage and promote differentiation. Cartilage tissue engineering scaffolds can be supplied from carbohydrate-based hyaluronic acid, agarose, alginate, chitosan, proteins or fibrin glue. Non-sulfated glycosaminoglycan harvested from tissue (hyaluronan) can be injected to the body [29]. Collagens are common to use as scaffolds. In addition, other natural scaffolds such as biodegradable fibrin, chitosan, or composites have also been studied and shown to be advantageous for cartilage tissue engineering [21]. Chondrogenesis favors a 3D environment with rounded cell morphology and limited cellular attachments, and there are some scaffolds are better at providing that environment than others. Agarose and alginate are hydrogels made from seaweed and are options for cartilage tissue engineering [30]. Steward et al. showed that 4% agarose (stiffer) is better than 1% and 2% for retention of the matrix products [31].

1.3.3.2 Synthetic, Nanostructured Scaffolds and Scaffold-free materials

Synthetic and nanostructured materials fabricated from polymers are interesting to study due to their easy fabrication, biocompatibility, versatility, controllable porosity and mechanical characteristics, and controllable degradability. Poly lactic acid (PLA), polyglycolic acid (PGA), and poly(lactic-co-glycolic) acid (PLGA) are common choices of scaffolds approved by the Food and Drug Administration [21]. There are different ways of manufacturing polymer materials to be used as scaffolds. Procedures which can be used to produce scaffolds include electrospinning, particulate leaching, chemical etching, 3D printing techniques, and phase separation [15]. Other than the tissue engineering through scaffolds, some scaffold-free methods can be used. Pellets, organ culture, aggregate culture, and self-assembling process are some examples of this method [15].

1.4 Growth Factors and Mechanical Stimuli for Improving Cartilage Tissue Repair and Regeneration

1.4.1 Growth Factors

Different hormonal and growth factors are used in order to regulate cells aggregation, adhesion, and metabolism. Some of the growth factors include insulin-like growth factors (IGF-I), basic fibroblast growth factor (bFGF), hepatocyte growth factor (HGF), platelet-derived growth factor (PDGF), and the TGF-β. TGF-β1 and TGF-β3 promote collagen formation and chondrogenic differentiation in mesenchymal stem cells [31–34].

1.4.2 Mechanical Stimuli

Many studies confirmed that different mechanical loading modalities regulate MSC fate. The deformations in the pericellular matrix can be sensed by cells mostly by

changes in ion concentration, changes in ATP concentration, and though integrins (which connects the outside of the cell to the cytoskeleton) as well as other factors (Figure 1.4) [35].

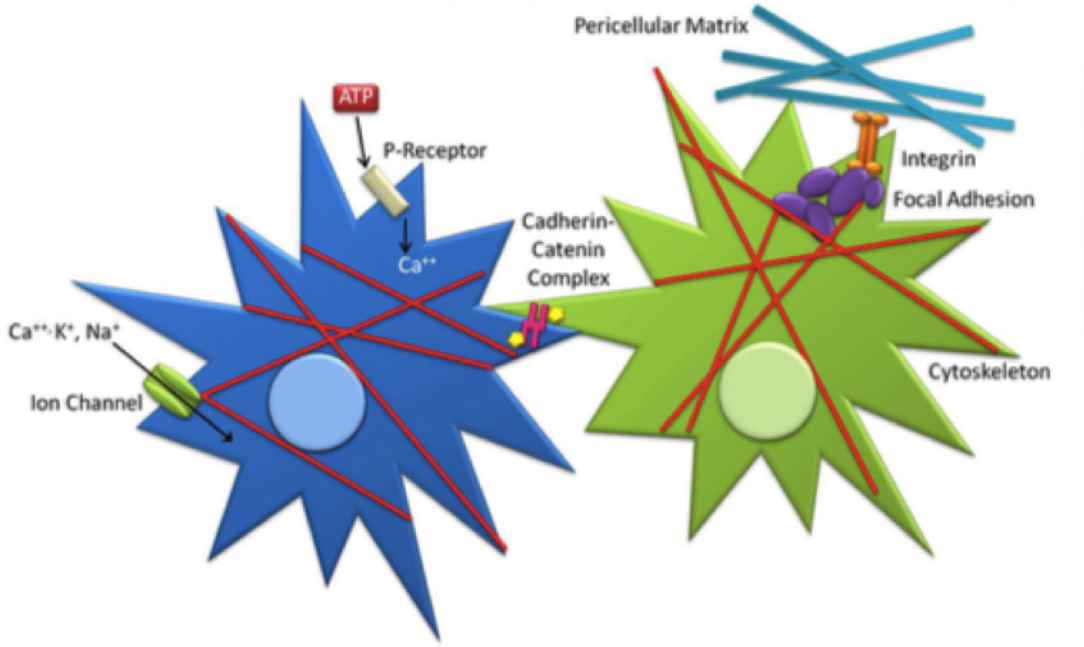

Fig. 1.4.: Integrins, focal adhesions, the cytoskeleton, ion channels, and P-receptors interact with the PCM to transmit signals into or out of the cell [31].

1.4.2.1 Hydrostatic Pressure

Cartilage is subjected to mechanical forces because of joint loading. Cartilage is mostly composed of water, which is mostly trapped inside the matrix due to the low matrix permeability. The result of this structure is that compressive loads are initially supported by the fluid phase. In fact, compressive loads are supported up to 90% by hydrostatic pressure in the fluid phase [36–38], causing a uniform normal stress on the cells (Figure 1.5). Physiologic levels of hydrostatic pressure have been determined to be 3 to 10 MPa [39]. Hydrostatic pressure (HP) is an important biomechanical

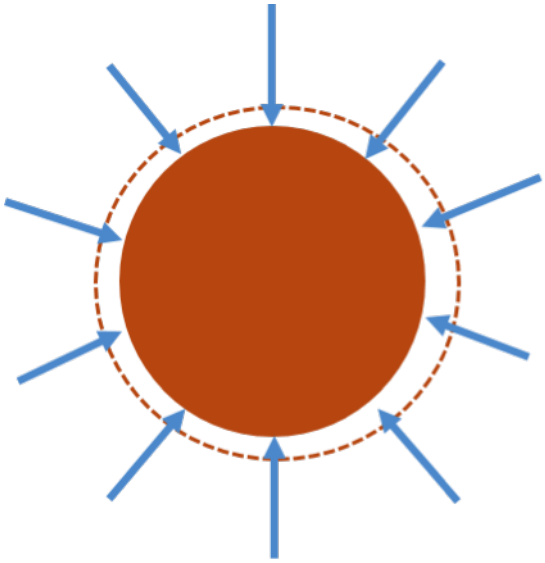

Fig. 1.5.: Hydrostatic pressure transmits a uniform normal compressive stress to the cells.

stimuli in cartilage tissue engineering. Different studies have shown beneficial or detrimental effects of hydrostatic pressure, depending on the magnitude of the load. Cyclic HP with magnitude in physiological range induced increasing GAGs production in chondrocytes [40]. Cyclic HP increased markers of chondrogenesis in different environments (e.g. 4% agarose gel, collagen I, synthetic scaffold, and pellets) including increasing gene expression and matrix production specific for cartilage [41]. All in all, frequency between 0.05 to 1 Hz (the human walking cadence [42]) and HP magnitude between 1 and 15 MPa was shown to be beneficial for cartilage tissue engineering [43].

Negative influences on cell viability and secretion may be caused by high magnitude static HP [44]. Proteoglycan secretion is inhibited by static HP at levels of 30 MPa [45]. Moreover, microtubule and actin fibers in epithelial cells were disrupted by high magnitude static HP [46].

Although mechanotransduction pathways are not well understood with hydrostatic pressure, the ion concentration changes inside the cells is suggested as a possible pathway [47]. It was shown that static HP inhibits the Na/K and Na/K/2Cl pump,

and increases Na/H interchanges [48]. Moreover, static HP for 5 minutes induced changes in calcium ion concentrations by activating stretch calcium channels [49]. It was also shown that that calcium signaling is required for HP mechanotransduction, and that it is likely activated by the purinergic pathway [50]. Beside calcium ion channel role, integrin binding can help to transduce HP [35, 51]. Integrin binding to the pericellular matrix could determine the response of MSCs to cyclic HP by regulating vimentin organization [35].

1.4.3 Shear Stress, Compression

Although cartilage is minimally loaded in shear in vivo because of the low friction, shear loading is effective at inducing cartilage matrix production. For example, 1% to 3% dynamic shear with a frequency of 1 Hz was beneficial for increasing ECM synthesis and cartilage oligomeric matrix protein expression [52]. Compression is another mechanical stimulus shown to be beneficial for cartilage tissue engineering. The mechanical load affects the cells response through their pericellular environment and through the mechanotransduction pathways, especially when the load is dynamic. Static compression has not shown a positive effect on the cells [5]. Tissue engineers have studied mechanotransduction to determine how cells respond to mechanical loading (Figure 1.6). For instance, mechanosensitive ion channels have been shown to be activated by compression and shear stress in several studies [47,48,53]. The changes in ion concentrations cause upregulation or downregulation of gene expression in cells. Integrins and the cytoskeleton have been shown to play roles in the responses to mechanical forces, with focal adhesion complexes as one of the messengers for these responses [54].

1.5 Question and Hypothesis

It is challenging to engineer cartilage tissue that has the same composition, structure and mechanical properties as native tissue. Understanding the pathways involved

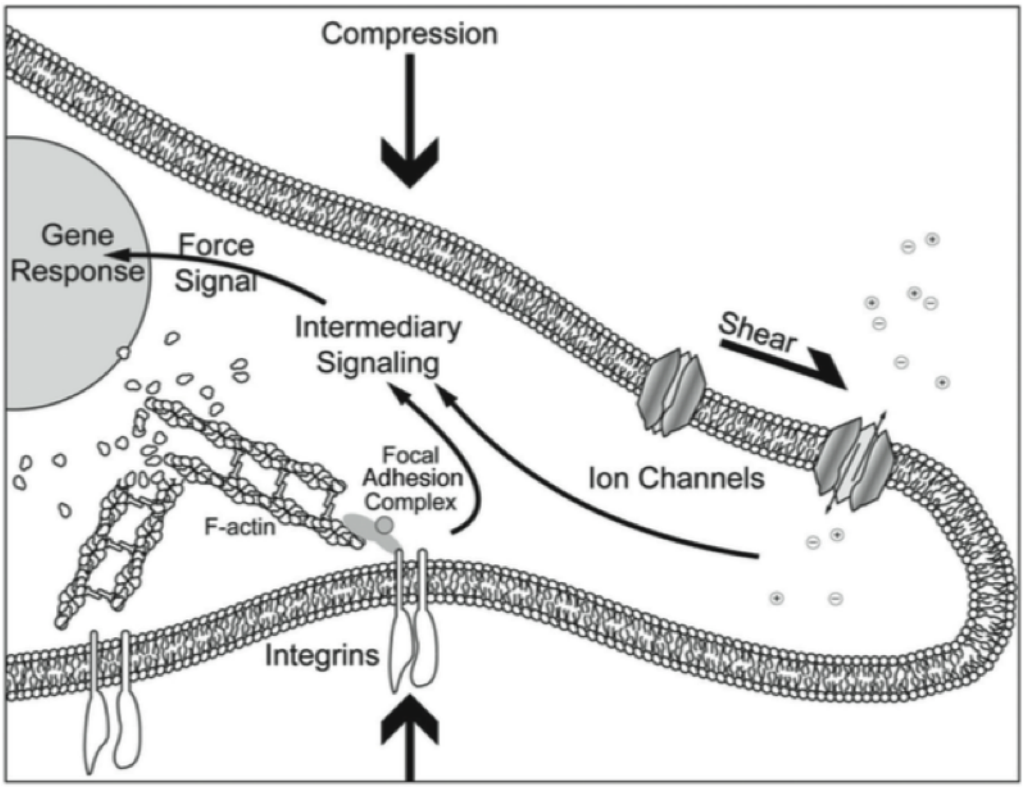

Fig. 1.6.: Cells can respond to mechanical forces via several mechanisms, such as stretch activated ion channels and focal adhesion complexes [6].

in HP mechanotransduction may provide targets to stimulate the desired change in cell behavior, and could help overcome these challenges. In this research we have investigated the role of Ca^{++} signaling, focal adhesion kinase (FAK) involvement, and sirtuin1 activity in the mechanotransduction of HP in MSCs. It was expected to be able to image changes in Ca^{++} concentration with mechanical loading and to investigate its correlation with other signaling molecules in MSC mechanotransduction. Furthermore, the role of FAK was examined in the study, because integrin binding to the pericellular matrix was previously shown to be necessary to transduce HP [55] to a cellular response, and also FAK is known as an early downstream regulator for transferring signals from integrin binding [56]. Therefore we hypothesized that FAK is necessary for transducing HP to MSCs and is part of its mechanotransduction path-

way. In another part of the study, it was questioned whether surtuin1 (an antiaging agent) activity could enhance chondrogenesis in MSCs or if it was part of HP mechanotransduction. These improved understandings about the mechanisms regulating the chondrogenesis in response to HP may reveal insights for cartilage tissue engineering and regenerative studies.

2. REAL TIME IMAGING OF CALCIUM ION SIGNALING WITH HYDROSTATIC PRESSURE BIOREACTOR

2.1 Introduction

2.1.1 Ca^{++} Signaling and Mechanotransduction

Calcium ions (Ca^{++}) are present in many cellular signaling pathways. The concentration of this ion is different in intracellular and extracellular spaces. There is a 10^4 times higher Ca^{++} concentration in extracellular fluid suggesting the potential for Ca^{++} flux into the cells, providing a message. Mechanical stimulations can cause the Ca^{++} flux from intracellular or extracellular space into the cytosol [57]. The change of Ca^{++} concentration in the cytosol can be a messenger for protein kinases and protein phosphatases resulting in cellular proliferation or differentiation [58]. Ca^{++} sensitive enzymes have been shown to play an important role in cartilage differentiation such as Ser/Thr specific protein kinases, PKCalpha, and Ser/Thr specific phosphatase calcineurin [59–61].

Many types of mechanical loading are beneficial for chondrogenesis of MSCs due to the involvement of Ca^{++} signaling pathways in mechanotransduction. For instance, cyclic tensile loading of MSCs caused them to produce more proteoglycans; this matrix deposition was suppressed by inhibiting stretch-activated ion channel activity that allows Ca^{++} flux through the membrane of cells [62]. Moreover, other studies have shown increased intracellular Ca^{++} and mitogen-activated protein (MAP) kinases in MSCs that influence their differentiation due to fluid flow stimulation [63–65]. Mechanical stress and deformation by compression in agarose constructs or deforming the cell surface with a micropipette in monolayer culture increased intracellular Ca^{++}

concentrations in chondrocytes [66–69]. In another study, Mizuno measured Ca^{++} concentration changes in chondrocytes exposed to 0.5 MPa static HP with a live-cell imaging bioreactor. He observed peaks during and after loading and claimed that these changes occurred through stretch activated calcium channels.

It is also suggested that the mechanism of how HP can transduce a mechanical load to a beneficial biological response is due to activation of Ca^{++} signaling pathways. Steward et al. demonstrated that Ca^{++} signaling is necessary in HP mechanotransduction. They further demonstrated that the purinergic pathway is involved in the Ca^{++} signaling in response to HP (Figure 2.1). In this pathway, adenosine triphosphate (ATP) is a paracrine or autocrine factor that initiates Ca^{++} signaling. The mechanical load causes the release of ATP into pericellular area. Afterwards, ATP binds to P-receptors that are coupled to Ca^{++} channels to activate voltage gated Ca^{++} channels (VGCCs) or sarcoendoplasmic reticulum Ca^{++} stores (SERCS) [70]. Pathways such as purinergic mechanotransduction pathway, activation of voltage-gated calcium channels, and integrin binding have been shown to be part of HP mechanotransduction by MSCs. However, the relation between these factors and Ca^{++} signaling is not known. Using a bioreactor that allows confocal imaging of cell-seeded gels that have been dyed with a fluorescent Ca^{++} indicator while HP is applied, our long term goal was to investigate the relationships between different signaling molecules and the Ca^{++} pathway. For the first step, the bioreactor was used to image the fluorescent Ca^{++} indicator with a single application of hydrostatic pressure to verify that this pathway is activated by the mechanical load. The previously designed and fabricated bioreactor maintained the pressure at 12 MPa and allowed confocal imaging of MSCs in their agarose scaffold.

2.1.2 Bioreactor Design

A bioreactor is defined as an apparatus in which a biological reaction or process is carried out, especially on an industrial scale. The bioreactor for detecting the

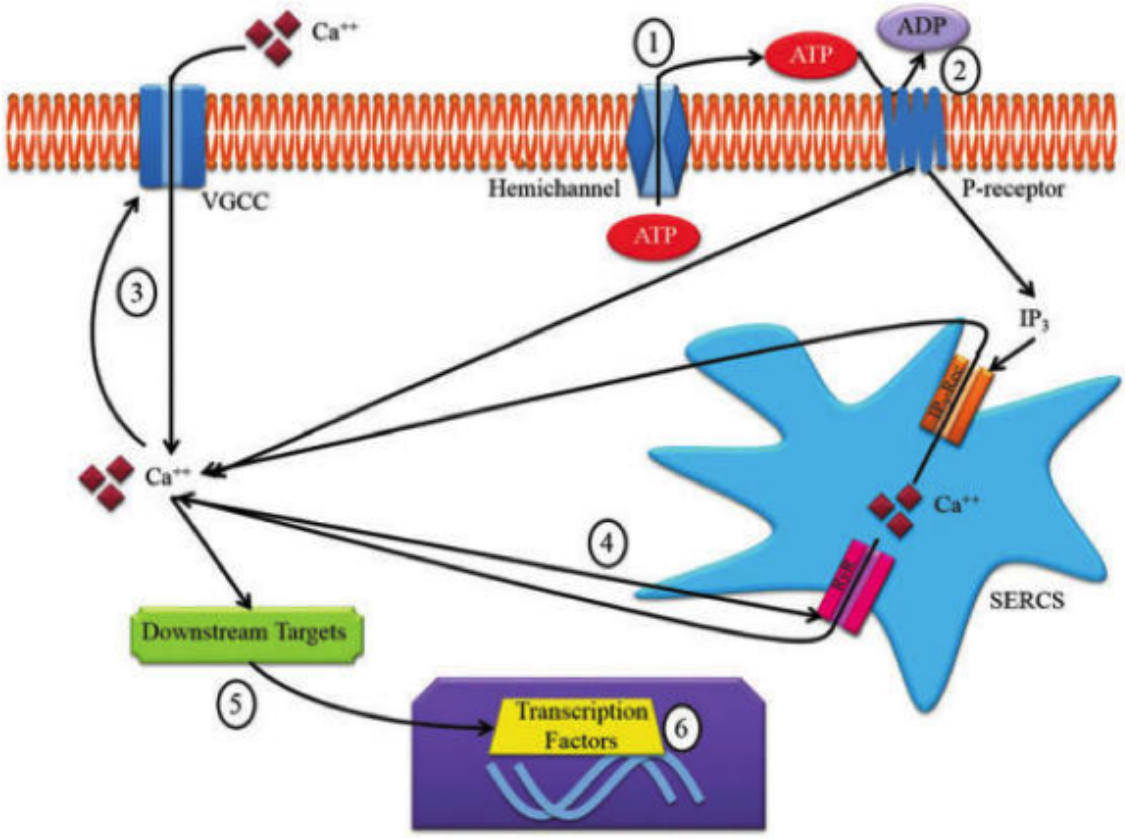

Fig. 2.1.: The purinergic and calcium signaling pathways proposed to act in the mechanotransduction of HP [50].

Ca^{++} changes in the cell-seeded gel has special features that allows it to hold a ϕ=5mm scaffold with thickness of 3mm, maintains pressure safely up to 20 MPa, is compatible with media and cells, has an optically clear window for imaging and has a temperature control system. The materials used to make the bioreactor are stainless steel, polyether ether ketone, sapphire, and Loctite (EA E-05MR, HYSOL) epoxy that are all non-toxic to cells.

The bioreactor has two major parts: the chamber and the pump (Figure 2.2). These two parts of the system is are connected with polyether ether ketone (PEEK) tubing. The chamber is a stainless steel cuboid that has 4 ports, which are designed to attach a pressure sensor, pressure release valve, tubing, and window. The pressure

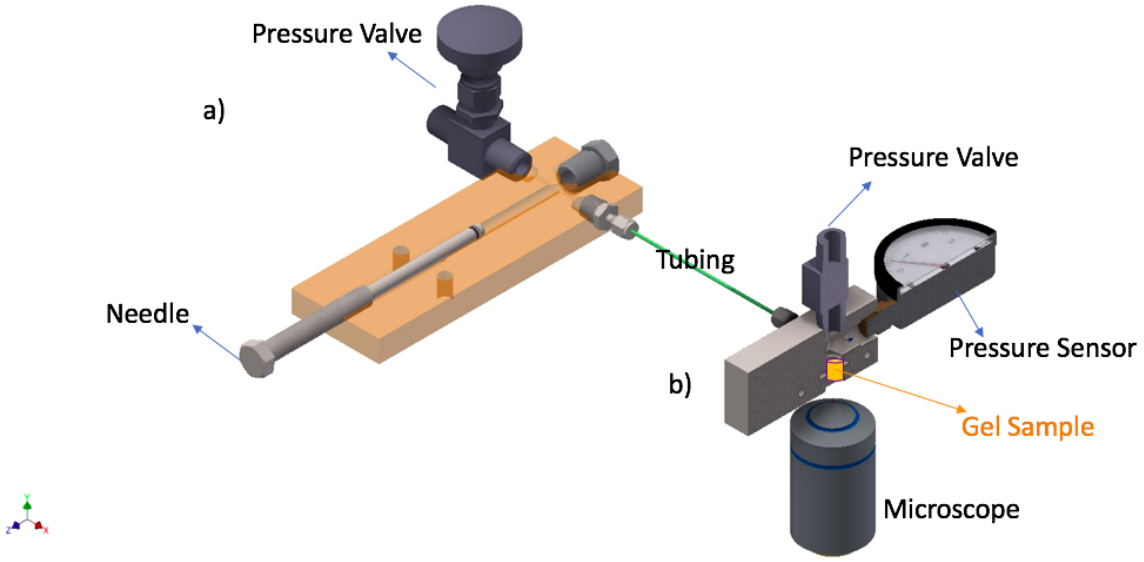

Fig. 2.2.: Custom bioreactor for real time confocal imaging of cell-seeded gels under 12 MPa static hydrostatic pressure (a) The pump generating the pressure (b) The chamber holding the cell-seeded gel sample.

sensor converts pressure to a voltage with a linear relationship. The pressure release valve is designed to eliminate air bubbles when running the system. The tubing port provides a connection to the pump. The window is a challenging part that needs to be optically clear, withstand up to 20 MPa of pressure and also needs to be sealed completely. The window subsystem consists of a metal holder, an O-ring and also a sapphire glass that is glued in place with Loctite (EA E-05MR, HYSOL) epoxy glue. There are also two cavities to insert heaters to maintain the temperature. The temperature and pressure are measured and monitored with an Arduino board.

The pump is another stainless-steel part that has 4 ports. The first port is sealed with a pressure release valve that is needed when the system is depressurized. The second port is for the tubing that connects it to the chamber. The other port is machined to have mating threads for the needle to advance. The last port contains a pressure rupture disc for safety, which bursts and releases the pressure if it becomes overloaded. Additionally, the tubing is made of polyether ether ketone (PEEK) that

connects the chamber to the pump. It also allows the pump to be operated away from the chamber and microscope.

2.2 Materials and Methods

2.2.1 Cell Isolation, Expansion and Encapsulation

MSCs were harvested under sterile conditions from the bone marrow of porcine femurs. MSCs were expanded in high glucose Dulbeccos modified Eagles Medium (hgDMEM with GlutaMAX) supplemented with 10% fetal bovine serum (FBS), penicillin-streptomycin, and Amphotericin B (Amp-B). At the end of passage 2, they were seeded in 4% agarose with the density of 15 million cells/mL. The heated cell/gel solution was poured to a 3 mm space between a stainless-steel mold and plexiglass cover. After solidification, a biopsy punch (ϕ=5mm) was used to obtain cell-seeded scaffolds, which were cultured for 3 weeks in chondrogenic differentiation media consisting of DMEM with sodium pyruvate, L-proline, bovine serum albumin (BSA), penicillin-streptomycin, Amp-B, 50 ng/mL transforming growth factor (TGF-β3), 50 ng/mL of L-ascorbic acid, 10 g/mL insulin-transferrin-selenium, 50 ng/mL lineoic acid, and 100 ng/mL dexamethasone. Half-media changes were done twice per week. The constructs deposited enough matrix to respond to mechanical loading after 21 days in culture [31].

For imaging calcium, 12 μM of fluorescent calcium indicator (Cal-520® AM, AAT Bioquest®) was applied to the media of gels one hour before imaging. After one hour, the gel construct was washed and placed in Hanks Balanced Salt Solution (HBSS).

2.2.2 Hydrostatic Pressure Application with Bioreactor

To pressurize the chamber, the pressure release valve was unscrewed from the chamber. This is right above the window, so the scaffold could be placed on the window. HBSS was added to the chamber until it was filled with fluid. Then the

pressure release valve was put in place but was left open. Fluid was added to the pump as the whole system filled with fluid. Some bubbles came out of the valve on chamber. Air is very compressible and the system does not have sufficient motion to obtain 12 MPa of pressure if the air is not out of the system as much as possible. Everything was sealed with Teflon sealing tape and no leakage should be observed during the experiment. After the pressure valve was closed, the needle was advanced on the threads to obtain the pressure. The needle was advanced by an electric drill to generate pressure quickly.

To depressurize the system, the needle was slightly unscrewed. Then to avoid letting air into the chamber again, the pressure release valve on the pump was opened. The needle could be removed then.

After each day of experiments, the whole system was filled with 70% ethanol and pressurized a little bit.

There are some challenges in using this bioreactor. First of all, the parts should not be washed with or exposed to bleach, since the bleach is corrosive and any residual bleach will kill the cells. However, components are autoclave compatible. No grease should be used as a sealant because it may clog the PEEK tubing.

2.2.3 Validation of Cell Imaging with Confocal Microscopy

The chamber of the bioreactor was placed on top of the microscope objective. The gel was placed on the sapphire glass inside the chamber. A drop of adenosine triphosphate (ATP) was applied to the gel and the fluorescence was recorded. The amplitude and duration of the spike in fluorescent intensity change (Ca^{++} concentration change) was analyzed with a self-provided custom-made MATLAB (Mathworks Inc, Natick, Massachusetts, USA) script (Appendix A).

2.2.4 Loading Constructs in Bioreactor with Hydrostatic Pressure

The gel was seated on top of the window inside the chamber, while the chamber was seated on top of the confocal microscope (Olympus 2) with an objective of 20x or 10x. The PEEK tubing allowed us to pressurize the pump away from the microscope. The Ca^{++} staining was observed with the fluorescent calcium indicator having excitation/emission at 492/514 nm at 4 different z stacks through the height of the cylindrical scaffold. The first z stack was chosen to be adjacent to the window and the bottom of gel construct. The space between the z-stacks was 45 μm (Figure 2.3). Images were taken at 5 second intervals for 374 seconds before pressurizing and during loading for approximately 500 seconds. The fluorescent intensity of individual cells was quantified with FIJI software [71].

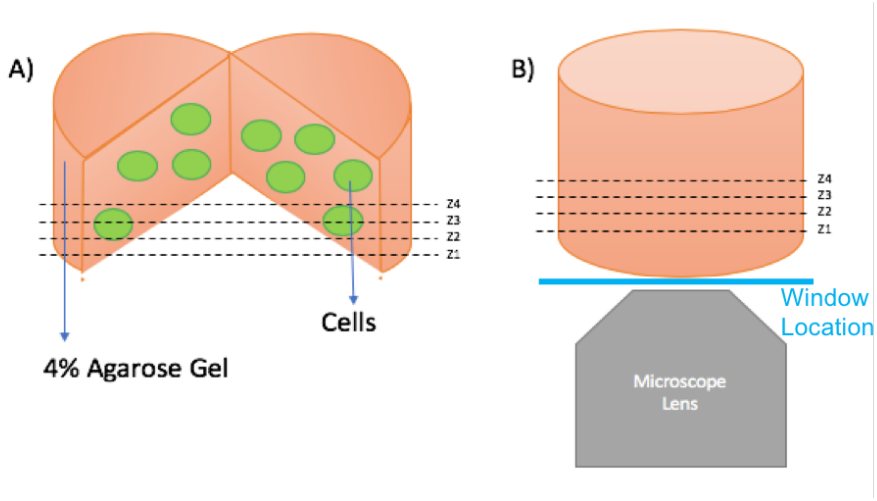

Fig. 2.3.: Schematic of seeded cells in (a) gel construct and 4 heights imaged by the microscope. (b) gel with microscope objective.

2.2.5 Fixing Gels

Due to the movement of the gel inside the bioreactor even before pressurizing the system, it was necessary to make the gel stay in place. It needed to be fixed next to

the window in a way that the HP load was transferred to the scaffold. It was decided to have the same gel structure (4% agarose) fill the chamber above the cell-seeded gel to keep it from floating around inside the chamber. This acellular gel was called fixing gel and was a cylinder with the diameter of 6.35 mm and height of 15.68 mm (Figure 2.4).

The fixing gels were made by hand. A clear plastic sheet was rolled with the desired diameter and the gel was poured in at an elevated temperature (around 80^0C) and was cooled down until the plastic sheet could be removed (Figure 2.4). The gel was cut into the required length.

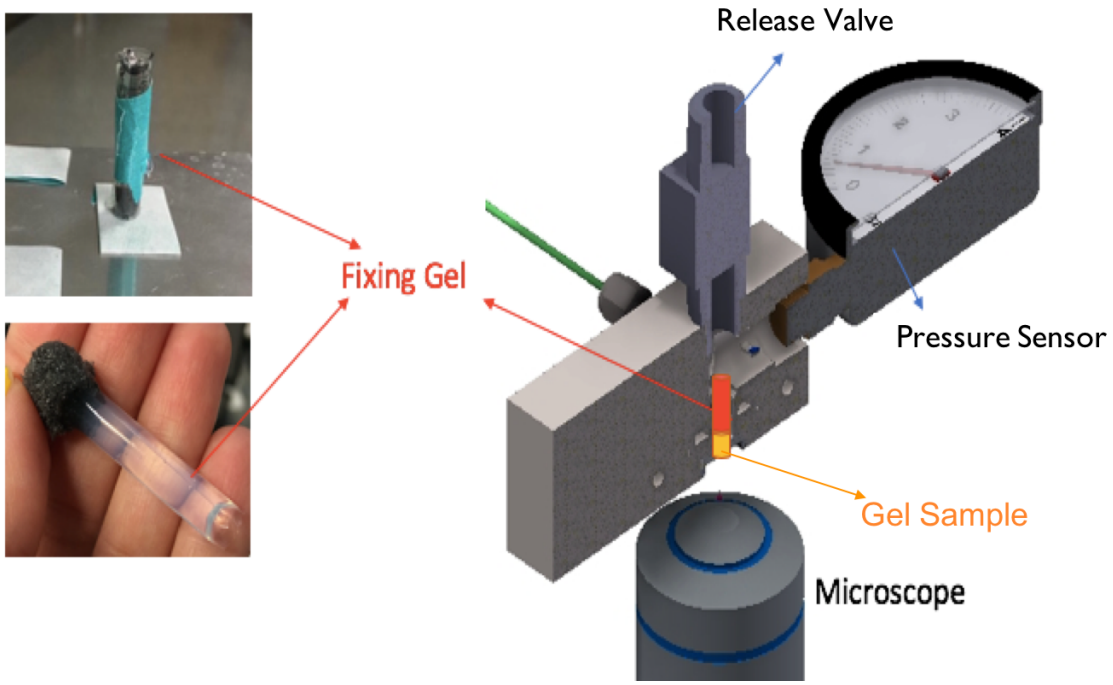

Fig. 2.4.: Acellular hand-made fixing gel to stop the construct sample from floating, placed on top of the cell-seeded gel inside the chamber.

2.3 Results

2.3.1 Activation of Ca^{++} Channels with ATP

To test the bioreactor, ATP could be used to generate a spike in Ca^{++} concentration (Figure 2.5). Four cells were individually selected and analyzed with a custom-made MATLAB script to quantify the amplitude and duration of the peaks in the intensity-time graph (Appendix A). The code provided the start time of the peak,

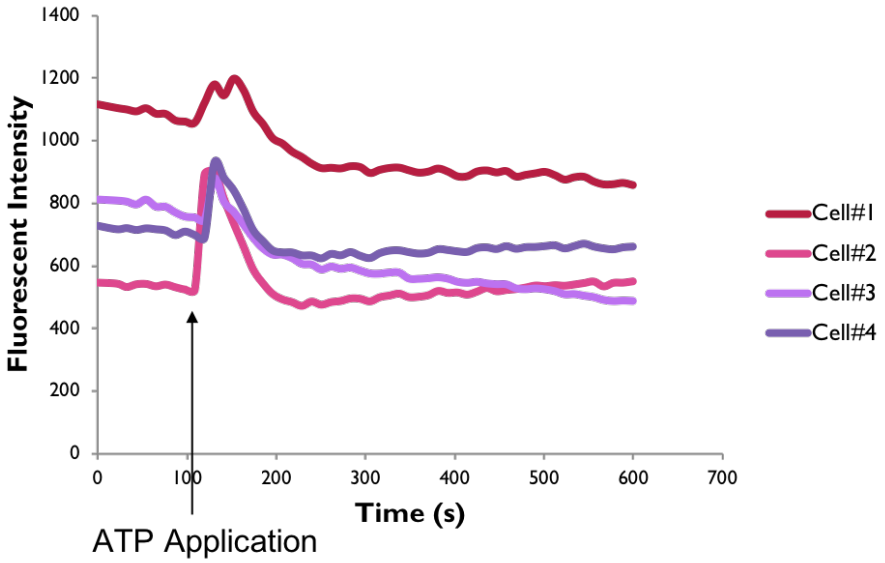

Fig. 2.5.: Fluorescent intensity change over time. Exogenous ATP was added to cell-seeded gels induced intracellular Ca++ concentration change. Confocal microscopy imaged the fluorescent intensity change inside the chamber, through the chambers window. Data collected by Komal Yadav.

the end time, duration, and the amplitude of intensity. The duration and amplitude of the Ca^{++} spike for four cells are shown in Table 2.1.

These results verify that the Ca^{++} response of the cells can be observed through the window of the bioreactor with confocal microscopy.

Table 2.1.: Amplitude and duration of the fluorescent intensity peak indicating interacellular Ca^{++} concentration change because of application of exogenous ATP to the cells.

Cell Code	**Duration of Peak (s)**	**Amplitude of Peak**
Cell#1	75.1720	140.3660
Cell#2	83.1580	378.5840
Cell#3	39.3489	132.1680
Cell#4	62.1907	239.8940

2.3.2 Loading Constructs in Bioreactor with Hydrostatic Pressure

In the first run, the fixing gel was not used. To analyze the data, the fluorescent intensity for each Z stack was graphed vs time for 5 different cells. If the Ca^{++} concentration is not changing in the cell and the cell is not moving, then the fluorescent intensity at each z-stack would have been stable over time. However, the maximum intensity was at Z2 at first (*), then was seen at Z3 before pressurizing (*) pressurizing (Figure 2.6). The change of intensities before loading suggest that the cell-seeded gel is floating in the chamber and is not resting on the window before loading. After loading, the fluorescent intensities changed again, suggesting that the gel was displaced downward with pressure. The cell-seeded gel was floating around with and without loading.

Next, the fixing gel was used on to hold the cell-seeded gel scaffold in place and the fluorescence intensity data was analyzed for 10 different cells. Unlike the previous run, the fluorescent intensity did not change without loading, and was relatively stable before applying the pressure (Figure 2.7). This proved that the fixing gel worked and stopped the gel from floating.

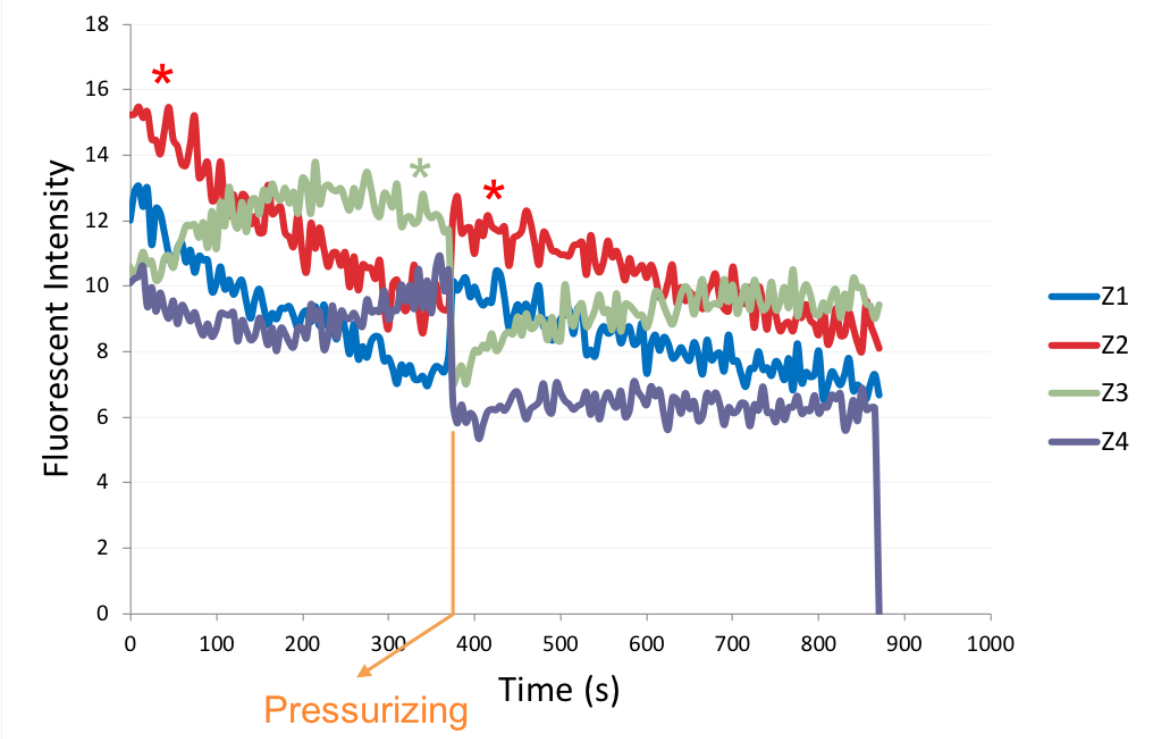

Fig. 2.6.: Fluorescent intensity of four Z-stacks over time for a representative cell before and after the application of 12 MPa of static hydrostatic pressure without fixing gel.

There was a change in fluorescent intensity during the time of loading. As can be seen in Figure 2.7, the intensity of upper heights (Z stacks 3 and 4) was decreased and the other two lower Z stacks were higher in intensity while the pressure was applied. However, when the pressure was released, the fluorescent signal came back to the intensity it was before loading. This suggests that the gel was displaced towards the microscope due to the mechanical load and was returned to its original place after depressurizing (Figure 2.8).

No Ca^{++} peaks were observed during or after applying the hydrostatic pressure for 10 minutes for any of the 10 cells that were analyzed.

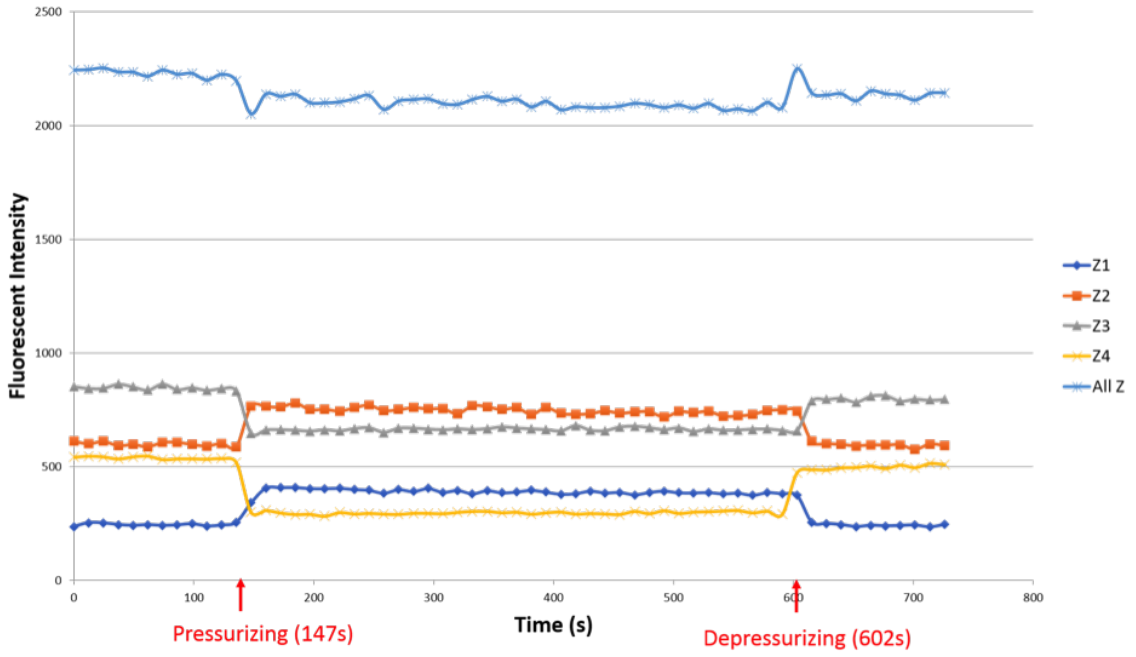

Fig. 2.7.: Fluorescence intensity of a representative cell at four Z-stacks and the sum of Z-stacks over time with the use of a fixing gel. The cell-seeded gel structure was pressurized with 12 MPa of static HP at 147s and depressurized at 602 s.

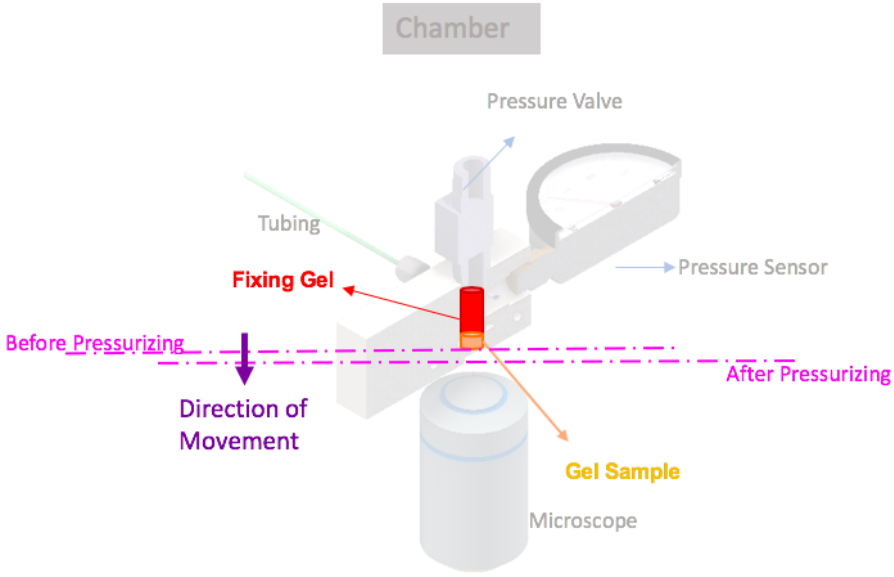

Fig. 2.8.: Schematic of gel displacement inside the chamber after stabilization by the fixing gel.

2.4 Discussion

Ca^{++} ion signaling was previously shown to be an important part of mechanotranduction for mesenchymal stem cells in different types of loading such as tension, compression, fluid flow, and osmotic pressure, as well as hydrostatic pressure [35, 62, 63, 67, 72–77]. As Ca^{++} seems to be necessary in mechanotransduction of many kinds of loading, we aimed to study different aspects of its role and later on its relationship to other factors involved in HP mechanotransduction.

The bioreactor was designed such that the Ca^{++} flux in the cells in a 3D construct could be imaged live while being pressurized by HP; the ability to image the Ca^{++} concentration changes was demonstrated by the addition of exogenous ATP. Firstly, the Ca^{++} concentration change (fluorescent intensity change) due to loading could not be imaged because the gel was floating around, even without loading. A cylindrical acellular 4% agarose gel (called fixing gel) was made and placed on top of the cell-seeded gel construct. By using the fixing gel, the cell-seeded gel was stopped from moving. Therefore, the fluorescent intensity (implying the Ca^{++} concentration) change during the time of HP application could be imaged. However no peaks detected during or after pressurizing.

Mizuno reported Ca^{++} concentration changes in bovine articular chondrocytes exposed to static HP with a magnitude of 500 kPa at the time of applying the pressure and after applying the load [48]. However, our results were not consistent with this previous study; we did not see any changes in Ca^{++} concentrations in our cells during or after loading. This may be because the two studies used different cell types and scaffolds. Mizuno used bovine chondrocytes in monolayer, as opposed to the mesenchymal stem cells in an agarose scaffold that were used in the current study. Another study by Steward et al. demonstrated Ca^{++} involvement in cyclic HP mechanotransduction by MSCs [76]. The varying responses to HP shows that the magnitude of loading, time of loading, and whether the pressure is cyclic or static can play roles in the response of the cells. Cyclic HP appears to activate Ca^{++} signaling,

but a single application of HP for 10 minutes may have no effect on intracellular Ca^{++} concentration.

3. ANALYSIS OF THE GEL DISPLACEMENT IN THE BIOREACTOR SYSTEM DUE TO HYDROSTATIC PRESSURE

3.1 Introduction

In our previous study, we used the bioreactor to image cells in 4% agarose gel live and real time as described in Chapter 2, and saw that the gel was being deformed or was moving when HP was applied.

In this chapter, the amount of movement and the cause of movement is analyzed. Firstly, the magnitude of the movement was estimated. After that, possible reasons for this movement, such as deformation of different parts of the bioreactor or the deformation of the gel were analyzed.

3.2 Quantification of Displacement

3.2.1 Materials and Methods

The overall goal was to fit curves to the fluorescent intensity of the cells as a function of z-height before and after loading and determine the shift in z due to loading. In order to analyze the magnitude of the movement, we assumed the calcium concentration in the cells was not changed by HP or cell movement. We further assumed that the z location of the maximum fluorescent intensity coincided with the location of the cell in z.

The intensity of fluorescent for 10 cells was determined at the moments before and after pressurizing for four z-stacks (Figure 3.1). The first z-stack was adjacent to the window near the bottom of gel construct ($z1$ =25 μm). The space between the

z-stacks was 45 μm, with the highest image taken at $z4$=160 μm. The data before pressurizing was fit to the quadratic equation:

$$f(z) = a(z)^2 + b(z) + c \tag{3.1}$$

while the data after pressurizing was fit to:

$$g(z) = a(z-d)^2 + b(z-d) + c \tag{3.2}$$

where a, b, and c are curve fitting parameters that are the same for both equations. Parameter d in $g(z)$ is the amount of shift between the two curves in z and represents the magnitude of the movement of the cells (Figure 3.2) and was calculated in two different ways.

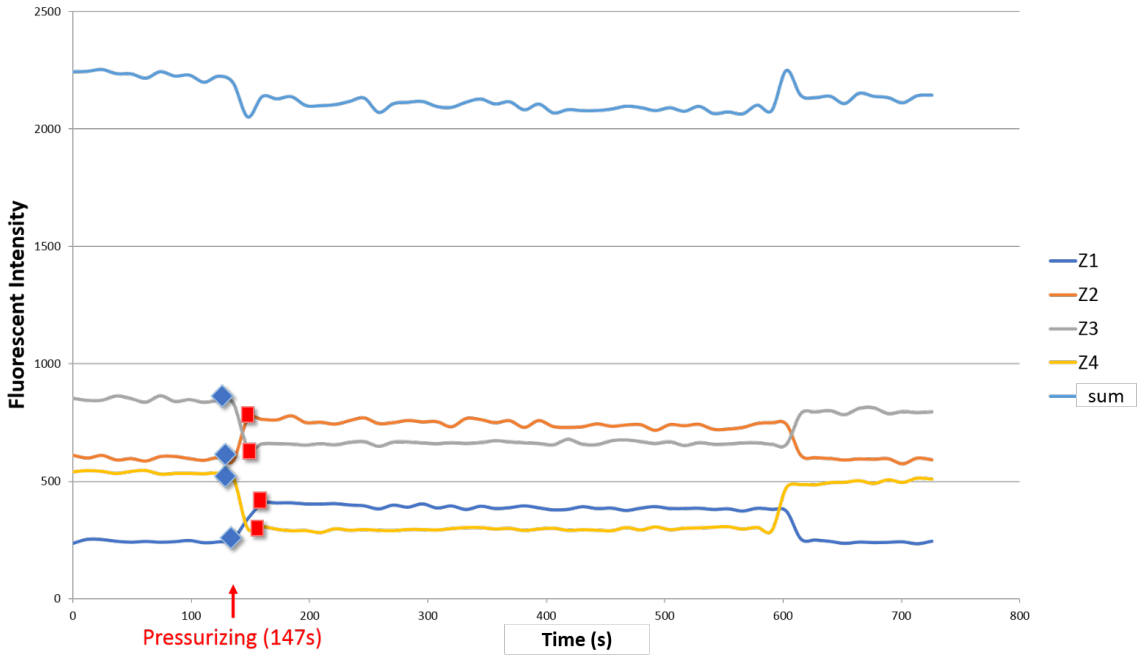

Fig. 3.1.: Fluorescent intensity changes during time for each height/z-stack. Dots indicates the intensities before (blue) and after (red) pressurizing selected and collected for further analysis for a representative cell.

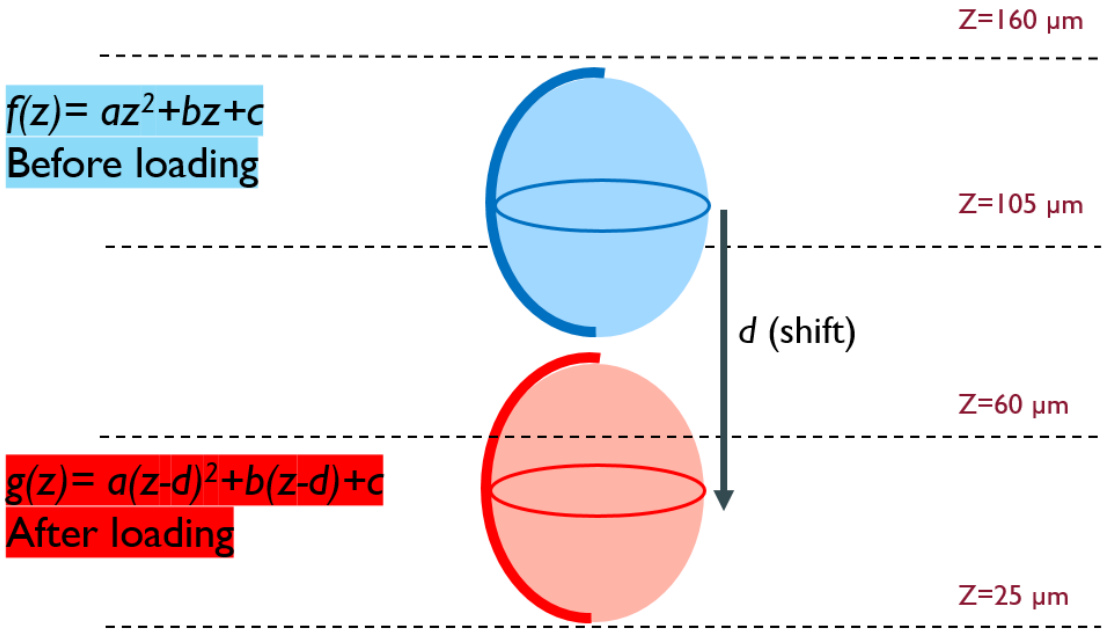

Fig. 3.2.: Schematic of cell before (blue) and after (red) loading and the displacement d in height (z). Quadratic functions were fit to the data before pressurizing ($f(z)$) and after pressurizing ($g(z)$) and the amount of shift between two functions (d) was determined.

3.2.1.1 Method#1

In this method the movement d was determined in two steps. First the intensity data before loading was used to determine the a, b, and c value for $f(z)$. The values were used in $g(z)$ and in the next fit only the undetermined parameter d was found. For finding best-fit parameters, a custom-made MATLAB (Mathworks) script was developed using the least square method (Appendix B).

3.2.1.2 Method#2

In this method the data before and after loading (8 data points) was simultaneously fit to equations $f(z)$ and $g(z)$, respectively to find optimized values for $a,\ b,\ c,$ and d. This was done by maximizing the coefficient of determination (R^2).

Assume an experimental data set with n values in form of $y_i(i = 1, 2, , n)$ with $\bar{y} = \frac{1}{n}\sum_{i=1}^{n}(y_i)$ and each data point is modeled and named as $f_i(i = 1, 2, , n)$. The residuals of each prediction would be in the form: $e_i = y_i - f_i$. The variability can be defined based on three sums:

$$SS_{tot} = \sum_i (y_i - \bar{y})^2 \tag{3.3}$$

$$SS_{reg} = \sum_i (f_i - \bar{y})^2 \tag{3.4}$$

$$SS_{res} = \sum_i (y_i - \bar{y})^2 = \sum_i (\bar{e_i})^2 \tag{3.5}$$

Then coefficient of determination is defined as:

$$R^2 = 1 - \frac{SS_{res}}{SS_{tot}} \tag{3.6}$$

The solver method in Excel (Microsoft) was used to find best fit values for $a, b, c,$ and d by maximizing R^2. The Excel solver uses GRG nonlinear method.

3.2.2 Results

3.2.2.1 Magnitude of Displacement

A quadratic polynomial adequately fit the data and provided unique coefficients (Figure 3.3). The magnitude of movement was determined for 10 selected cells with two methods.

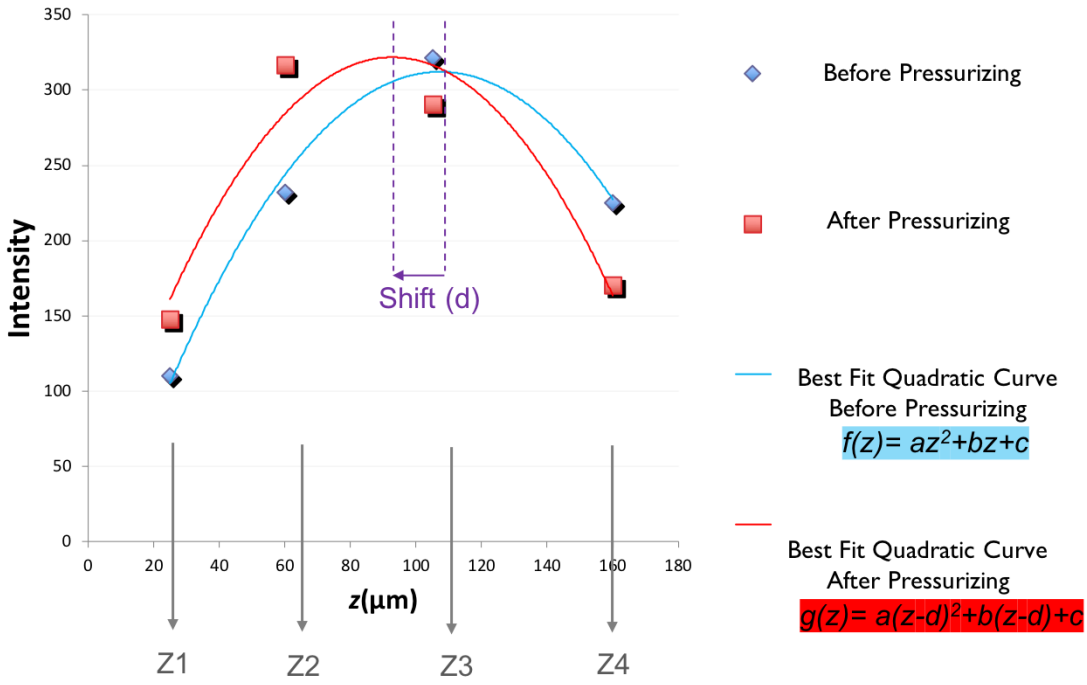

Fig. 3.3.: Fluorescent intensity changes during time for each height/z-stack. Dots indicates the intensities before (blue) and after (red) pressurizing selected and collected for further analysis for a representative cell.

3.2.2.2 Method#1

This method first used the data before loading to determine the best-fit values of a, b, and c from $f(z)$. Then these values were used in $g(z)$ and the undetermined parameter d was calculated. Values were found with self-developed MATLAB code (Table 3.1). The average shift between two curves was $d = 13.46 \pm 1.68$ μm.

Table 3.1.: Best-fit parameters of functions $f(z) = a(z)^2 + b(z) + c$ and $g(z) = a(z-d)^2 + b(z-d) + c$ from method #1 to determine the displacement d in z.

Cell Code	$\|d\|$ (μm)	a	b	c
Cell#1	11.89	-0.78	12.08	305.96
Cell#2	13.61	-0.91	15.83	94.098
Cell#3	14.75	-0.11	16.91	489.15
Cell#4	11.19	-0.045	6.79	212.26
Cell#5	14.11	-0.037	7.12	85.51
Cell#6	14.63	-0.030	6.55	-39.43
Cell#7	15.96	-0.089	18.69	-172.18
Cell#8	11.50	-0.085	15.68	-119.50
Cell#9	14.94	-0.054	11.92	-93.42
Cell#10	12.02	-0.041	8.55	-37.90
Average	13.46			
STDEV	1.68			

3.2.2.3 Method#2

This method simultaneously used the data before and after loading and found optimized values of $a,\ b,\ c$, and d for 10 cells with GRG nonlinear method (Tale 3.2). The average shift between the two curves was $d = 16.73 \pm 4.19$ μm for method#2.

Table 3.2.: Best-fit parameters of functions $f(z) = a(z)^2 + b(z) + c$ and $g(z) = a(z-d)^2 + b(z-d) + c$ from method #2 to determine the displacement d in z. * Outlier data.

Cell Code	$\|d\|$ (μm)	a	b	c
Cell#1	15.22	-0.05	6.93	517.68
Cell#2	19.90	-0.060	10.03	274.64
Cell#3	27.05*	0.05	4.80	875.651
Cell#4	15.19	-0.028	3.51	334.62
Cell#5	18.67	-0.029	5.66	140.20
Cell#6	13.59	-0.033	6.96	-53.33
Cell#7	14.84	-0.91	18.70	-192.13
Cell#8	15.22	-0.06	11.58	7.49
Cell#9	13.25	-0.062	13.31	138.29
Cell#10	14.39	-0.034	7.29	3.92
Average	16.73			
STDEV	4.19			

3.2.2.4 Quality of Fit

Method 1 fit the data before loading well, but had poor fitting to the data after loading because it did not use them to determine a, b or c. On the other hand, method 2 used all the data to simultaneously find best-fit values for the parameters and had better overall R^2 values. R^2 values for the equation $f(z)$ before loading were only slightly different at 0.95 and 0.89 for methods 1 and 2, respectively. However the average R^2 after loading ($g(z)$) was 0.65 for method 1 and was substantially higher at 0.84 for method 2 (Table 3.3). This suggests that method 2 was an overall better

fit for the 10 cells and therefore the magnitude of displacement was determined from the second method; d was estimated to be 16.73 μm.

Table 3.3.: R^2 values of curve fittings for methods 1 and 2.

Cell Code	R^2 for $f(z)$ in Method 1	R^2 for $g(z)$ in Method 1	R^2 for $f(z)$ in Method 2	R^2 for $g(z)$ in Method 2
Cell#1	0.92	0.66	0.83	0.84
Cell#2	0.94	0.46	0.84	0.73
Cell#3	0.82	0.41	0.69	0.82
Cell#4	0.91	0.66	0.83	0.84
Cell#5	0.96	0.53	0.90	0.76
Cell#6	0.99	0.89	0.99	0.90
Cell#7	0.98	0.80	0.96	0.87
Cell#8	0.99	0.48	0.93	0.79
Cell#9	0.99	0.92	0.99	0.95
Cell#10	0.99	0.68	0.97	0.84
Average	**0.95**	**0.65**	**0.89**	**0.84**
STDEV	0.06	0.18	0.09	0.06

3.3 Source of Displacement

3.3.1 Materials and Methods

To determine the source of the displacement of the gel, three possible sources were considered: deformation of the gel scaffold, deformation of the glass window, and deformation of the epoxy glue.

3.3.1.1 Scaffold Gel Deformation

As described in section 2.2.1, cells were seeded into 4% agarose gels. This means the scaffolds contained 96% water and as a result the properties of water were used to estimate the deformation of scaffold due to 12 MPa of hydrostatic pressure. The change of volume in gels due to HP was determined through the following equation:

$$\Delta p = k\frac{\Delta v}{v} \tag{3.7}$$

where p is HP, k is bulk modulus, and v is volume.

From the change in volume, can also be calculated as:

$$\frac{\Delta v}{v} = \frac{\pi r^2 h - \pi r_0^2 h_0}{\pi r_0^2 h_0} \tag{3.8}$$

where r_0 and h_0 are the undeformed radius and height of the gel, respectively, and r and h are the radius amd height of the deformed scaffold. Expanding the terms and neglecting higher order terms in small displacement:

$$\frac{\Delta v}{v} = \frac{(r_0 - \Delta r)^2(h_0 - \Delta h) - r_0^2 h_0}{r_0^2 h_0} \tag{3.9}$$

$$\frac{\Delta v}{v} = \frac{(r_0^2 - 2r_0\Delta r)(h_0 - \Delta h) - r_0^2 h_0}{r_0^2 h_0} \tag{3.10}$$

Assuming small displacements, higher order terms can be neglected:

$$\frac{\Delta v}{v} = \frac{r_0^2 h_0 - r_0^2 h_0 + r_0^2\Delta h + 2r_0 h_0 \Delta r}{r_0^2 h_0} \tag{3.11}$$

Simplifying,

$$\frac{\Delta v}{v} = \frac{\Delta h}{h_0} + \frac{2\Delta r}{r_0} \tag{3.12}$$

For isotropic material under the uniform load of HP, $\frac{\Delta h}{h_0} \approx \frac{\Delta r}{r_0}$, so:

$$\frac{\Delta h}{h_0} = \frac{1}{3}\frac{\Delta v}{v_0} \tag{3.13}$$

These equations were solved using the following values:

p= 12 MPa, $k = 2.15 \times 10^9$ Pa, h_0 as primary height =3 mm

3.3.1.2 Sapphire Glass Deformation

The movement of cells may be due to the glass deformation under the pressure. To estimate the deformation of the glass, a finite element model was made of the glass window. The simulations were modeled in Abaqus (ABAQUS (2011), Dassault Systmes, Providence, RI, USA) with 3-D tetrahedron meshes.

The sapphire glass window was modeled as 0.5" in diameter, 0.08" in height with a Youngs modulus of 462.6 GPa and Poissons ratio of 0.309 (data from www.ispoptics.com).

The boundary conditions were determined based on how the window is held in the chamber (Figure 3.4). Three different boundary conditions were applied to the window in separate Abaqus simulations, as the epoxy glue does not provide simple fixation.

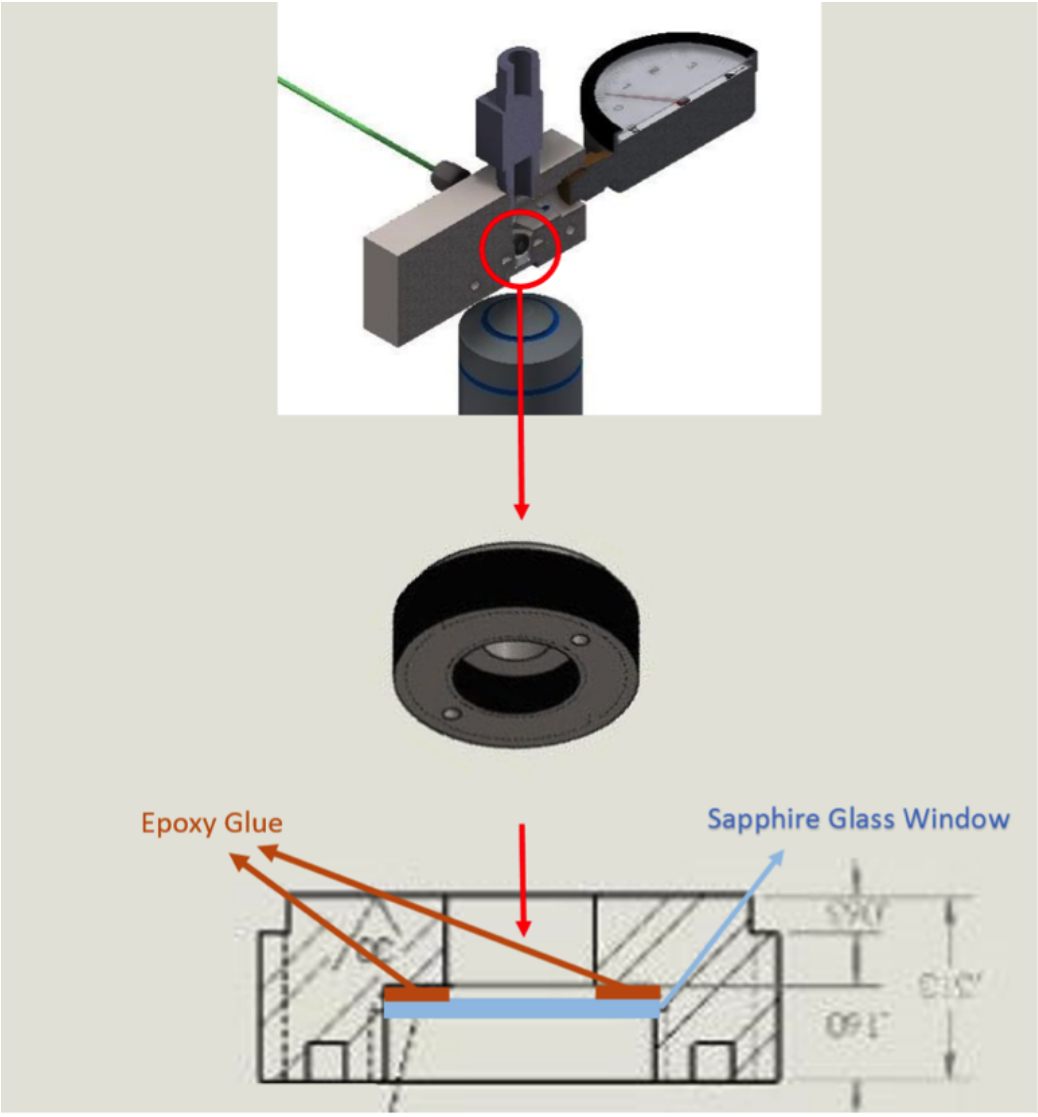

Fig. 3.4.: Schematic of the sapphire glass window epoxied to the window holder.

In the first model, it was assumed that the top edge of the window was fixed and 12 MPa of pressure was applied to the entire top surface of the window (Figure 3.5).

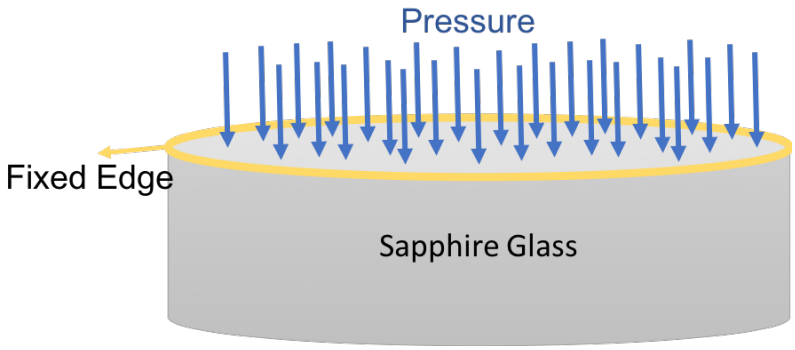

Fig. 3.5.: Schematic of the finite element model of sapphire window with fixed top edge and 12 MPa pressure on top surface.

In the second model, it was assumed that the side of the window was fixed and 12 MPa pressure was applied to the entire top surface of the window (Figure 3.6).

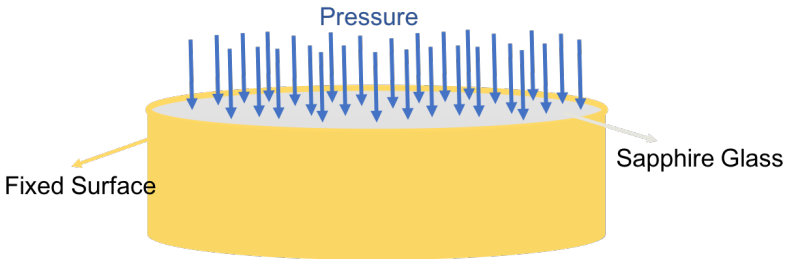

Fig. 3.6.: Schematic of the finite element model of the sapphire window with fixed side surface and 12 MPa pressure on top surface.

In the third model, it was assumed that the outer top surface is fixed and 12 MPa pressure was applied to the non-fixed circle on the top surface with a diameter of 0.25" (Figure 3.7).

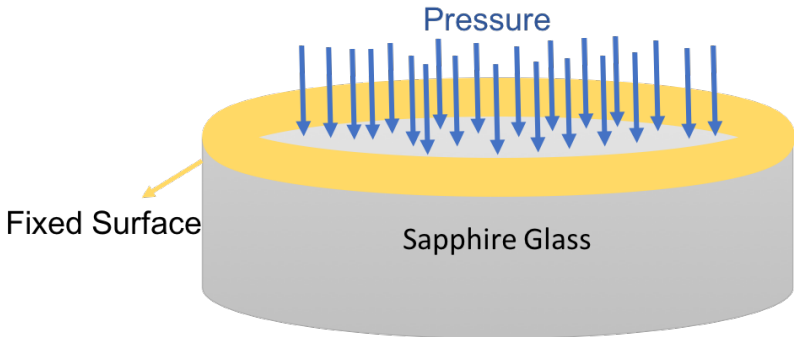

Fig. 3.7.: Schematic of the finite element model of the sapphire window with fixed outer top surface and 12 MPa pressure in the center.

3.3.1.3 Epoxy Glue Deformation

The movement of cell-seeded gels may be due to the epoxy tension under the pressure, as the window is glued to chamber with epoxy (Figure 3.4). Models with different thicknesses were generated because the actual thickness could not be determined. The deformation was modeled for thicknesses of 0.5, 0.6, 0.7, 0.8. 0.9 and 1 mm. The epoxy (EA E-05MR, HYSOL) was modeled as a cirlcular strip with inner diameter of 0.25" and outer diameter of 0.5" (Figure 3.8). The Young's modulus and Poisson's ratio were 723 MPa and 0.433 respectively [78]. The simulations were modeled in Abaqus (ABAQUS (2011), Dassault Systmes, Providence, RI, USA) with 3-D tetrahedron meshes and 12 MPa of pressure was applied to the epoxy.

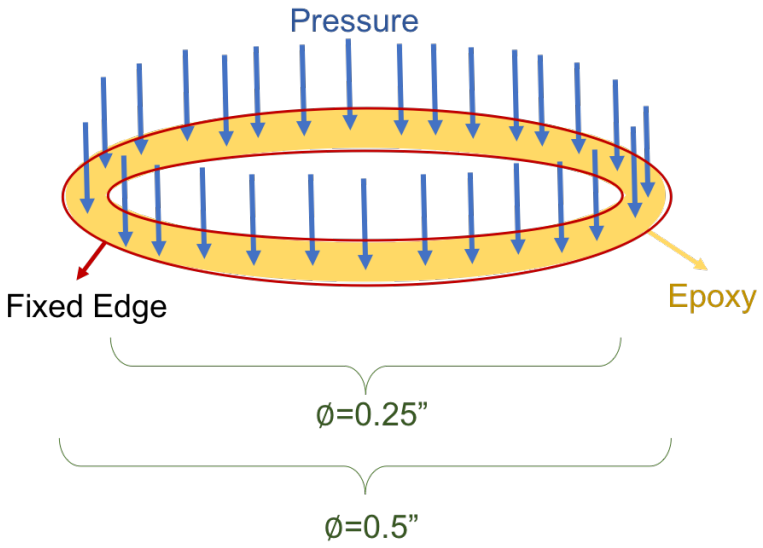

Fig. 3.8.: Schematic of finite element model of epoxy with 12 MPa of applied pressure on top.

3.3.2 Results

In Chapter 2, it was determined that although the gel was stopped from floating around with a fixing gel, there was still $\sim$ 16 μm downward movement during pressurizing. The cause for this movement was determined next.

3.3.2.1 Scaffold Gel Deformation

The change of volume and height in gels due to HP was determined through the equation 3.7 to 3.11 and the properties of water. The volumetric strain was first calculated:

$$\frac{\Delta v}{v} = 5.58 \times 10^{-3} \tag{3.14}$$

The strain in the vertical direction was:

$$\frac{\Delta h}{h_0} \approx \frac{1}{3}\frac{\Delta v}{v_0} = 1.86 \times 10^{-3} \tag{3.15}$$

This was used to calculate the theoretical change in the height of the scaffold.

$$\Delta h = 5.58 \mu m \tag{3.16}$$

We only imaged the bottom 4.5% of the scaffold height. Therefore, the theoretical change in the height of imaging would be:

$$\Delta h_{imaged} = 0.045 \times 5.58 = 0.25 \mu m \tag{3.17}$$

3.3.2.2 Sapphire Glass Deformation

In the first model of the sapphire glass, it was assumed that the circular edge at the top of the window was fixed and the pressure was applied to the entire top surface. The maximum displacement in this model was 0.3135 μm (Figure 3.9).

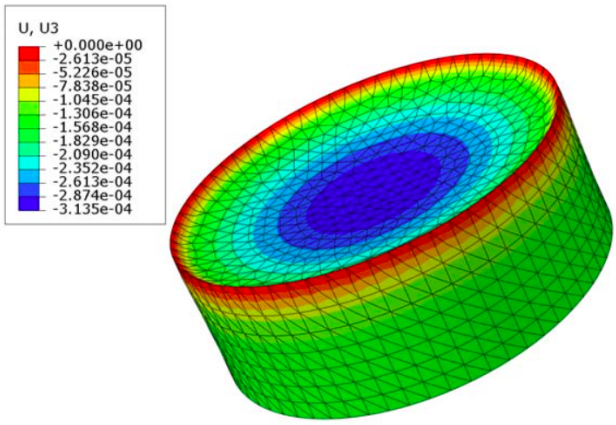

Fig. 3.9.: Displacement of the sapphire glass with a fixed top edge in the finite element model.

In the second model of the sapphire window with a fixed side surface, the maximum displacement was 0.1543 μm (Figure 3.10).

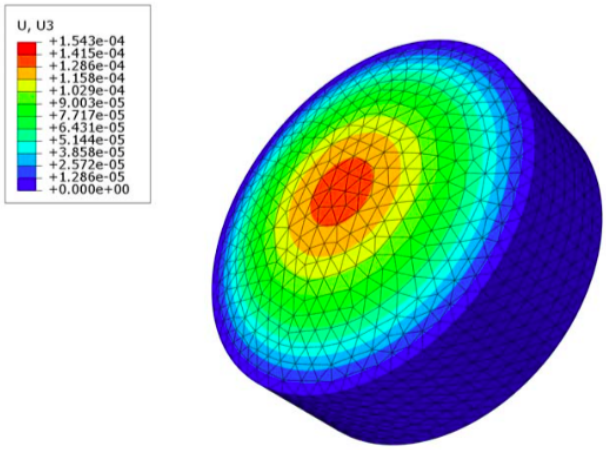

Fig. 3.10.: Displacement of the sapphire glass with a fixed side surface in the finite element model.

The finite element model of the sapphire glass window with the top surface partially fixed resulted in a maximum displacement of 0.2220 μm (Figure 3.11).

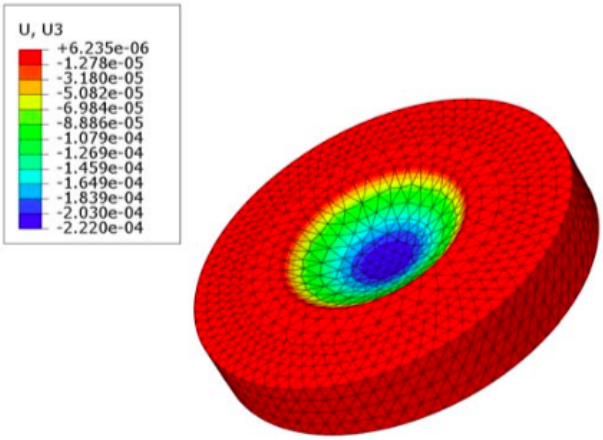

Fig. 3.11.: Displacement of the sapphire glass with a partially fixed top surface in the finite element model.

Overall, the models suggest a maximum displacement of the glass between 0.1544 μm and 0.3135 μm, which is small compared to our estimate of the movement of the gel. Therefore, this displacement cannot be the main reason for the movement.

Another material which is more deformable is the epoxy used to glue the window to the chambers body, and this a cause of movement was also considered.

3.3.2.3 Epoxy Deformation

Epoxy thicknesses of 0.5, 0.6, 0.7, 0.8. 0.9 and 1 mm were modeled; the maximum displacement increased with thickness and the relationship was linear (Figure 3.13). The displacement for thickness of 1.0 mm were as high as 16.97 μm (Figure 3.12).

The calculations in the previous section show that the movement of the gel inside the chamber was about 16.73 μm. If we assume the movement is due entirely to epoxy deformation, the thickness of epoxy is approximately 0.98 mm.

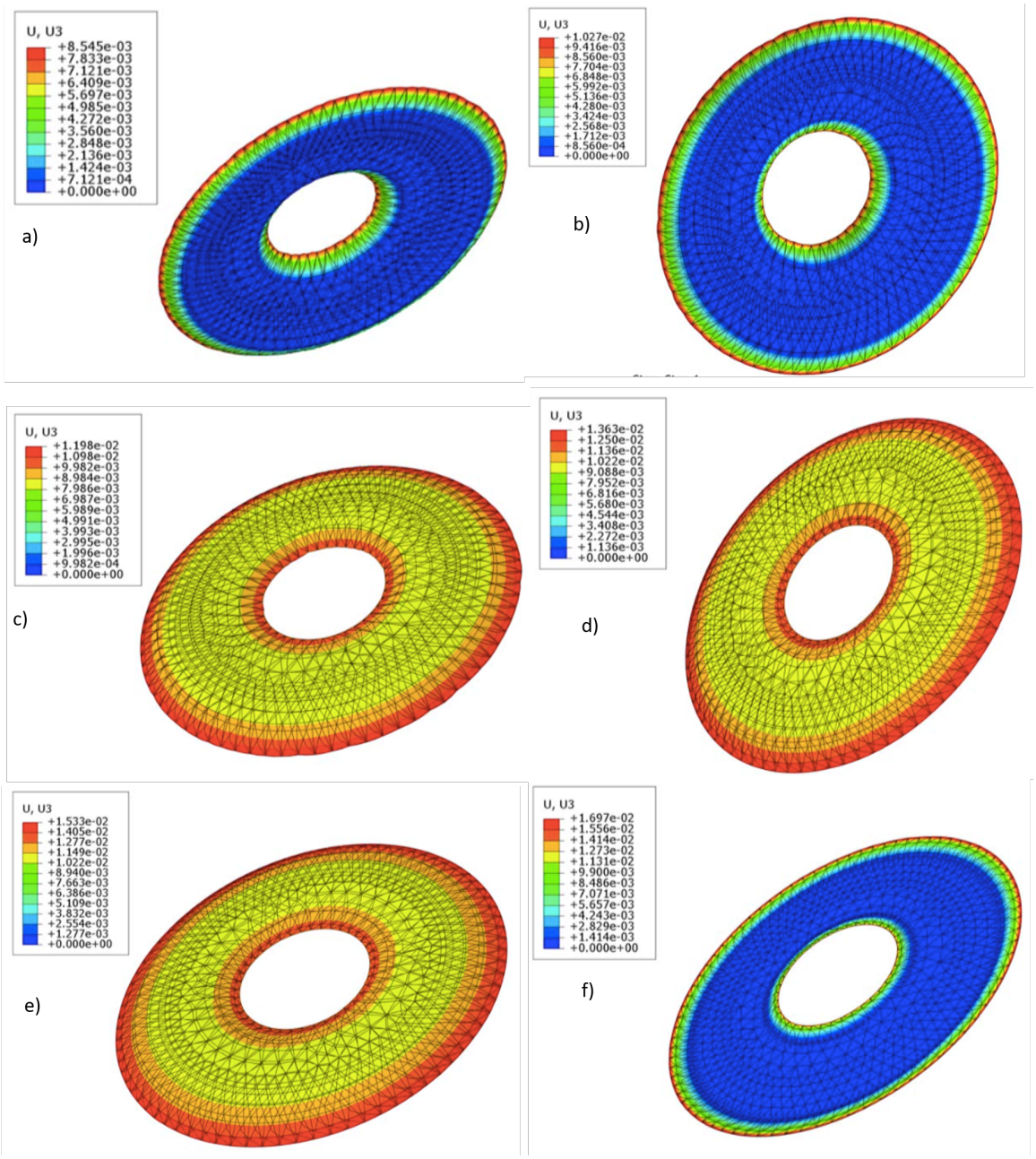

Fig. 3.12.: Displacement of epoxy with thickness of (a) 0.5 mm (b) 0.6 mm (c) 0.7 mm (d) 0.8 mm (e) 0.9 mm and (f) 1 mm. Simulated in Abaqus.

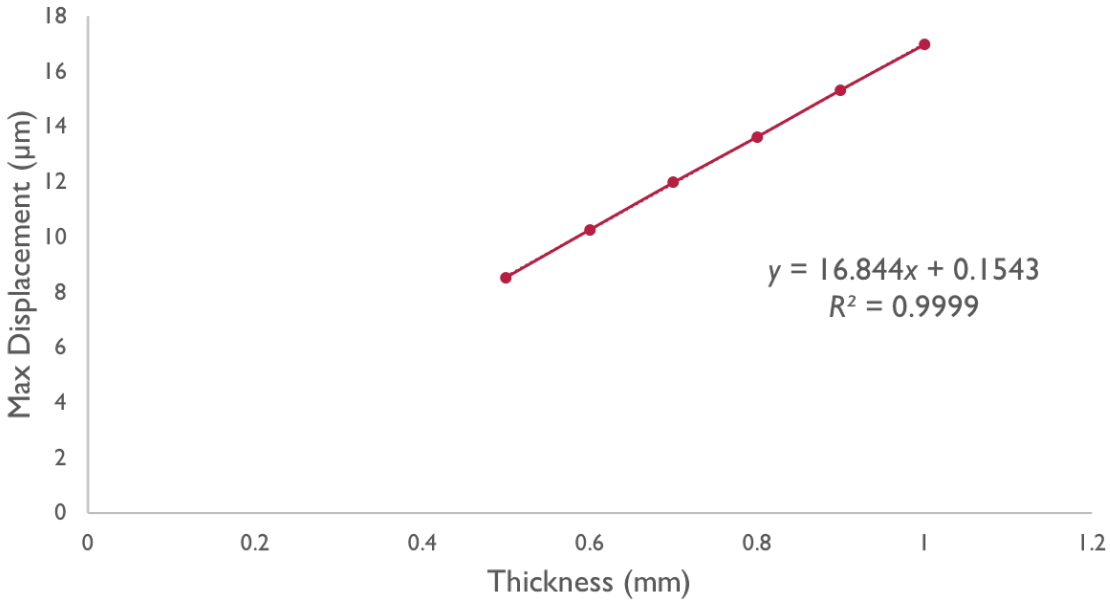

Fig. 3.13.: Linear relationship between maximum epoxy displacement (determined in Abaqus) and epoxy thickness.

3.4 Discussion

The fixing gel stopped the cell-seeded gel from moving in the absence of applied load but there were still some movement due to the application of HP. The movement was quantified by fitting quadratic curves to the fluorescent intensity data as a function of z before and after loading. Two methods were used to fit the data. In the first method, 4 data points from before loading were used to fit the curve and determine parameters a, b, and c and then the curve was fit to data after pressurizing and parameter d was calculated. In the second method, all 8 data from before and after loading were simultaneously utilized to determine the optimum values for parameters a, b, c, and d. The second method showed overall better quality fitting based on R^2 values. About 16 μm displacement or movement of the gel in the bioreactor was esti-

mated. Further analysis determined that this was due more to the bioreactor design rather than the gel construct deformation.

Deformation of the epoxy between the window of the bioreactor and its chamber seemed to be one of main reasons for the displacement of the gel. Other causes of the movement could be due to deforming or slipping of threads between the window holder and chamber. In reality, all these sources of deformation combine to cause the movement. The bioreactor provides live imaging of cells when they are seeded in ϕ=5 mm gels and also can hold up to 12 MPa of hydrostatic pressure. However, further studies and efforts would have to be done on the bioreactor design to minimize the deformations and maximize the quality of the images.

4. THE EFFECT OF FAK INHIBITION IN EARLY AND LATE CHONDROGENESIS AND HP MECHANOTRANSDUCTION

4.1 Introduction

Mechanotransduction pathways for hydrostatic pressure are poorly understood, and all of the signaling molecules are not known. A better understanding of how the mechanical load is translated into a beneficial response could help to overcome current limitations in cartilage tissue engineered structures. In this study, the involvement of focal adhesion kinase (FAK) was considered as one of the agents in HP mechanotransduction and chondrogenesis of MSCs.

Integrin binding to the extracellular matrix (ECM) outside the cell and to the cytoskeleton inside the cell, triggers intracellular pathways controlling cell behavior such as proliferation, migration, and differentiation [79]. Focal adhesions are a response to integrin binding formation, contain multiple integrins and are a concentrated site of actin filaments and proteins such as talin, vinculin, paxillin (pax), Srx, and FAK (Figure 4.1). FAK is one of the downstream regulators that transfers signals from focal adhesions. The role of FAK in MSC proliferation and migration has been more studied than differentiation. However, reports indicate a function for FAK in the differentiation of MSCs and preosteoblasts [56, 79–81].

Integrin binding and focal adhesions are mainly thought to inhibit chondrogenesis [83]. FAK signaling pathways were shown to suppress early chondrogenesis [84]. On the other hand, type II collagen decreased with FAK knockdown when the chondrocytes were cultured in alginate hydrogel [85]. Moreover, GAG secretion as well as aggrecan was not affected by FAK knockdown in chondrocytes [85]. These results showed the important role of FAK signaling in chondrogenesis but did not support

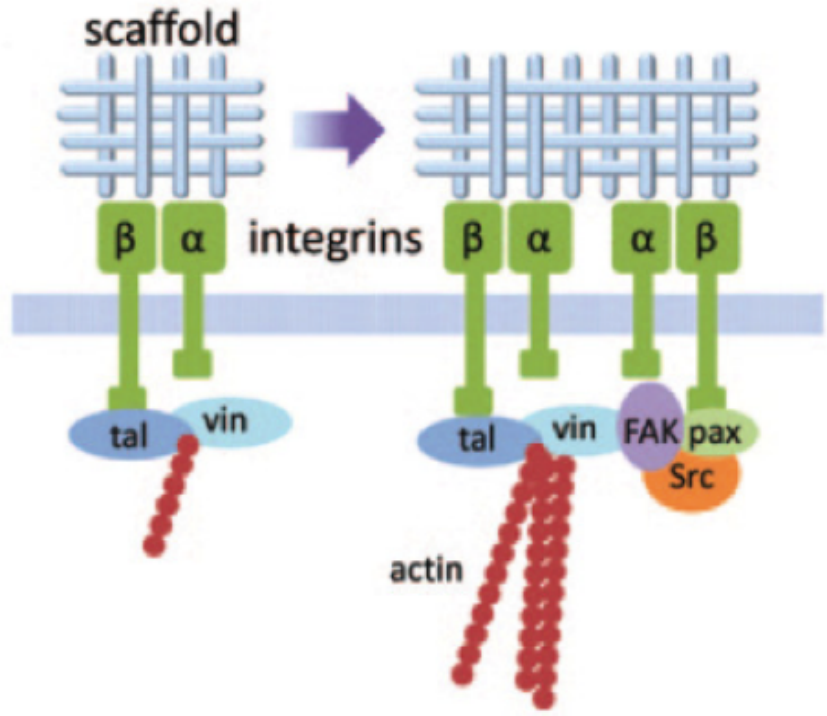

Fig. 4.1.: Left: An integrin with and subunits attached to a scaffold. Right: A focal adhesion containing multiple integrins is a concentrated site of actin filament and protein binding [82].

each other in every aspect. In our lab, Huseyin Arman previously showed a dose-dependent decrease in matrix production when FAK inhibitor was used on MSCs seeded in 4% agarose gel. In addition, Komal Yadav from our lab confirmed this with Alcian Blue staining (Figure 4.2).

There are many studies on FAK activity in response to different mechanical stimuli for various types of cells. Fluid shear stress has been shown to activate FAK in bovine aortic endothelial cells [86]. Moreover, FAK involvement was shown in mechanotransduction of fluid shear stress by osteoblasts [87]. Wang et al. demonstrated that FAK is involved in mechanosensing of mouse embryonic fibroblasts [88]. However, FAK involvement in HP mechanotransduction had not been previously studied.

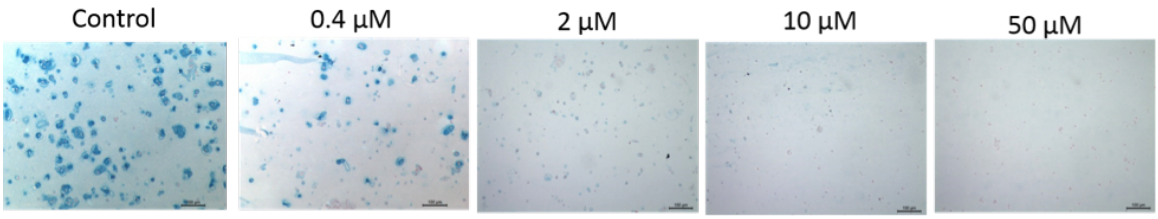

Fig. 4.2.: Alcian blue staining of MSCs in agarose scaffold, cultured with different concentrations of FAK inhibitor PF 573228 from day 1 to day 21 (early chondrogenesis).

In this chapter the FAK participation in early and late chondrogenesis was investigated. The study utilized a pharmacological FAK inhibitor at early and late stages of MSC chondrogenic differentiation, and chondrogenic gene expression and matrix production was assessed. Additionally, FAKs involvement in HP mechanotransduction was studied.

4.2 Materials and Methods

4.2.1 Cell Isolation, Expansion, Encapsulation and Culture

The same procedure of seeding porcine MSCs in 4% agarose gels was done as in Chapter 2, Part 2.2.1; cell-seeded gels were cultured in chondrogenic differentiation medium for up to 6 weeks.

In some studies different concentrations of FAK inhibitor PF573228 (Sigma Aldrich) were added to the culture medium on the gels from day1 to day 21 (early chondrogenesis) or from day 22 to 42 (late chondrogenesis). The concentrations were: 0 μM (control), 0.4 μM, 2 μM, 10 μM, and 50 μM. Gels were harvested either at day 21 (early chondrogenesis) or day 42 (late chondrogenesis).

In another study, cell-seeded gels were treated with 50 μM of the FAK inhibitor overnight in their culture medium at days 6 and 20. The vehicle control for each

group received the same volume of DMSO. Gels were harvested at day 7 (week1) and day 21 (week3).

To investigate FAK involvement in mechanotransduction, gels were treated with 50 μM of the FAK inhibitor overnight after 3 weeks of culture. The same volume of DMSO was added to each well as vehicle control. Gels were loaded the next day.

4.2.2 RNA Isolation and Real-time Polymeric Chain Reaction

Real-time reverse transcription polymerase chain reaction (RT-PCR) was used to quantify relative changes in the expression of chondrogenic genes in different groups. RNA was extracted by homogenizing each construct in 1 mL of TRIzol® reagent (Fisher Scientific Co.), followed by chloroform (Sigma-Aldrich) extraction. The extracted amount was incubated with an equal volume of 2-propanol in -20 ^{0}C freezer overnight. The solution was then centrifuged at 4 ^{0}C and the precipitate was washed once with 70 % ethanol. The precipitate was suspended in 100 μL DNAse and RNAse free water and an equal volume of 75% ethanol was added. The RNA then was purified with a PureLink RNA Mini kit (Ambion) according to manufacturers instructions. 3 gels were pooled together per replicate for higher concentrations of RNA. Total RNA yield and purity were analyzed using a NanoDrop Spectrophotometer. To quantify mRNA expression, 100 ng total RNA was reverse transcribed into cDNA using Applied Biosystems™ High-Capacity cDNA Reverse Transcription Kit (Fisher Scientific Co.). Forward and reverse primers including Sox9, aggrecan (Agc), collagen type II alpha 1 (Col2), and housekeeping gene (18s) were used in this study (Table 4.1). RT-PCR was performed using an SYBR® Green MasterMix (Applied Biosystems, A25742). 5 μL cDNA preparation (diluted 1:5 with RNase free water), 0.1 μL gene assay, 10 μL Master mix and 4.8 μL RNase free water (20 μL total volume) were added to each well. Samples were analyzed in duplicate or triplicate in one run (40 cycles). RT-PCR data were analyzed using the $\Delta\Delta C_T$ method with 18s as the endogenous control (n=3). In FAK inhibitor and early/late chondrogenesis study, data

are presented as fold changes in gene expression relative to the control group. For investigating FAK involvement in mechanotransduction, data are presented relatively as fold changes in gene expression relative to the unloaded group.

Table 4.1.: Reverse and forward gene primers for polymeric chain reaction. 18s is housekeeping gene.

Gene	**Forward 5'-3'**	**Reverse 5'-3'**
18s	TCGGAACTACGACGGTATCTCT	CGGAACTGAGGCCATGATTA
Agc	CGGTAATGGAACACAACCCCT	TGCAGGTGACCATGGCC
Sox9	CTTGTAATCCGGGTGGTCCTT	ATCAGTACCCGCACCTGCAC
Col2	CCACGAGGCCAGGAGCT	CCATCTGGCTTCCAGGGAC

4.2.3 Biochemical Analysis

Gel constructs (n=4 for each group) were digested with papain (125 μg/mL) in 0.1 M sodium acetate, 5 mM L-cysteine-HCl, and 0.05 M EDTA (pH 6.0, all Sigma-Aldrich) at 60 ^{0}C overnight. Sulphated glycosaminoglycan (sGAG) content was quantified using the dimethylmethylene blue dye-binding assay (DMMB; Sigma) with a chondroitin sulphate standard. Media samples from the twice weekly half media changes were also analyzed using the DMMB assay. Total sGAG was determined by summing the amount of sGAG in each gel with the corresponding amount in the media.

A Pico Green assay was also performed on the papain digests to measure the total DNA in the constructs using Quant-iT™ PicoGreen™ dsDNA Assay Kit (Thermo Scientific P11496) following the manufacturers protocol.

4.2.4 Histology and Immunohistochemistry

One sample from each group (0, 0.4, 2, 10, 50 μM of FAK inhibitor) was fixed in paraformaldehyde (PFA) overnight and then embedded in paraffin and sectioned with a thickness of 5 μm. Sections were stained with 1 % Alcian blue 8GX (Sigma- Aldrich) in 0.1 M HCl for to visualize sGAG distribution. Collagen types I and II and X were determined with immunohistochemistry. Sections were treated with peroxidase, followed by chondroitinase ABC (Sigma-Aldrich) in a humidified chamber at 37 ^{0}C for 1 h to make the extracellular matrix permeable. Samples were then blocked with goat serum diluted in PBS with 1 % BSA (Hyclone). Afterwards, the primary antibodies for collagen types I, II and X(mouse monoclonal, Abcam) were applied for 1 h. Next, the secondary antibody (anti-Mouse IgG biotin conjugate, Sigma-Aldrich) was applied for 1 h, followed by incubation with ABC Peroxidase Standard Staining Kit (Fisher Scientific Co.) for 45 minutes all in a humidity chamber. Finally, the slides were developed with DAB peroxidase (Vector Labs) for 10 minutes. Samples were washed with PBS between each step and Permount (Fisher Scientific Co.) was used under a cover slip. Negative and positive controls of pig ligament and meniscus (positive for type I collagen, negative for type II collagen) and cartilage (positive for type II collagen, negative for type I collagen) were also stained.

4.2.5 Application of Hydrostatic Pressure

Constructs were sealed into sterile bags with 1.5 mL of medium per construct. Cyclic HP was applied in a metal pressure vessel filled with water within a 37 ^{0}C water bath. The sealed bags exposed to HP were placed into the pressure vessel while the controls were placed into a similar container in the same water bath. The pressure vessel was connected by tubing to a hydraulic cylinder (PHD Inc., Fort Wayne, IN, USA) that was loaded using a computer controlled MTS (858 Mini Bionix) testing machine. The pressure inside the vessel was measured using a pressure gauge (Omega Engineering Inc.). The load applied to the hydraulic cylinder by the MTS was set

such that the HP inside the vessel reached an amplitude of 10 MPa at a frequency of 1 Hz, for 4 hours. Immediately after loading, constructs were snap-frozen and stored at -80 ^{0}C until further analysis.

4.2.6 Protein Extraction and Western Blot

Snap frozen samples were transferred to 500 μL of RIPA buffer (Alfa Aesar J60629) with EDTA and Halt Phosphatase-Proteinase cocktail (Thermo scientific 78440). The samples incubated in the solution for 10-15 minutes and then they were homogenized for 1 minute. The blade of the homogenizer was washed twice with 200 μL of RIPA buffer solution to reach a total volume of 900 μL for each sample. Samples were in 4^{0}C for 2 hours while shaking. The samples were centrifuged at 12000 g for 20 minutes and the supernatant was taken to new tubes. The solution that contains protein then was concentrated with Amicon Ultra Centrifugal Filters (3k) following the protocol provided in the kit. The amount of protein was then determined by BCA Protein Assay Kit, Thermo scientific 23227. Western blots were performed by Yao Fan in Dr. Yokota's lab.

4.2.7 Statistical Analysis

Data were reported in form of mean $\pm$ standard deviation. Statistical analyses performed using Student's t-test (for difference between 2 groups) or one-way ANOVA with Tukey's post hoc test (for difference between multiple groups). A level of $p < 0.05$ was considered significant.

4.3 Results

4.3.1 Chondrogenic Gene Expression with FAK Inhibition in Early Chondrogenesis

The chondrogenic gene expression for different concentrations of FAK inhibitor applied during the first 3 weeks of culture was determined. The expression of Agc and Col2 decreased with increasing concentrations of the FAK inhibitor in a dose-dependent manner (Figure 4.3).

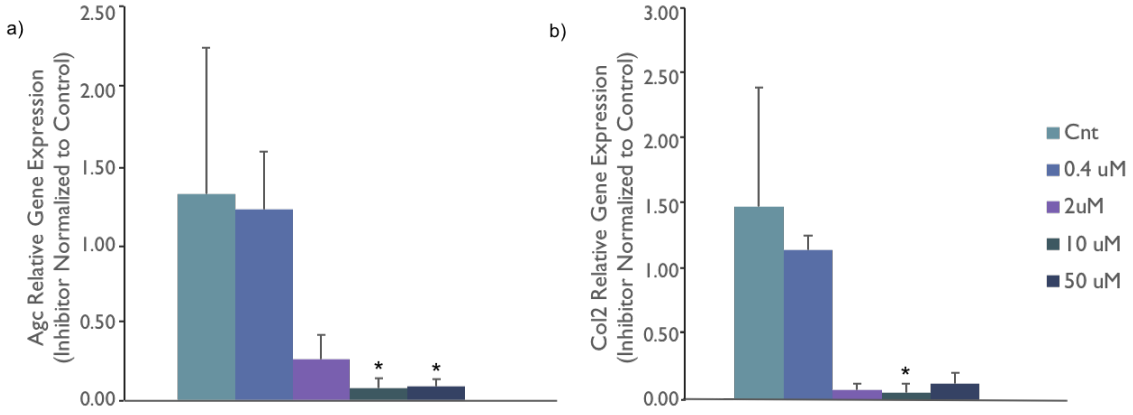

Fig. 4.3.: (a) Agc and (b)Col2 relative gene expression with different concentrations of FAK inhibitor in early chondrogenesis (day 1 to 21), relative to vehicle control. * indicates significant difference from control group (cnt), $p < 0.05$.

The results are consistent with the DMMB assay and Alcian Blue staining that had been done in our lab by Huseyin Arman and Komal Yadav respectively.

4.3.2 Total DNA and Total sGAG and Collagen Decrease by Increasing FAK Inhibition in Late Chondrogenesis

Cell seeded agarose constructs were cultured in differentiation medium for 6 weeks with the FAK inhibitor added in the last 3 weeks. The results show decreasing in DNA

from 3.54±0.44 μg for the control group to 1.74±0.18 μg for the highest concentration of FAK inhibitor (Figure 4.4a). The total sGAG also decrease from 811.63±133.5 3μg for the control group to 188.48±56.8 μg for the highest concentration of FAK inhibitor (Figure 4.4b). No trend was seen in Total sGAG/DNA for late chondrogenesis and just the highest concentration of FAK inhibitor application was different from the control group (Figure 4.4c).

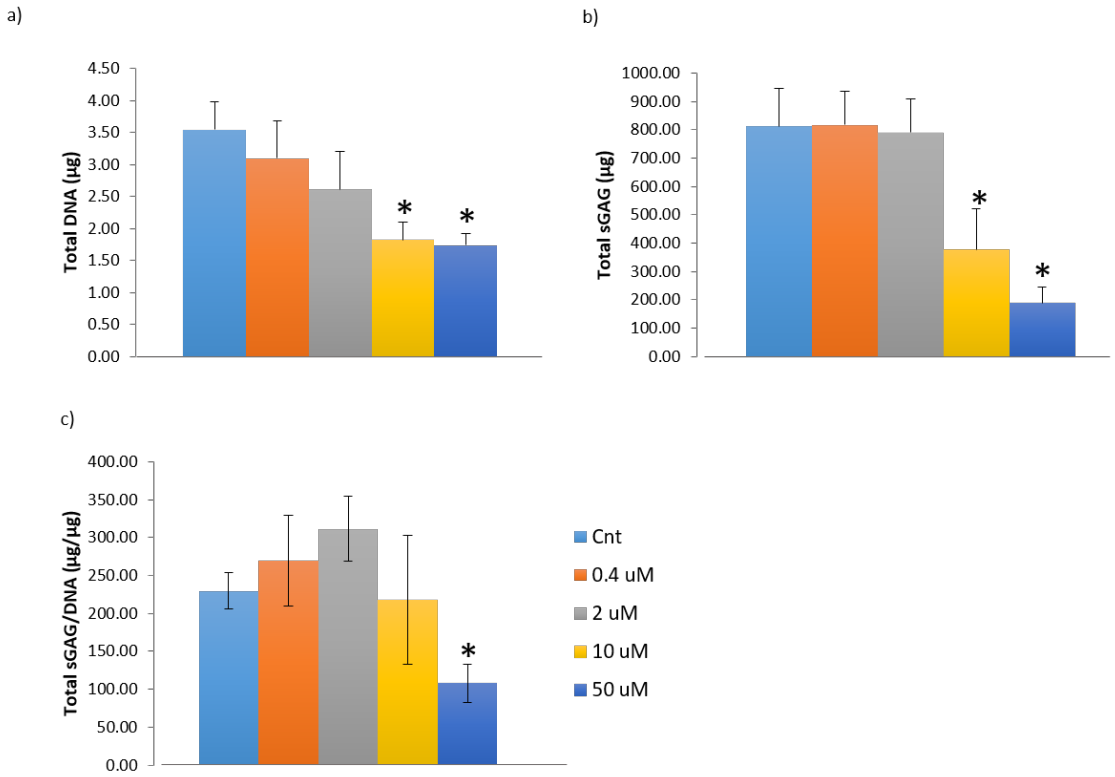

Fig. 4.4.: Total DNA, (b) Total sGAG and (c) toal sGAG/DNA for different concentrations of FAK inhibitor applied in weeks 4 to 6 (late chondrogenesis). * indicates significant difference from control, $p < 0.05$.

Immunohistochemistry staining for Col II, I and X generally showed less staining for higher concentrations of the FAK inhibitor. However, one concentration (0.4 μM) did not follow this trend. This sample may have had a defect as other results seem consistent (Figure 4.5a).

Alcian blue staining was also done to visualize sGAG production with different FAK inhibitor concentrations. The matrix production in the gel construct decreased in a dose-dependent manner with FAK inhibition, suggesting that FAK may be important to MSC functionality (Figure 4.5b).

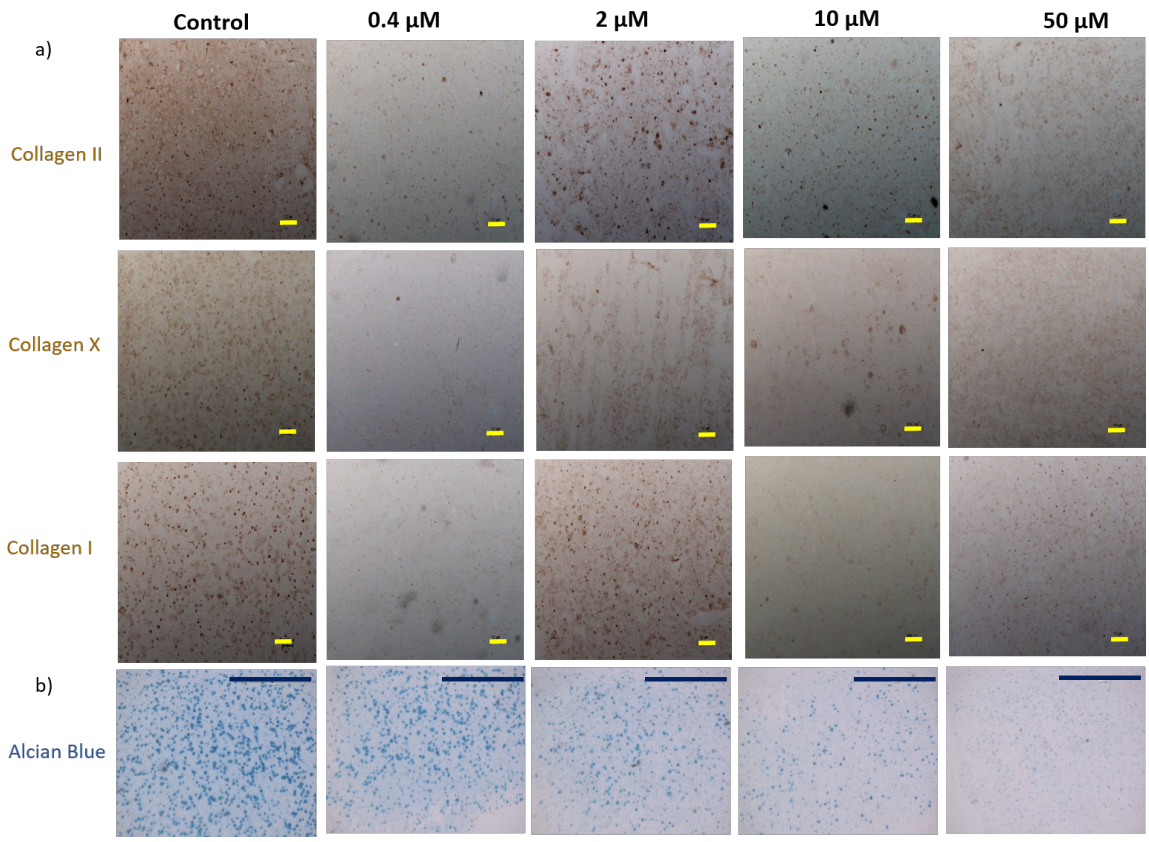

Fig. 4.5.: Representative images of (a) collagen II, X and I IHC staining for different concentrations of FAK inhibitor (scale bars = 50 μm) and (b) Alcian blue staining of sGAG deposition for different concentrations of FAK inhibitor (scale bars = 1000 μm) in late chondrogenesis (FAK inhibitor applied from week 4 to week6).

4.3.3 Time-dependent Response of MSCs to FAK Inhibition

It had been shown that the FAK signaling suppressed early chondrogenesis [84]. We examined possible difference in gene expression when the matrix is not fully produced (day 7) and when matrix is observed around the cells (day 21). In this study, the inhibitor was on gels overnight. The results showed a decrease in expression of all genes with FAK inhibition at day 7. At day 21, the expression of Agc and Sox9 was less with the FAK inhibitor, but the decrease was not as great as at day 7 (Figure 4.6a,b). At day 21 the expression of Col2 did not decrease with overnight application of the FAK inhibitor (Figure 4.6c).

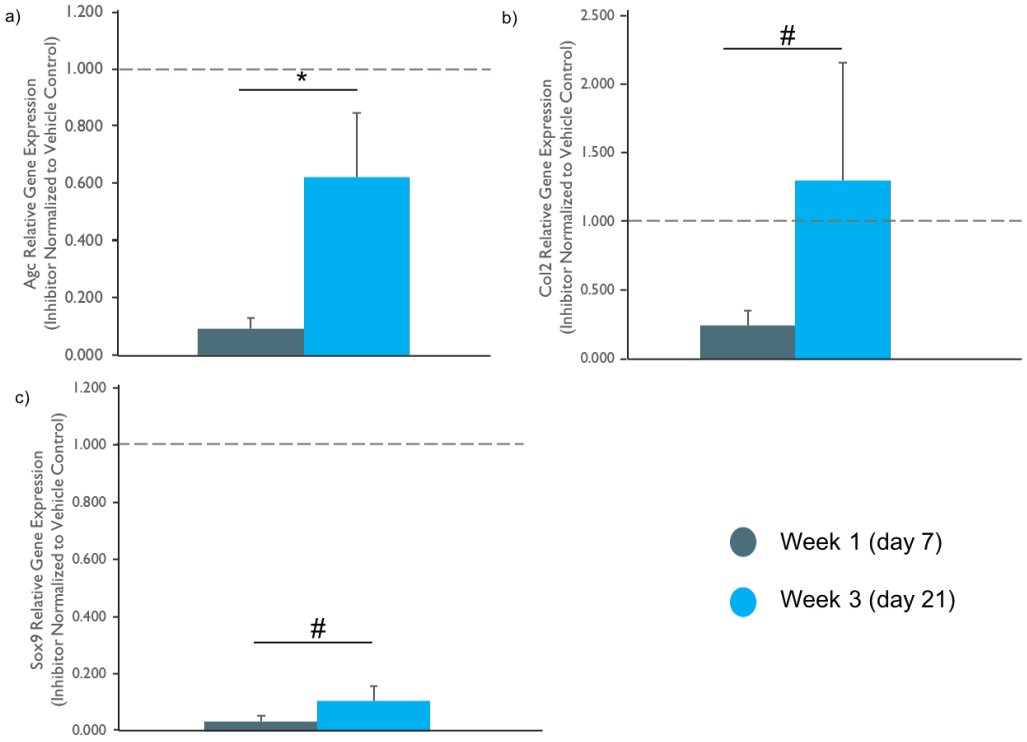

Fig. 4.6.: (a) Agc, (b) Col2 and (c) Sox9 relative gene expression with overnight application of FAK inhibitor relative to vehicle control at days 7 and 21. * indicates significant difference between days 7 and 21, $p < 0.05$; # tends to be different between days 7 and 21, $0.05 \leqslant p \leqslant 0.1$. Dashed line indicates a normalized value of 1.0 (no difference between treated (inhibitor) and control samples).

4.3.4 Hydrostatic Pressure Activates FAK

Western Blot analysis of p-FAK, FAK and -actin was performed for loaded and unloaded cells treated with either the FAK inhibitor or the vehicle control. With the vehicle control, higher levels of FAK phosphorylation were seen with HP loading than in the unloaded cells, suggesting that HP loading leads to an increase in FAK activity and that FAK may be a part of MSCs mechanotransduction. On the other hand, groups that were treated with the FAK inhibitor did not show a difference between loaded and unloaded conditions (Figure 4.7).

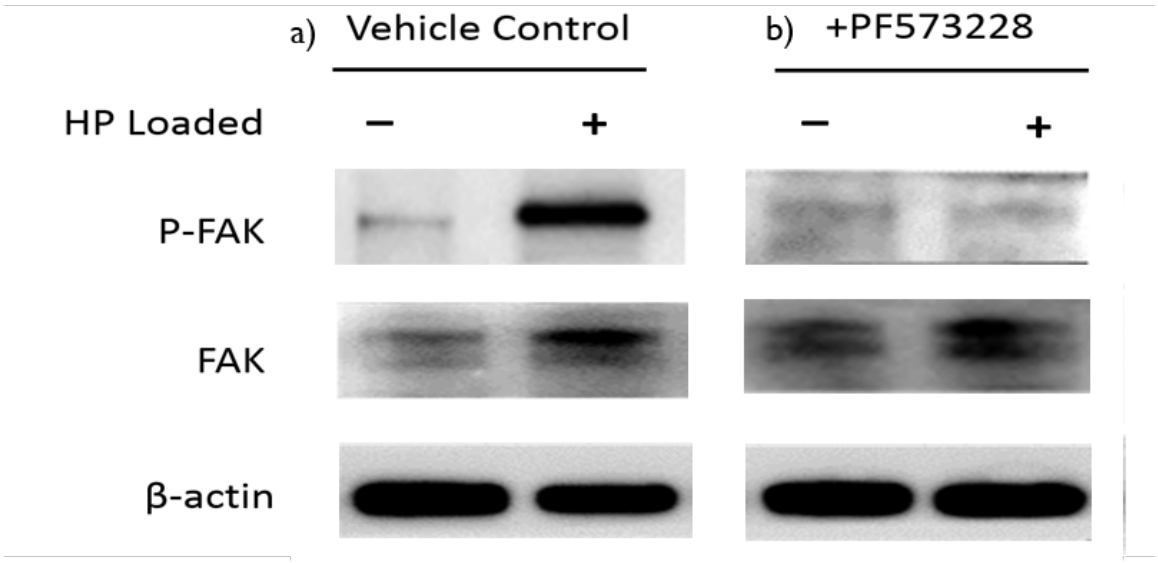

Fig. 4.7.: Western Blot analysis of p-FAK and FAK for loaded (1 Hz of 10 MPa hydrostatic pressure for 4 hours on day 21) and unloaded groups exposed to (a) vehicle control and (b) overnight FAK inhibitor. β-actin was a loading control for the Western blot.

4.3.5 FAK Inhibition Eliminates the Beneficial Effect of Hydrostatic Pressure

Integrin binding had been shown to play a part in the mechanotransduction of hydrostatic pressure by MSCs [32, 82], therefore we examined if FAK also plays a role in the chondrogenic response to mechanical loading. The results confirm that HP increases chondrogenic gene expression, and also show that FAK inhibition suppressed MSCs′ response to HP (Figure 4.8). This outcome suggests that FAK is a part of the pathway of HP mechanotransduction by MSCs.

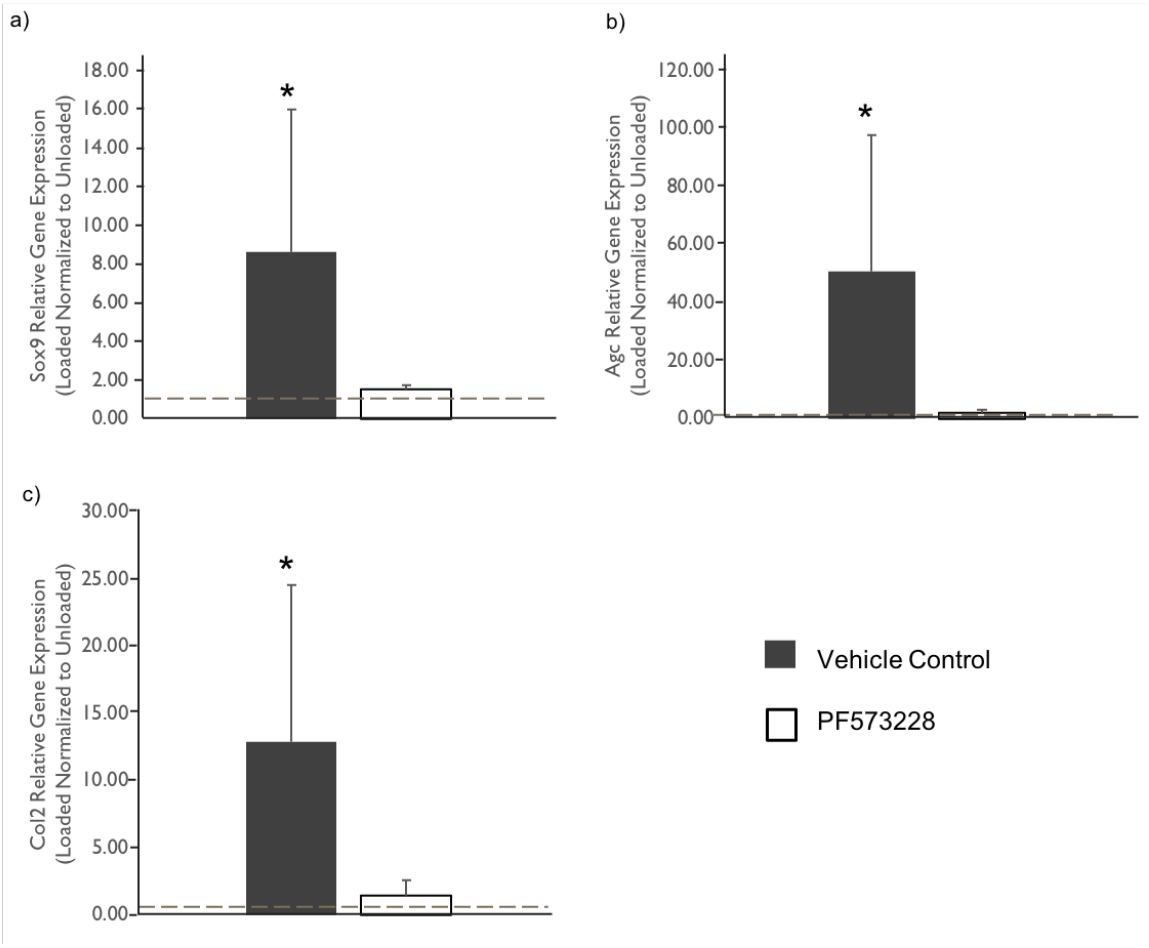

Fig. 4.8.: (a)Sox9, (b) Agc, and (c) Col2 relative gene expression for cells treated with PF573228 or vehicle control. Expression of loaded (1 Hz of 10 MPa hydrostatic pressure for 4 hours on day 21) cells normalized to the unloaded condition. * indicates a significant difference between loaded and unloaded conditions, $p < 0.05$. Dashed line indicates a normalized value of 1.0 (no difference between loaded and unloaded samples).

4.4 Discussion

Cell-matrix interactions been have shown to control chondrogenesis [89]. It has also been shown that FAK might play a role in chondrocyte specific gene expression and is required in chondrocyte communication with type II collagen and the mainte-

nance of chondrocyte phenotypes [85]. On the other hand, Pala et al. demonstrate that FAK/Src suppresses early chondrogenesis [84]. In this study, chondrogenic gene expression of MSCs with the application of 50 μM FAK inhibitor at days 7 and 21 was studied. The Agc gene expression increased at day 21 in comparison to day 7. This difference helps to explain the contradiction between different studies and guided us to further study of FAK.

Furthermore, FAK inhibition for MSCs in the early stage of chondrogenesis (weeks 1 to 3) decreased the amount of matrix production in a dose-dependent manner. This observation was consistent between sGAG production per DNA, gene expression, and immunohistochemistry and agrees the study done by Pala et al [84]. However, in the late chondrogenic stage (weeks 4 to 6) no trend was observed in sGAG production between groups. The DNA was higher in control group and decreased in higher concentrations of FAK inhibitor. This suggest either the cells died in higher concentrations or proliferated in the control group. Immunohistochemistry for collagens II, I and X and Alcian blue histology showed less staining with increasing FAK inhibitor concentration. Therefore, more study is needed to have more consistent data between techniques.

Mechanotransduction varies based on cell type, scaffold material, media supplement and culture condition. Therefore, defining the conditions that allow for cells to respond to mechanical loading is important. FAK was shown to be part of different mechanotransduction pathways for shear stress [86, 87] and cyclic tensile strain [78] for different types of cells. In the current study, 10 MPa cyclic HP of 1 Hz increased FAK activation in MSCs (shown by Western blot) and also increased the chondrogenic gene expression. Furthermore, the beneficial chondrogenic effect of HP on MSCs was suppressed by inhibition of FAK. These observations suggest that focal adhesion kinase is involved in the HP mechanotransduction of MSCs.

5. THE EFFECT OF SIRTUIN1 INHIBITION ON CHONDROGENESIS AND HYDROSTATIC PRESSURE MECHANOTRANSDUCTION

5.1 Introduction

A better understanding of the signaling pathways involved in the cells response to beneficial mechanical loading may uncover new molecular targets to enhance cartilage matrix production and address limitations in cartilage tissue engineering and regenerative medicine. To this end, the potential role of surtuin1 (SIRT1) was studied in HP mechanotransduction and chondrogenesis for MSCs.

SIRT1 is a NAD^+-dependent histone deacetylase that is known to be an anti-aging gene [90]. As SIRT1 can de-acetylate various transcription factors and also reacts with chromatin and nonchromatin proteins, it cooperates in cell differentiation, survival, tumorigenesis, inflammation, and metabolism [91]. SIRT1 can be activated by resveratrol (3,5,4-trihydroxy-tran-stilbene), which is found in the skin of red grapes, cranberries, and peanuts [90]. Investigations show that resveratrol has anti-inflammatory, antioxidant, and antitumor effects on tumor cells [92–94] and other cell types.

Although SIRT1 is the best-studied of the 7 sirtuins, there are some considerations about SIRT6 as well. It has been shown in vivo that SIRT1 and SIRT6 play important roles in cartilage homeostasis and their activators might be effective in cartilage anabolism [95]. It has been suggested to activate sirtuins to treat OA and joint degenerative pathologies as the sirtuins are thought to encourage chondrocyte survival, especially under stress conditions. Therefore, the function and pathway of sirtuin activity is under investigation in different aspects of cartilage biology, such as skeletal development, osteoarthritis (OA), and rheumatoid arthritis (RA) [95].

SIRT1 is known as a mammalian ortholog of yeast SIR2, and one of the genes involving in aging [96]. Aging is a destructive factor in MSCs capability to self-renew, stemness, and differentiation. The loss of SIRT1 expression is partly responsible for older individuals to have fewer MSCs and for their harvested MSCs to poorly proliferate and differentiate. MSCs also tend to differentiate to the adipose lineage with decreased SIRT1 expression and age [97]. These factors might explain increasing tissue degeneration diseases (such as osteoporosis, arthritis, and sarcopenia) with aging. SIRT1 activation can protect MSCs from DNA damage, reactive oxygen species, hyperinflammatory, and apoptotic signaling and help them maintain their self-renewal characteristic [98]. The protective role of SIRT1 in MSCs has been demonstrated in ex vivo growth of human MSCs in culture [99] and the in vivo maintenance and function of MSCs in mice [100]. In addition, SIRT1 is responsible for various biological functions besides aging, such as stress responses [101–103].

In actuality, an early study showed reduction of sirtuin protein level and activity with osteoarthritis development [104]. Afterwards, the sirtuin activity and influence in biology were widely studies and it was observed that this protein plays roles in metabolism and heath of articular cartilage. There is evidence that SIRT1 plays a role in regulating cartilage homeostasis [105]. In this regard, chondrocytes from patients with osteoarthritis were harvested and SIRT1 overexpression or activation increased cartilage related gene expression (Collagen II and Aggrecan) [106]. On the other hand, SIRT1 knockout in mice leads to osteoarthritis [107]. Another study of chondrocytes confirmed that SIRT1 inactivation caused hypertrophy and catalytic activity in this type of cell [108].

Although there has not been sufficient study, some evidences demonstrate potential role of SIRT1 in mechanotransduction. Recently, Chen et al. claimed the decrease of reactive oxygen species generation caused by mechanical stretch in skeletal muscle cells was due to upregulation of SIRT1 [109]. Moreover, human periodontal ligament cells expressed immune response genes through the SIRT1 pathway under mechanical stretch [110]. Additionally, mechanical stretch encouraged antioxidant response

and osteogenic differentiation in human MSCs by the activation of the AMPK-SIRT1 signaling pathway [111].

In this chapter, the possible role of SIRT1 in differentiation and HP mechanotransduction of mesenchymal stem cells was investigated. Due to beneficial effect of SIRT1 in MSC differentiation and survival and its response to mechanical stimuli, we hypothesized that SIRT1 is activated in response to cyclic hydrostatic pressure and is necessary for the mechanotransduction of HP and MSC chondrogenesis.

5.2 Materials and Methods

5.2.1 Cell Isolation, Expansion, Encapsulation and Culture

The procedure of seeding 4% agarose gels was done as described in Chapter 2, Part 2.2.1. Briefly, MSCs were harvested from porcine femoral bone marrow and were expanded in for 2 passages. Afterwards, they were seeded in 4% agarose gel at a density of 15 million cells/mL, and scaffolds with dimension ϕ=5mm$\times$3mm thickness were obtained. They were cultured in chondrogenic differentiation medium containing TGF-β3 for 3 weeks. A day before the application of hydrostatic pressure, 0.1 mM SIRT1 inhibitor (EX527, Sigma, St. Louis, MO) was added to the media overnight on the cell-seeded gel constructs. The same volume of DMSO was added to other gels as vehicle control.

5.2.2 Application of Hydrostatic Pressure

As explained in Chapter 4, part 4.2.1, constructs were sealed into sterile bags with 1.5 mL of medium per construct. Cyclic HP was applied in a pressure vessel filled with water within a 37 ^{0}C water bath. The sealed bags exposed to HP were placed into the pressure vessel while the controls were placed into a similar container in water bath next to the pressure vessel. The load applied to the hydraulic cylinder by the MTS was set such that the HP inside the vessel reached an amplitude of 10

MPa at a frequency of 1 Hz, for 4 hours. Immediately after loading, constructs were snap-frozen and stored at -80^{0}C until further analysis.

5.2.3 RNA Isolation and Quantitative Real-time Polymeric Chain Reaction

As described in Chapter 4, part 4.2.3, the total RNA was extracted using TRIzol (Invitrogen) followed by an RNA purification kit. Then 100 ng of RNA for each sample went through reverse transcription and cDNA was obtained. RT-PCR was done with SYBR® Green protocol for aggrecan, Sox9, and collagen II genes with 18s as the housekeeping gene and analyzed with $\Delta\Delta C_T$ method. The primer sequences are found in Table 4.1.

5.2.4 Protein Extraction and Sirtuin Activity Measurement

Snap frozen samples were transferred to 500 μL of DL-Dithiothreitol (DTT; Sigma, 43815) with EDTA solution and protease inhibitor cocktail (Sigma, P8340) and were homogenized for 1 minute for each sample. The blade of the homogenizer was washed with 100 μL of the DTT solution to reach a total volume of 600 μL for each sample. Samples were placed in 4^{0}C for 10-15 minutes while shaking. Then, samples were centrifuged at 16000 g for 20 minutes at 4^{0}C and the supernatant was taken to new tubes. The protein was concentrated with Amicon Ultra Centrifugal Filters (50k) following the manufacturers protocol. The activity of protein was then determined by SIRT1 Assay Kit (Sigma Aldrich, Cat# CS1040) following the protocol provided by the manufacturer.

5.2.5 Statistical Analysis

Biochemical measurement were reported in the form of mean ± standard deviation. Differences between groups were determined using Students t-test (Excel, Microsoft office). A level of $p < 0.05$ was considered significant.

5.2.6 Results

5.2.6.1 Effect of SIRT1 Inhibitor on Gene Expression

First the effect of SIRT1 inhibition on the chondrogenic gene expression was assessed via RT-PCR. Sox9, Agc and Col2 gene expression all increased significantly by application of SIRT1 inhibitor EX527 overnight (Sox9: 79.16 ± 31.13 fold, Agc: 20.83 ± 9.45 fold, Col2: 13.95 ± 5.65 fold) (Figure 5.1).

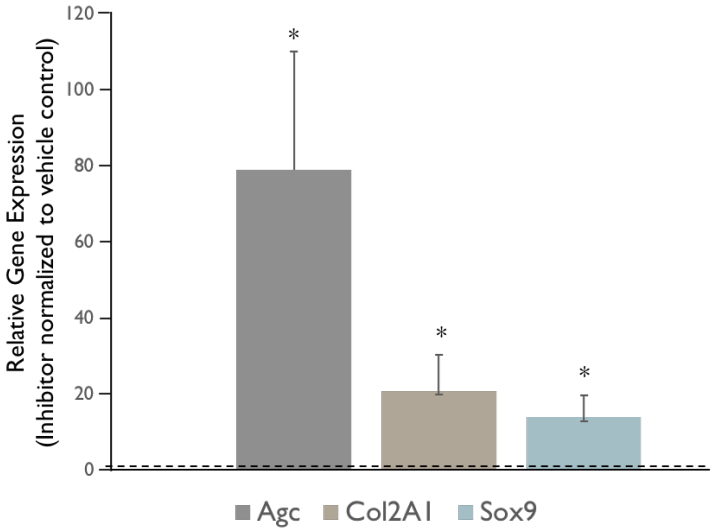

Fig. 5.1.: Agc, Col2, and Sox9 relative gene expression, SIRT1 inhibitor EX527 normalized to the vehicle control. * indicates significant difference between inhibitor group and vehicle control group; $p < 0.05$. Dashed line indicates a normalized value of 1.0 (no difference between treated (inhibitor) and control samples).

5.2.6.2 EX527 and Hydrostatic Pressure Decreasing SIRT1 Activity

SIRT1 activity was measured in cell-seeded gels that were exposed to vehicle control and were either loaded with hydrostatic pressure or were left unloaded. The activity of SIRT1 was decreased by the application of cyclic HP (Figure 5.2).

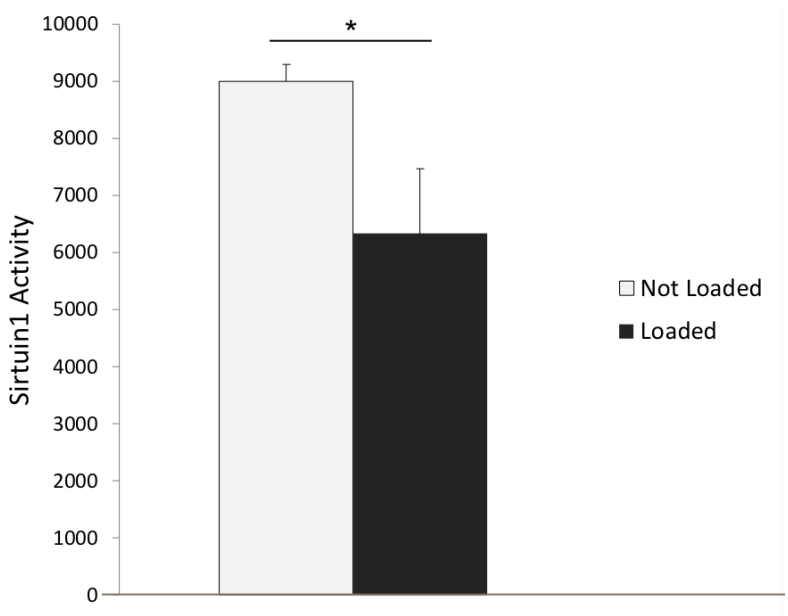

Fig. 5.2.: SIRT1 activity of unloaded and loaded vehicle controls (1 Hz of 10 MPa hydrostatic pressure at 1 Hz for 4 hours on day 21). * indicates significant difference between groups; $p < 0.05$.

To verify that EX527 was effective at inhibiting SIRT1 activity, it was used with the SIRT1 activity kit. The kit was used with purified SIRT1, an inhibitor that was provided with the kit, and EX527. Blank readings were subtracted from readings for each inhibitor. The SIRT1 activity was lower with EX527 than with the kit's inhibitor, suggesting that the EX527 effectively inhibited the SIRT1 enzyme (Figure 5.3).

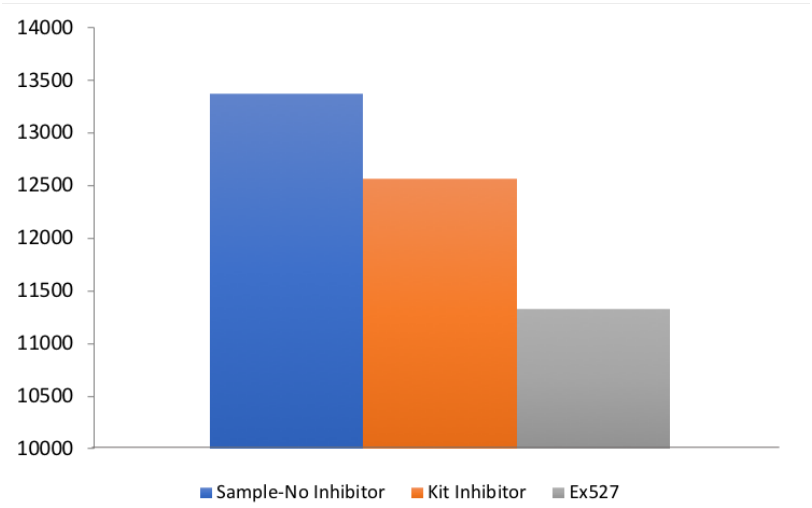

Fig. 5.3.: SIRT1 activity with different inhibitors confirms that EX527 provides sufficient SIRT1 inhibition. Data compared to SIRT1 activity when no inhibitor was used on the sample.

5.2.7 SIRT1 Inhibition Suppressed the Beneficial Effect of Hydrostatic Pressure

As before, cyclic HP increased the expression of the 3 chondrogenic genes that were assessed. The beneficial effect of HP was suppressed in these genes when EX527 was applied to gels overnight (Figure 5.4).

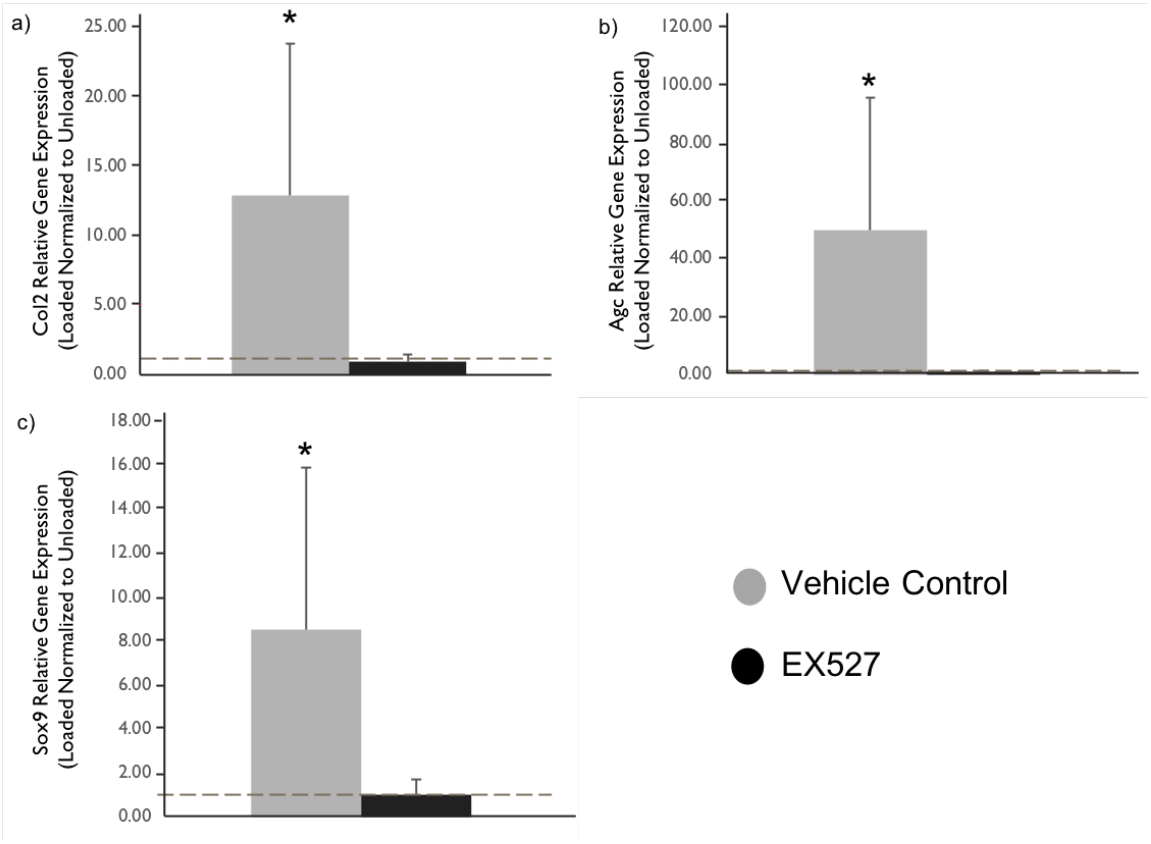

Fig. 5.4.: (a)Col2, (b) Agc, and (c) Sox9 relative gene expression for SIRT1 inhibitor EX527 and vehicle control loaded (10 MPa hydrostatic pressure at 1 Hz for 4 hours on day 21) normalized to the unloaded condition. * indicates a significant difference between loaded and unloaded cell-seeded gels, $p < 0.05$. Dashed line indicates a normalized value of 1.0 (no difference between loaded and unloaded samples).

5.2.8 Discussion

SIRT1 is involved in biological responses such as stress responses, DNA repair and inflammation, differentiation, and survival [101–103,112]. Some data suggest the potential role of SIRT1 in mechanotransduction. However, SIRT1 activity had not been previously studied with HP or with chondrogenic mechanical loading.

The results show that the SIRT1 inhibitor EX527 increased chondrogenic gene expression in mesenchymal stem cells in chondrogenic conditions. Since this was a surprising result, we verified that the inhibitor decreased the SIRT1 activity using purified SIRT1 and the SIRT1 activity kit, and saw that it was effective. This study also confirmed that mechanical loading improves MSCs chondrogenesis, as has been observed previously using various scaffolds [31, 40, 41]. The results also suggest that SIRT1 is involved in hydrostatic pressure mechanotransduction as the SIRT1 activity decreased with HP loading and also the inhibition of SIRT1 suppressed the beneficial effect of HP for chondrogenesis.

Results from our study suggest that SIRT1 inhibition increased chondrogenesis in MSCs, as cells exposed to EX527 demonstrated increased chondrogenic gene expression (Agc, Col2, and Sox9) and the activity of SIRT1 was decreased with both cyclic hydrostatic pressure and EX527 application to MSCs. SIRT1 inhibition appeared to improve chondrogenesis, which is opposite from what had been reported in previous studies. Buhrmann et al. demonstrated that SIRT1 activity enhances chondrogenic differentiation of human MSCs [91]. Other studies demonstrated that SIRT1 overexpression or activation increased cartilage related gene expression (Col2 and Agc) in human chondrocyte [109] or that deletion of SIRT in mice leads to more severe osteoarthritis [107]. On the other hand, it has been shown that sirtuin1 (SIRT1) activity was higher in growth plate endochondral ossification than chondrogenic lineage. Our hypothesis that mechanical load would increase SIRT1 activity and enhance chondrogenesis was not supported by the data. This may due to the short term duration of the inhibition, or to differences in cell types and treatments between the current study and previous reports. The contradictions may reveal new insights for cartilage tissue engineering if the role of SIRT1 is better understood.

6. CONCLUSIONS

The work in this thesis aimed to determine the role of different signaling pathways in the chondrogenic responses of MSCs to HP. Firstly, we tried to image the Ca^{++} signaling response of a single application of HP, as Ca^{++} signaling was previously shown to be involved in the mechanotransduction of HP. The eventual goal of this study was to investigate its relationship with other factors that are involved in HP mechanotrasduction in MSCs. We applied HP for 10 minutes to the cells and saw no change in Ca^{++} concentration. Additionally, we discovered that cell-seeded gels moved during mechanical loading due to deformations in the bioreactor. The magnitude and the cause of the deformation was analyzed, however, there are some other elements that should also be considered as possible sources of deformation.

Moreover, the result from investigating the role of FAK in chondrogenesis showed a differential responses of MSCs to FAK inhibition in early and late stages of chondrogensis. Previous studies from our lab showed a dose-dependent loss of matrix production with increasing concentration of a pharmacological FAK inhibitor in early chondrogenesis. In this study the matrix production with FAK inhibition during late chondrogenesis was investigated; some differences were shown in matrix production between early and late chondrogenesis. Additionally, FAK phosphorylation increased with 10 MPa of cyclic HP loading for 4 hours, and the inhibition of FAK suppressed the increase in chondrogenic gene expression with loading. These results suggesting the FAK signaling is important for MSCs mechanotransduction. For further study, some improvements are needed for different result to be consistent. Moreover, the study should be done using more donors to verify the results.

Another part of our study explored SIRT1 involvement in MSC chondrogenesis. Firstly, the chondrogenic gene expression increased when a SIRT1 inhibitor was used overnight on MSCs. Secondly, SIRT1 activity decreased with a beneficial chondro-

genic load of 10 MPa of cyclic HP for 4 hours. These two results suggest that SIRT1 inhibition could enhance chondrogenesis. In other studies in the literature, SIRT1 was shown to be necessary for chondrogenesis, and to be important for cartilage homeostasis. This discrepancy between published reports and our results may be due to differences in cell type or the duration of SIRT1 inhibition. Additionally, SIRT1 inhibition suppressed the beneficial effect of HP in chondrogenic gene expression, implicating SIRT1 involvement in HP mechanotransduction. Exploring the contradictions between studies may lead to new insights into SIRT1 activity in chondrogenesis. Further investigation is needed about the relation of sirtuin1 inhibition and its activity with mechanical stimuli.

In conclusion, the results from this study help explain the role of different factors such as Ca^{++}, FAK, and sirtuin1 in cyclic HP mechanotransduction by MSCs (Figure 6.1). Understanding and investigating the relation between these different factors could be the goal of future studies. Additionally, the duration of loading might be important for the activity and expression of these factors and could be the subject of additional studies. Moreover, our study used the inhibitors overnight and more study could be done about the difference between overnight application and long-term application of sirtuin1 inhibitor on cells. If the biochemical pathway of MSC mechanotransduction is clarified, it could serve as a guideline for improving current cartilage tissue engineering strategies.

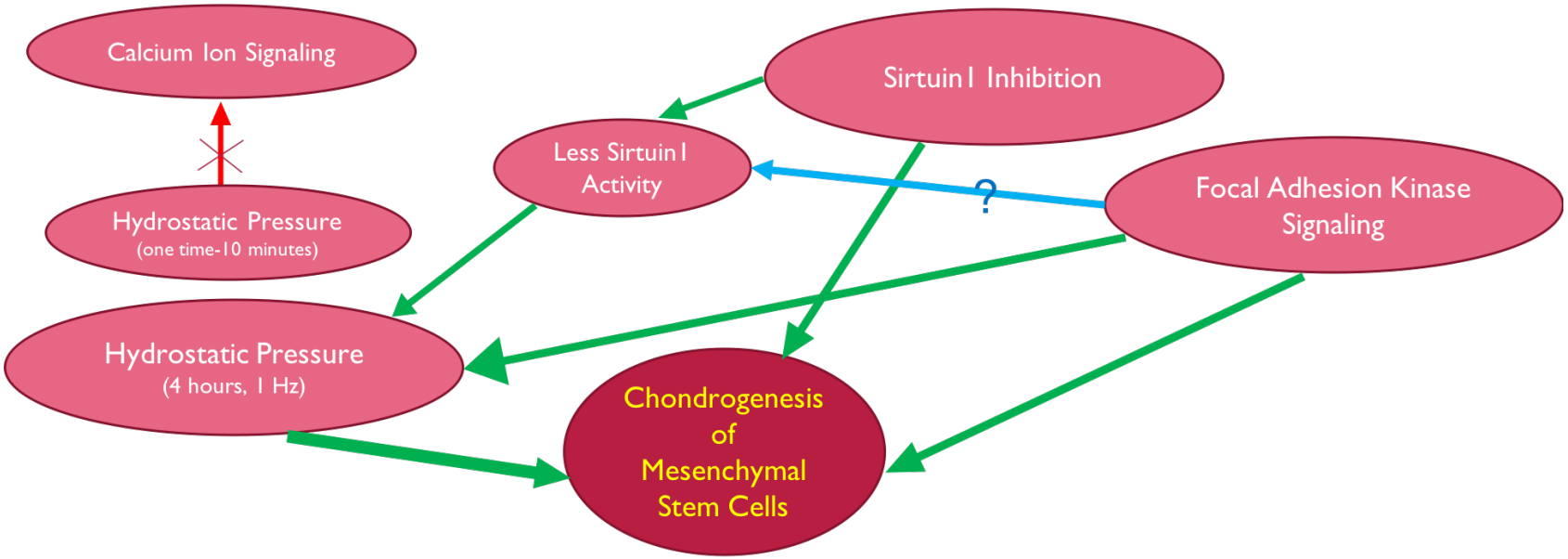

Fig. 6.1.: Relations between chondrogenesis, hydrostatic pressure and different biochemical factors.

LIST OF REFERENCES

LIST OF REFERENCES

[1] F. Eckstein, M. Reiser, K.-H. Englmeier, and R. Putz, "In vivo morphometry and functional analysis of human articular cartilage with quantitative magnetic resonance imagingfrom image to data, from data to theory," *Anatomy and embryology*, vol. 203, no. 3, pp. 147–173, 2001.

[2] J. Buckwalter, "Articular cartilage: composition and structure," *Injury and repair of the musculoskeletal soft tissues*, 1991.

[3] J. S. Temenoff and A. G. Mikos, "Tissue engineering for regeneration of articular cartilage," *Biomaterials*, vol. 21, no. 5, pp. 431–440, 2000.

[4] D. J. Responte, R. M. Natoli, and K. A. Athanasiou, "Collagens of articular cartilage: structure, function, and importance in tissue engineering," *Critical Reviews in Biomedical Engineering*, vol. 35, no. 5, 2007.

[5] F. Guilak, L. G. Alexopoulos, M. L. Upton, I. Youn, J. B. Choi, L. Cao, L. A. Setton, and M. A. Haider, "The pericellular matrix as a transducer of biomechanical and biochemical signals in articular cartilage," *Annals of the New York Academy of Sciences*, vol. 1068, no. 1, pp. 498–512, 2006.

[6] M. Schwartz, P. Leo, and J. Lewis, "A microstructural model for the elastic response of articular cartilage," *Journal of biomechanics*, vol. 27, no. 7, pp. 865–873, 1994.

[7] L. Zhang, J. Hu, and K. A. Athanasiou, "The role of tissue engineering in articular cartilage repair and regeneration," *Critical Reviews in Biomedical Engineering*, vol. 37, no. 1-2, 2009.

[8] J. Hu, "Chondrocyte self-assembly and culture in bioreactors," Thesis, 2005.

[9] M. Wong, P. Wuethrich, P. Eggli, and E. Hunziker, "Zone-specific cell biosynthetic activity in mature bovine articular cartilage: a new method using confocal microscopic stereology and quantitative autoradiography," *Journal of Orthopaedic Research*, vol. 14, no. 3, pp. 424–432, 1996.

[10] A. M. Bhosale and J. B. Richardson, "Articular cartilage: structure, injuries and review of management," *British medical bulletin*, vol. 87, no. 1, pp. 77–95, 2008.

[11] F. T. Moutos and F. Guilak, "Functional properties of cell-seeded three-dimensionally woven poly (ε-caprolactone) scaffolds for cartilage tissue engineering," *Tissue Engineering Part A*, vol. 16, no. 4, pp. 1291–1301, 2009.

[12] S. Akizuki, V. C. Mow, F. Mller, J. C. Pita, D. S. Howell, and D. H. Manicourt, "Tensile properties of human knee joint cartilage: I. influence of ionic conditions, weight bearing, and fibrillation on the tensile modulus," *Journal of Orthopaedic Research*, vol. 4, no. 4, pp. 379–392, 1986.

[13] E. B. Hunziker, "Articular cartilage repair: are the intrinsic biological constraints undermining this process insuperable?" *Osteoarthritis and Cartilage*, vol. 7, no. 1, pp. 15–28, 1999.

[14] A. I. Caplan, M. Elyaderani, Y. Mochizuki, S. Wakitani, and V. M. Goldberg, "Principles of cartilage repair and regeneration," *Clinical orthopaedics and related research*, no. 342, pp. 254–269, 1997.

[15] L. Zhang and T. J. Webster, "Nanotechnology and nanomaterials: promises for improved tissue regeneration," *Nano today*, vol. 4, no. 1, pp. 66–80, 2009.

[16] B. L. Clair, A. R. Johnson, and T. Howard, "Cartilage repair: current and emerging options in treatment," *Foot ankle specialist*, vol. 2, no. 4, pp. 179–188, 2009.

[17] R. Bergman, D. Gazit, A. Kahn, H. Gruber, S. McDougall, and T. Hahn, "Agerelated changes in osteogenic stem cells in mice," *Journal of Bone and Mineral Research*, vol. 11, no. 5, pp. 568–577, 1996.

[18] C. T. Laurencin, A. Ambrosio, M. Borden, and J. Cooper Jr, "Tissue engineering: orthopedic applications," *Annual review of biomedical engineering*, vol. 1, no. 1, pp. 19–46, 1999.

[19] A. Getgood, R. Brooks, L. Fortier, and N. Rushton, "Articular cartilage tissue engineering: todays research, tomorrows practice?" *The Journal of bone and joint surgery. British volume*, vol. 91, no. 5, pp. 565–576, 2009.

[20] K. Bobacz, L. Erlacher, J. Smolen, A. Soleiman, and W. Graninger, "Chondrocyte number and proteoglycan synthesis in the aging and osteoarthritic human articular cartilage," *Annals of the rheumatic diseases*, vol. 63, no. 12, pp. 1618–1622, 2004.

[21] K. A. Athanasiou, E. M. Darling, and J. C. Hu, "Articular cartilage tissue engineering," *Synthesis Lectures on Tissue Engineering*, vol. 1, no. 1, pp. 1–182, 2009.

[22] H. Koga, L. Engebretsen, J. E. Brinchmann, T. Muneta, and I. Sekiya, "Mesenchymal stem cell-based therapy for cartilage repair: a review," *Knee Surgery, Sports Traumatology, Arthroscopy*, vol. 17, no. 11, pp. 1289–1297, 2009.

[23] B. A. Ashton, T. D. Allen, C. Howlett, C. Eaglesom, A. Hattori, and M. Owen, "Formation of bone and cartilage by marrow stromal cells in diffusion chambers in vivo," *Clinical orthopaedics and related research*, no. 151, pp. 294–307, 1980.

[24] K. Miyanishi, M. C. Trindade, D. P. Lindsey, G. S. Beaupr, D. R. Carter, S. B. Goodman, D. J. Schurman, and R. L. Smith, "Effects of hydrostatic pressure and transforming growth factor- 3 on adult human mesenchymal stem cell chondrogenesis in vitro," *Tissue Engineering*, vol. 12, no. 6, pp. 1419–1428, 2006.

[25] H. A. Awad, M. Q. Wickham, H. A. Leddy, J. M. Gimble, and F. Guilak, "Chondrogenic differentiation of adipose-derived adult stem cells in agarose, alginate, and gelatin scaffolds," *Biomaterials*, vol. 25, no. 16, pp. 3211–3222, 2004.

[26] S. Wakitani, K. Imoto, T. Yamamoto, M. Saito, N. Murata, and M. Yoneda, "Human autologous culture expanded bone marrow mesenchymal cell transplantation for repair of cartilage defects in osteoarthritic knees," *Osteoarthritis and Cartilage*, vol. 10, no. 3, pp. 199–206, 2002.

[27] E. J. Koay, G. M. Hoben, and K. A. Athanasiou, "Tissue engineering with chondrogenically differentiated human embryonic stem cells," *Stem cells*, vol. 25, no. 9, pp. 2183–2190, 2007.

[28] S. Mizuno and J. Glowacki, "Low oxygen tension enhances chondroinduction by demineralized bone matrix in human dermal fibroblasts in vitro," *Cells Tissues Organs*, vol. 180, no. 3, pp. 151–158, 2005.

[29] B. Grigolo, L. Roseti, M. Fiorini, M. Fini, G. Giavaresi, N. N. Aldini, R. Giardino, and A. Facchini, "Transplantation of chondrocytes seeded on a hyaluronan derivative (hyaff-11) into cartilage defects in rabbits," *Biomaterials*, vol. 22, no. 17, pp. 2417–2424, 2001.

[30] C. L. Murphy and A. Sambanis, "Effect of oxygen tension and alginate encapsulation on restoration of the differentiated phenotype of passaged chondrocytes," *Tissue engineering*, vol. 7, no. 6, pp. 791–803, 2001.

[31] A. J. Steward, D. R. Wagner, and D. J. Kelly, "The pericellular environment regulates cytoskeletal development and the differentiation of mesenchymal stem cells and determines their response to hydrostatic pressure," *Eur Cell Mater*, vol. 25, pp. 167–178, 2013.

[32] C. N. Salinas and K. S. Anseth, "The enhancement of chondrogenic differentiation of human mesenchymal stem cells by enzymatically regulated rgd functionalities," *Biomaterials*, vol. 29, no. 15, pp. 2370–2377, 2008. [Online]. Available: http://www.sciencedirect.com/science/article/pii/S0142961208000616

[33] C. G. Williams, T. K. Kim, A. Taboas, A. Malik, P. Manson, and J. Elisseeff, "In vitro chondrogenesis of bone marrow-derived mesenchymal stem cells in a photopolymerizing hydrogel," *Tissue engineering*, vol. 9, no. 4, pp. 679–688, 2003.

[34] S. J. Bryant and K. S. Anseth, "Hydrogel properties influence ecm production by chondrocytes photoencapsulated in poly (ethylene glycol) hydrogels," *Journal of Biomedical Materials Research: An Official Journal of The Society for Biomaterials and The Japanese Society for Biomaterials*, vol. 59, no. 1, pp. 63–72, 2002.

[35] A. J. Steward, *The mechanotransduction of hydrostatic pressure by mesenchymal stem cells*. University of Notre Dame, 2014.

[36] D. Shin, J. Lin, C. Agrawal, and K. Athanasiou, "Zonal variations in microindentation properties of articular cartilage," in *TRANSACTIONS OF THE ANNUAL MEETING-ORTHOPAEDIC RESEARCH SOCIETY*. ORTHOPAEDIC RESEARCH SCOIETY, Conference Proceedings, pp. 903–903.

[37] R. M. Schinagl, D. Gurskis, A. C. Chen, and R. L. Sah, "Depthdependent confined compression modulus of fullthickness bovine articular cartilage," *Journal of Orthopaedic Research*, vol. 15, no. 4, pp. 499–506, 1997.

[38] K. Athanasiou, A. Agarwal, and F. Dzida, "Comparative study of the intrinsic mechanical properties of the human acetabular and femoral head cartilage," *Journal of Orthopaedic Research*, vol. 12, no. 3, pp. 340–349, 1994.

[39] A. C. Hall, E. R. Horwitz, and R. J. Wilkins, "The cellular physiology of articular cartilage," *Experimental Physiology*, vol. 81, no. 3, pp. 535–545, 1996.

[40] B. D. Elder and K. A. Athanasiou, "Synergistic and additive effects of hydrostatic pressure and growth factors on tissue formation," *PloS one*, vol. 3, no. 6, p. e2341, 2008.

[41] P. Angele, J. Yoo, C. Smith, J. Mansour, K. Jepsen, M. Nerlich, and B. Johnstone, "Cyclic hydrostatic pressure enhances the chondrogenic phenotype of human mesenchymal progenitor cells differentiated in vitro," *Journal of Orthopaedic Research*, vol. 21, no. 3, pp. 451–457, 2003.

[42] B. D. Elder and K. A. Athanasiou, "Hydrostatic pressure in articular cartilage tissue engineering: from chondrocytes to tissue regeneration," *Tissue Engineering Part B: Reviews*, vol. 15, no. 1, pp. 43–53, 2009.

[43] R. L. Smith, S. Rusk, B. Ellison, P. Wessells, K. Tsuchiya, D. Carter, W. Caler, L. Sandell, and D. Schurman, "In vitro stimulation of articular chondrocyte mrna and extracellular matrix synthesis by hydrostatic pressure," *Journal of orthopaedic research*, vol. 14, no. 1, pp. 53–60, 1996.

[44] J. Parkkinen, J. Ikonen, M. Lammi, J. Laakkonen, M. Tammi, and H. Helminen, "Effects of cyclic hydrostatic pressure on proteoglycan synthesis in cultured chondrocytes and articular cartilage explants," *Archives of biochemistry and biophysics*, vol. 300, no. 1, pp. 458–465, 1993.

[45] M. J. Lammi, R. Inkinen, J. Parkkinen, T. Hkkinen, M. Jortikka, L. Nelimarkka, H. Jrvelinen, and M. Tammi, "Expression of reduced amounts of structurally altered aggrecan in articular cartilage chondrocytes exposed to high hydrostatic pressure," *Biochemical Journal*, vol. 304, no. 3, pp. 723–730, 1994.

[46] B. Bourns, S. Franklin, L. Cassimeris, and E. Salmon, "High hydrostatic pressure effects in vivo: changes in cell morphology, microtubule assembly, and actin organization," *Cell motility and the cytoskeleton*, vol. 10, no. 3, pp. 380–390, 1988.

[47] J. Browning, K. Saunders, J. Urban, and R. Wilkins, "The influence and interactions of hydrostatic and osmotic pressures on the intracellular milieu of chondrocytes," *Biorheology*, vol. 41, no. 3-4, pp. 299–308, 2004.

[48] J. Browning, R. Walker, A. Hall, and R. Wilkins, "Modulation of na+ x h+ exchange by hydrostatic pressure in isolated bovine articular chondrocytes," *Acta physiologica scandinavica*, vol. 166, no. 1, pp. 39–45, 1999.

[49] S. Mizuno, "A novel method for assessing effects of hydrostatic fluid pressure on intracellular calcium: a study with bovine articular chondrocytes," *American Journal of Physiology-Cell Physiology*, vol. 288, no. 2, pp. C329–C337, 2005.

[50] A. J. Steward, D. J. Kelly, and D. R. Wagner, "Purinergic signaling regulates the transforming growth factor-3-induced chondrogenic response of mesenchymal stem cells to hydrostatic pressure," *Tissue Engineering Part A*, vol. 22, no. 11-12, pp. 831–839, 2016.

[51] A. J. Steward, D. R. Wagner, and D. J. Kelly, "Exploring the roles of integrin binding and cytoskeletal reorganization during mesenchymal stem cell mechanotransduction in soft and stiff hydrogels subjected to dynamic compression," *Journal of the mechanical behavior of biomedical materials*, vol. 38, pp. 174–182, 2014.

[52] E. G. Lima, L. Bian, K. W. Ng, R. L. Mauck, B. A. Byers, R. S. Tuan, G. A. Ateshian, and C. T. Hung, "The beneficial effect of delayed compressive loading on tissue-engineered cartilage constructs cultured with tgf-3," *Osteoarthritis and cartilage*, vol. 15, no. 9, pp. 1025–1033, 2007.

[53] A. Joukar, H. Niroomand-Oscuii, and F. Ghalichi, "Numerical simulation of osteocyte cell in response to directional mechanical loadings and mechanotransduction analysis: Considering lacunar–canalicular interstitial fluid flow," *Computer methods and programs in biomedicine*, vol. 133, pp. 133–141, 2016.

[54] C. Zhu, G. Bao, and N. Wang, "Cell mechanics: mechanical response, cell adhesion, and molecular deformation," *Annual review of biomedical engineering*, vol. 2, no. 1, pp. 189–226, 2000.

[55] A. Katsumi, A. W. Orr, E. Tzima, and M. A. Schwartz, "Integrins in mechanotransduction," *Journal of Biological Chemistry*, vol. 279, no. 13, pp. 12 001–12 004, 2004.

[56] R. F. Loeser, "Integrins and cell signaling in chondrocytes," *Biorheology*, vol. 39, no. 1, 2, pp. 119–124, 2002.

[57] C. Matta, J. Fodor, Z. Szíjgyártó, T. Juhász, P. Gergely, L. Csernoch, and R. Zákány, "Cytosolic free ca2+ concentration exhibits a characteristic temporal pattern during in vitro cartilage differentiation: a possible regulatory role of calcineurin in ca-signalling of chondrogenic cells," *Cell calcium*, vol. 44, no. 3, pp. 310–323, 2008.

[58] D. Chin and A. R. Means, "Calmodulin: a prototypical calcium sensor," *Trends in cell biology*, vol. 10, no. 8, pp. 322–328, 2000.

[59] I. S. Han, S. Lew, and M. H. Han, "Photometric glucose measurement system using glucose-sensitive hydrogel," Dec. 28 2004, uS Patent 6,835,553.

[60] M. Tomita, M. I. Reinhold, J. D. Molkentin, and M. C. Naski, "Calcineurin and nfat4 induce chondrogenesis," *Journal of Biological Chemistry*, vol. 277, no. 44, pp. 42 214–42 218, 2002.

[61] R. Zákány, Z. Szíjgyártó, C. Matta, T. Juhász, C. Csortos, K. Szűcs, G. Czifra, T. Bíró, L. Módis, and P. Gergely, "Hydrogen peroxide inhibits formation of cartilage in chicken micromass cultures and decreases the activity of calcineurin: implication of erk1/2 and sox9 pathways," *Experimental cell research*, vol. 305, no. 1, pp. 190–199, 2005.

[62] L. A. McMahon, V. A. Campbell, and P. J. Prendergast, "Involvement of stretch-activated ion channels in strain-regulated glycosaminoglycan synthesis in mesenchymal stem cell-seeded 3d scaffolds," *Journal of biomechanics*, vol. 41, no. 9, pp. 2055–2059, 2008.

[63] R. C. Riddle, A. F. Taylor, D. C. Genetos, and H. J. Donahue, "Map kinase and calcium signaling mediate fluid flow-induced human mesenchymal stem cell proliferation," *American Journal of Physiology-Cell Physiology*, vol. 290, no. 3, pp. C776–C784, 2006.

[64] R. K. Jaiswal, N. Jaiswal, S. P. Bruder, G. Mbalaviele, D. R. Marshak, and M. F. Pittenger, "Adult human mesenchymal stem cell differentiation to the osteogenic or adipogenic lineage is regulated by mitogen-activated protein kinase," *Journal of Biological Chemistry*, vol. 275, no. 13, pp. 9645–9652, 2000.

[65] Y. J. Li, N. N. Batra, L. You, S. C. Meier, I. A. Coe, C. E. Yellowley, and C. R. Jacobs, "Oscillatory fluid flow affects human marrow stromal cell proliferation and differentiation," *Journal of Orthopaedic Research*, vol. 22, no. 6, pp. 1283–1289, 2004.

[66] Q.-q. Wu and Q. Chen, "Mechanoregulation of chondrocyte proliferation, maturation, and hypertrophy: ion-channel dependent transduction of matrix deformation signals," *Experimental cell research*, vol. 256, no. 2, pp. 383–391, 2000.

[67] S. R. Roberts, M. M. Knight, D. A. Lee, and D. L. Bader, "Mechanical compression influences intracellular ca2+ signaling in chondrocytes seeded in agarose constructs," *Journal of applied physiology*, vol. 90, no. 4, pp. 1385–1391, 2001.

[68] B. D. Idowu, M. M. Knight, D. L. Bader, and D. A. Lee, "Confocal analysis of cytoskeletal organisation within isolated chondrocyte sub-populations cultured in agarose," *The Histochemical journal*, vol. 32, no. 3, pp. 165–174, 2000.

[69] K. L. Ryan, J. A. D'andrea, J. R. Jauchem, and P. A. Mason, "Radio frequency radiation of millimeter wave length: potential occupational safety issues relating to surface heating." *Health physics*, vol. 78, no. 2, pp. 170–181, 2000.

[70] D. R. Wagner, D. P. Lindsey, K. W. Li, P. Tummala, S. E. Chandran, R. L. Smith, M. T. Longaker, D. R. Carter, and G. S. Beaupre, "Hydrostatic pressure enhances chondrogenic differentiation of human bone marrow stromal cells in osteochondrogenic medium," *Annals of biomedical engineering*, vol. 36, no. 5, pp. 813–820, 2008.

[71] J. Schindelin, I. Arganda-Carreras, E. Frise, V. Kaynig, M. Longair, T. Pietzsch, S. Preibisch, C. Rueden, S. Saalfeld, and B. Schmid, "Fiji: an open-source platform for biological-image analysis," *Nature methods*, vol. 9, no. 7, p. 676, 2012.

[72] B. PingguanMurphy, M. ElAzzeh, D. Bader, and M. Knight, "Cyclic compression of chondrocytes modulates a purinergic calcium signalling pathway in a strain rateand frequencydependent manner," *Journal of cellular physiology*, vol. 209, no. 2, pp. 389–397, 2006.

[73] C. E. Yellowley, C. R. Jacobs, and H. J. Donahue, "Mechanisms contributing to fluidflowinduced ca2+ mobilization in articular chondrocytes," *Journal of cellular physiology*, vol. 180, no. 3, pp. 402–408, 1999.

[74] W. B. Valhmu, "myo-inositol 1, 4, 5-trisphosphate and ca2+/calmodulin-dependent factors mediate transduction of compression-induced signals in bovine articular chondrocytes," *Biochemical Journal*, vol. 361, no. 3, pp. 689–696, 2002.

[75] A. Mobasheri, S. Carter, P. MartinVasallo, and M. Shakibaei, "Integrins and stretch activated ion channels; putative components of functional cell surface mechanoreceptors in articular chondrocytes," *Cell biology international*, vol. 26, no. 1, pp. 1–18, 2002.

[76] P.-h. G. Chao, A. C. West, and C. T. Hung, "Chondrocyte intracellular calcium, cytoskeletal organization, and gene expression responses to dynamic osmotic loading," *American Journal of Physiology-Cell Physiology*, vol. 291, no. 4, pp. C718–C725, 2006.

[77] J. Campbell, D. Bader, and D. Lee, "Mechanical loading modulates intracellular calcium signaling in human mesenchymal stem cells," *Journal of Applied Biomaterials and Biomechanics*, vol. 6, no. 1, pp. 9–15, 2008.

[78] H. Cease, P. Derwent, H. Diehl, J. Fast, and D. Finley, "Measurement of mechanical properties of three epoxy adhesives at cryogenic temperatures for ccd construction," *Fermi National Accelerator Laboratory*, 2006.

[79] D. Ward, W. A. Williams, N. E. Schapiro, S. R. Christy, G. L. Weber, M. Salt, R. F. Klees, A. Boskey, and G. E. Plopper, "Focal adhesion kinase signaling controls cyclic tensile strain enhanced collagen i-induced osteogenic differentiation of human mesenchymal stem cells," *Molecular and Cellular Biomechanics*, vol. 4, no. 4, p. 177, 2007.

[80] R. M. Salasznyk, R. F. Klees, W. A. Williams, A. Boskey, and G. E. Plopper, "Focal adhesion kinase signaling pathways regulate the osteogenic differentiation of human mesenchymal stem cells," *Experimental Cell Research*, vol. 313, no. 1, pp. 22–37, 2007. [Online]. Available: http://www.sciencedirect.com/science/article/pii/S0014482706003958

[81] M. Suzawa, Y. Tamura, S. Fukumoto, K. Miyazono, T. Fujita, S. Kato, and Y. Takeuchi, "Stimulation of smad1 transcriptional activity by rasextracellular signalregulated kinase pathway: a possible mechanism for collagendependent osteoblastic differentiation," *Journal of Bone and Mineral Research*, vol. 17, no. 2, pp. 240–248, 2002.

[82] A. J. Steward, Y. Liu, and D. R. J. J. Wagner, "Engineering cell attachments to scaffolds in cartilage tissue engineering," vol. 63, no. 4, pp. 74–82, 2011.

[83] J. T. Connelly, A. J. Garca, and M. E. Levenston, "Inhibition of in vitro chondrogenesis in rgd-modified three-dimensional alginate gels," *Biomaterials*, vol. 28, no. 6, pp. 1071–1083, 2007.

[84] D. Pala, M. Kapoor, A. Woods, L. Kennedy, S. Liu, S. Chen, L. Bursell, K. M. Lyons, D. E. Carter, and F. Beier, "Focal adhesion kinase/src suppresses early chondrogenesis central role of ccn2," *Journal of Biological Chemistry*, vol. 283, no. 14, pp. 9239–9247, 2008.

[85] Y. H. Kim and J. W. Lee, "Targeting of focal adhesion kinase by small interfering rnas reduces chondrocyte redifferentiation capacity in alginate beads culture with type ii collagen," *Journal of cellular physiology*, vol. 218, no. 3, pp. 623–630, 2009.

[86] S. Li, M. Kim, Y.-L. Hu, S. Jalali, D. D. Schlaepfer, T. Hunter, S. Chien, and J. Y. J. J. o. B. C. Shyy, "Fluid shear stress activation of focal adhesion kinase linking to mitogen-activated protein kinases," vol. 272, no. 48, pp. 30 455–30 462, 1997.

[87] S. R. Young, R. GerardO'Riley, J. Kim, F. M. J. J. o. b. Pavalko, and m. research, "Focal adhesion kinase is important for fluid shear stressinduced mechanotransduction in osteoblasts," vol. 24, no. 3, pp. 411–424, 2009.

[88] H.-B. Wang, M. Dembo, S. K. Hanks, and Y.-l. Wang, "Focal adhesion kinase is involved in mechanosensing during fibroblast migration," *Proceedings of the National Academy of Sciences*, vol. 98, no. 20, pp. 11 295–11 300, 2001.

[89] R. McBeath, D. M. Pirone, C. M. Nelson, K. Bhadriraju, and C. S. Chen, "Cell shape, cytoskeletal tension, and rhoa regulate stem cell lineage commitment," *Developmental cell*, vol. 6, no. 4, pp. 483–495, 2004.

[90] M. D. Knutson and C. Leeuwenburgh, "Resveratrol and novel potent activators of sirt1: effects on aging and age-related diseases," *Nutrition reviews*, vol. 66, no. 10, pp. 591–596, 2008.

[91] C. Buhrmann, F. Busch, P. Shayan, and M. Shakibaei, "Sirtuin-1 (sirt1) is required for promoting chondrogenic differentiation of mesenchymal stem cells," *Journal of Biological Chemistry*, pp. jbc–M114, 2014.

[92] S. Gautam, Y. Xu, M. Dumaguin, N. Janakiraman, and R. Chapman, "Resveratrol selectively inhibits leukemia cells: a prospective agent for ex vivo bone marrow purging," *Bone marrow transplantation*, vol. 25, no. 6, p. 639, 2000.

[93] Y.-J. Surh, Y.-J. Hurh, J.-Y. Kang, E. Lee, G. Kong, and S. J. Lee, "Resveratrol, an antioxidant present in red wine, induces apoptosis in human promyelocytic leukemia (hl-60) cells," *Cancer letters*, vol. 140, no. 1-2, pp. 1–10, 1999.

[94] M. Tsan, J. E. White, J. G. Maheshwari, T. A. Bremner, and J. Sacco, "Resveratrol induces fas signallingindependent apoptosis in thp1 human monocytic leukaemia cells," *British journal of haematology*, vol. 109, no. 2, pp. 405–412, 2000.

[95] M. Dvir-Ginzberg, A. Mobasheri, and A. Kumar, "The role of sirtuins in cartilage homeostasis and osteoarthritis," *Current rheumatology reports*, vol. 18, no. 7, p. 43, 2016.

[96] K. Zainabadi, "The variable role of sirt1 in the maintenance and differentiation of mesenchymal stem cells," *Regenerative medicine*, vol. 13, no. 3, pp. 343–356, 2018.

[97] S. Zhou, J. S. Greenberger, M. W. Epperly, J. P. Goff, C. Adler, M. S. LeBoff, and J. Glowacki, "Agerelated intrinsic changes in human bonemarrowderived mesenchymal stem cells and their differentiation to osteoblasts," *Aging cell*, vol. 7, no. 3, pp. 335–343, 2008.

[98] C. Ma, C. Pi, Y. Yang, L. Lin, Y. Shi, Y. Li, Y. Li, and X. He, "Nampt expression decreases age-related senescence in rat bone marrow mesenchymal stem cells by targeting sirt1," *PloS one*, vol. 12, no. 1, p. e0170930, 2017.

[99] H.-F. Yuan, C. Zhai, X.-L. Yan, D.-D. Zhao, J.-X. Wang, Q. Zeng, L. Chen, X. Nan, L.-J. He, and S.-T. Li, "Sirt1 is required for long-term growth of human mesenchymal stem cells," *Journal of molecular medicine*, vol. 90, no. 4, pp. 389–400, 2012.

[100] P. Simic, K. Zainabadi, E. Bell, D. B. Sykes, B. Saez, S. Lotinun, R. Baron, D. Scadden, E. Schipani, and L. Guarente, "Sirt1 regulates differentiation of mesenchymal stem cells by deacetylating catenin," *EMBO molecular medicine*, vol. 5, no. 3, pp. 430–440, 2013.

[101] F. Liang, S. Kume, and D. Koya, "Sirt1 and insulin resistance," *Nature Reviews Endocrinology*, vol. 5, no. 7, p. 367, 2009.

[102] M. C. Haigis and D. A. Sinclair, "Mammalian sirtuins: biological insights and disease relevance," *Annual Review of Pathological Mechanical Disease*, vol. 5, pp. 253–295, 2010.

[103] G. Blander and L. Guarente, "The sir2 family of protein deacetylases," *Annual review of biochemistry*, vol. 73, no. 1, pp. 417–435, 2004.

[104] I. Peytremann-Bridevaux, D. Faeh, and B. Santos-Eggimann, "Prevalence of overweight and obesity in rural and urban settings of 10 european countries," *Preventive medicine*, vol. 44, no. 5, pp. 442–446, 2007.

[105] X. Kang, W. Yang, R. Wang, T. Xie, H. Li, D. Feng, X. Jin, H. Sun, and S. Wu, "Sirtuin-1 (sirt1) stimulates growth plate chondrogenesis by attenuating the perk-eif-2-chop pathway in the unfolded protein response," *Journal of Biological Chemistry*, p. jbc. M117. 809822, 2018.

[106] M. Dvir-Ginzberg, V. Gagarina, E.-J. Lee, and D. J. Hall, "Regulation of cartilage-specific gene expression in human chondrocytes by sirt1 and nicotinamide phosphoribosyltransferase," *Journal of Biological Chemistry*, vol. 283, no. 52, pp. 36 300–36 310, 2008.

[107] T. Matsuzaki, T. Matsushita, K. Takayama, T. Matsumoto, K. Nishida, R. Kuroda, and M. Kurosaka, "Disruption of sirt1 in chondrocytes causes accelerated progression of osteoarthritis under mechanical stress and during ageing in mice," *Annals of the rheumatic diseases*, vol. 73, no. 7, pp. 1397–1404, 2014.

[108] N. Fujita, T. Matsushita, K. Ishida, S. Kubo, T. Matsumoto, K. Takayama, M. Kurosaka, and R. Kuroda, "Potential involvement of sirt1 in the pathogenesis of osteoarthritis through the modulation of chondrocyte gene expressions," *Journal of Orthopaedic Research*, vol. 29, no. 4, pp. 511–515, 2011.

[109] X. Chen, J. Yan, F. He, D. Zhong, H. Yang, M. Pei, and Z.-P. Luo, "Mechanical stretch induces antioxidant responses and osteogenic differentiation in human mesenchymal stem cells through activation of the ampk-sirt1 signaling pathway," *J Free Radical Biology and Medicine*, vol. 126, pp. 187–201, 2018.

[110] S. Lee, K. Park, S. Kim, Y. Kang, Y. Lee, and E. Kim, "Mechanical stressactivated immune response genes via sirtuin 1 expression in human periodontal ligament cells," *Clinical and Immunology, Experimental*, vol. 168, no. 1, pp. 113–124, 2012.

[111] H.-C. Chen, L.-Y. Sung, W.-H. Lo, C.-K. Chuang, Y.-H. Wang, J.-L. Lin, and Y.-C. Hu, "Combination of baculovirus-expressed bmp-2 and rotating-shaft bioreactor culture synergistically enhances cartilage formation," *Gene therapy*, vol. 15, no. 4, p. 309, 2008.

[112] A. A. Sauve, C. Wolberger, V. L. Schramm, and J. D. Boeke, "The biochemistry of sirtuins," *Annu. Rev. Biochem.*, vol. 75, pp. 435–465, 2006.

APPENDICES

A. MATLAB CODE TO RECOGNIZE PEAKS IN DATA

This MATLAB Script is developed for recognizing peaks and determining their duration and amplitude in Fluorescent intensity-time Graphs.

```
clear;
clc;
IU1 = xlsread('DATAcopy.xlsx','sheet1');\%intensity of the cell1
IU2 = xlsread('DATA.xlsx','sheet2');\%intensity of the cell2
IU3 = xlsread('DATA.xlsx','sheet3');\%intensity of the cell3
IU4 = xlsread('DATA.xlsx','sheet4');\%intensity of the cell4
time = xlsread('DATAcopy.xlsx','sheet5');\%time
tao=1100/110;\%tao=real time of experiment(sec)/pics created by Fiji

duration = [];
amplitude = [];
start = [];
finish = [];

\%Cell\#1 analysis
for i=1:size(IU1,1)-1\%number of data
    IU1dif(:,i)=IU1(i+1)-IU1(i);
end

M1=abs(IU1dif);
avg1=mean(M1); \%avg of subtraction of IU(i+1)-IU(i)
```

```
std1=std(M1);
L1=std1+avg1; \%standard definition for finding peaks
timehold = 1;
IUdifff1 = IU1dif;
while max(IUdifff1) > L1
    c=0;
for i=timehold:size(IU1dif',1)\%number of data
    if IU1dif(i)-L1>0
    c=c+1;
    more1(c)=IU1dif(i);
    end
end
IUdiff1 = IU1dif(timehold:size(IU1dif',1));
s1=find(IUdiff1==more1(1));
s1 = s1 + timehold -1;
tbegin1=tao*(s1-1); \%where the peak starts
A1 = [];
for j=1:(size(IU1dif',1)-s1)
    A1(j)=IU1(j+s1)-IU1(s1); \%subtraction of points after
    the start point from the start point
end

N1=A1(A1<0);
a1=N1(1);
jj1=find(A1==a1); \%shows the place of the first negative number in matrix A
jj1 = jj1(1,1);

eL1=s1+jj1; \%ending point later
eF1=eL1-1; \%ending point former
```

```
\%linear interpolation between two ending points:
te1=(IU1(s1)-IU1(eF1))/(IU1(eL1)-IU1(eF1))+eF1;
tend1=te1*tao;
duration1=tend1-tbegin1
amplitude1=max(IU1)-IU1(s1)
s1
amplitude = [amplitude;amplitude1];
finish = [finish;tend1];
start = [start;tbegin1];
duration = [duration;tend1];
timehold = eL1;
IUdifff1 = IU1dif(timehold:size(IU1dif',1));
end
IUs=[amplitude, start, finish, (finish-start)]
\%Plotting:
plot(time,IU1,'-','linewidth',1.2);

xlabel('Time')
ylabel('Fluorescent Intensity')
```

B. MATLAB CODE TO FIT QUADRATIC POLYNOMIAL CURVE ON DATA

This MATLAB Script is developed for fitting quadratic poly to the data before pressurizing.

% fitting quadratic poly to the data before(f(x)) and finding delta for the poly fit after(g(x)=f(x+delta)) for

```
\% fitting quadratic poly to the data before(f(x)) and finding delta
for the poly fit after(g(x)=f(x+delta)) for
clear;
clc;
cell_1 = xlsread('movement.xlsx','sheet1');
$z$ = cell_1(:,1) \% before loading height
int_be = cell_1(:,2) \%before loading intensity
int_af = cell_1(:,3) \%after loading intensity

F= @(x,z)(x(1)+x(2)*z+x(3)*(z.^2)); \%x(i)'s are model parameters to be fit.
x0 = [1 1 1]; \% Initial guess of x(i)'s
\%nonlinear least squares solver
[x,resnorm,residual,exitflag,output]= lsqcurvefit(F,x0,z,int_be);
\%print the results
fprintf(['There were \%d iterations using lsqcurvefit.\n'],output.iterations);
fprintf(['There were \%d function evaluations,lsqcurvefit.\n'],output.funcCount);
fprintf(['The value of error \%f.\n'],resnorm);\%resnorm is the sum of the
residuals squared,
```

```
gives a measure of the overall error
c=x(1);
b=x(2);
a=x(3);

G= @(y,z)(c+b*(z-y(1))+a*((z-y(1)).^2)); \%d is the shifting parameter
y0 = [0];
\% Initial guess of d
\%nonlinear least squares solver
[y,resnorm,residual,exitflag,output]= lsqcurvefit(G,y0,z,int_af);
\%print the results
fprintf(['There were \%d iterations using lsqcurvefit.\n'],output.iterations);
fprintf(['There were \%d function evaluations,lsqcurvefit.\n'],output.funcCount);
fprintf(['The value of shift.\n'],y(1));
fprintf(['The value of error \%f.\n'],resnorm);\%resnorm is the sum of
the residuals squared,
gives a measure of the overall error
d=y(1);

fprintf(['before(z)=a*z.^2+b*z+c, after(z)=a*(z-d).^2+b*(z-d)+c, with:.\n']);
fprintf(['and after(z)=a*(z-d).^2+b*(z-d)+c.\n']);
fprintf('a= \%f.\n',x(3));
fprintf('b= \%f.\n',x(2));
fprintf('c= \%f.\n',x(1));
fprintf('d= \%f.\n',y(1));

times = linspace(25,160);
plot(z,int_be,'bo',times,F(x,times),'b-')
hold on;
```

```
plot(z,int_af,'go',times,G(y,times),'g-')
legend('Data','Fitted curve')
title('Data and Model');
xlabel('height, um');
ylabel('intensity');
hold off;
```